QUASI-STATIC AND FATIGUE DELAMINATION CHARACTERISATION FOR CARBON FIBRE REINFORCED WOVEN LAMINATES:

INVESTIGATION INTO THE NESTING EFFECT BETWEEN LAYERS

MIREIA OLAVE IRIZAR

Directores de tesis:

Dr. D. Laurentzi Aretxabaleta Ramos

Dr. D. Dirk Vandepitte

Para obtener el título de **DOCTOR**

por MONDRAGON UNIBERTSITATEA

Departamento de Mecánica y Producción Industrial

Mondragon Unibertsitatea

Mayo 2016

DECLARACIÓN DE ORIGINALIDAD

Declaro que el trabajo desarrollado y presentado en esta tesis es original y ha sido llevado a cabo por mí dentro del Departamento de Mecánica y Producción Industrial de la Escuela Politécnica Superior de Mondragon Unibertsitatea, y el departamento de Ingeniería Mecánica de la Universidad de KULeuven, y que ninguna parte de él ha sido empleada para obtener un título o grado similar.

Mireia Olave

Mayo 2016

ACKNOWLEDGEMENTS

Kostatu zait baina amaitu dut tesia, hori da garrantzitsuena. Eta zuen babes gabe ez zen posible izango. Lerro hauen bitartez eskerrik beroenak eman nahi dizkizuet; hor zaudete, eta egongo zarete. Seguru nago.

Mila esker departamentu osoari, lankide guztiei, eta batez ere L3ko lankide paregabe guztiei; nik tesia amaitzea lortu badut, zuek ere egingo duzue! Amaitu ostean afari bat egin beharko dugu, promesa hori eginda daukat-eta.

Mila esker tesian zehar lagunkide izan diren Sheilari eta Igorri.

Mila esker koadrillakoei. Saioak eta Maiderrek badakite zer den hau; euren animoek idarberritu naute.

Mila esker tesian bideratu nauten zuzendari eta ikuskatzaileei. Euren laguntza gabe ez nintzateke honaino iritsiko.

Mila esker Lovainan ezagututako jende zoragarriari. Tesi honengatik izango ez balitz, ez genuke topo egingo, eta merezi izan du!

Mila esker etxekoei: Guraso, ahizpa, koinatu eta koinata, loba, lehengusu... eta batez ere Xabiri, Juneri eta Unaxeri.

Mila esker denoi, bihotz-bihotzetik.

Mireia

ABSTRACT

Low weight is one of the most important design criteria to be considered during the selection of the material for different applications. Weight saving is necessary in the applications where the components are in motion. Materials for transportation systems such as high-speed trains, automobiles, aircraft, or mobile components like wind turbine blades need to fulfil the strength requirement without increasing the component's thickness and, consequently, weight. Accordingly, composite materials offer the advantage of providing a lightweight structure because of their low density but with a considerable increase in strength-to-weight ratio.

Under different load conditions, static and/or dynamic, the layers of the composite material may try to debound. This phenomenon is called delamination and it is a common damage mechanism that ends up in a loss of stiffness and strength. This is the reason why in order to prevent delamination damage in composite materials, the correct characterisation and modelling of the interlaminar fracture behaviour can play an important role in the design of composite parts. The initiation of a delamination does not mean that there is a catastrophic failure in the material. The delamination may not grow any further for the rest of its service life if the loading condition does not exceed a specified crack propagation limit. The design procedure must not only cover the static interlaminar strength calculation of the component, but also the dynamic interlaminar strength calculation, and be able to support maximum load levels and fatigue dynamic

loads without total failure. Good knowledge of interlaminar fracture behaviour can facilitate reliable and efficient design criteria to prevent the final failure of the component.

Carbon fibre reinforced woven textile laminates are widely used in aeronautics, automotive or sport equipment applications due to their excellent performance and low weight. One of the reasons is that as the drapability of these textiles is high compared to unidirectional laminates, curved shapes can be manufactured easily. Due to the yarn alignment in orthotropic directions, woven structures show good in-plane mechanical behaviour, but low delamination resistance because of poor through-thickness properties. Many authors have seen in their experimental tests that fracture toughness and surface geometry can be affected because of textile structure geometry characteristics; the inner structure of the woven material has an impact on the delamination damage evolution in the laminate. The nesting effect, for example, which is the interaction between neighbouring layers of a textile composite laminate, can be strongly linked to the fracture surface geometry and the delamination behaviour.

In this work the internal structure geometry is linked to the static and dynamic fracture toughness values. The analysed properties are the nesting and the unit cell size effect. The most suitable test methods are proposed for measuring the static and fatigue fracture toughness values for the selected textile composite material. The conclusions show that fracture behaviour of the woven textile composite material changes depending on the internal structure.

LIST OF ABBREVIATIONS

UD	Unidirectional composite material
DCB	Double Cantilever Beam
ENF	End notch flexure
4ENF	Four point end notch flexure
ELS	End loaded split
C-ELS	Calibrated end-loaded split
MMB	Mixed Mode Bending
DMMB	Double Mixed Mode Bending
AE	Acoustic emission
ERR	Energy release rate
FBG	Long Fiber Bragg Grating
SAM	Scanning Acoustic Microscopy
VCCT	Virtual Crack closure technique

VARTM	Vacuum Assisted Resin Transfer Molding
RTM	Resin Transfer Molding
MSBL	Misalignment Scatter Between Layers
SM	Sample misalignment
COV	Coefficient of variation
CBTE	Effective crack length method
BTBE	Beam Theory including Bending rotations effects method
ONF	Over notched flexure
CBBM	Compliance Based Beam method
DIC	Digital image correlation

CONTENTS

LIST OF FIGURES

LIST OF TABLES

1. CHAPTER 1: INTRODUCTION

1.1 GENERAL INTRODUCTION

Today, low weight is one of the most important design criteria to be considered during the selection of the material for different applications. Weight saving is necessary in the applications where the components are in motion. Materials for transportation systems such as high-speed trains, automobiles, aircraft, or mobile components like wind turbine blades need to fulfil the strength requirement without increasing the component's thickness and, consequently, weight. Accordingly, composite materials offer the advantage of providing a lightweight structure because of their low density but with a considerable increase in strength-to-weight ratio.

Under different load conditions, static and/or dynamic, the layers of the composite material may try to debound. This phenomenon is called delamination and it is a common damage mechanism that ends up in a loss of stiffness and strength. This is the reason why in order to prevent delamination damage in composite materials, the correct characterisation and modelling of the interlaminar fracture behaviour can play an important role in the design of composite parts. The initiation of a delamination does not mean that there is a catastrophic failure in the material. The delamination may not

grow any further for the rest of its service life if the loading condition does not exceed a specified crack propagation limit. The design procedure must not only cover the static interlaminar strength calculation of the component, but also the dynamic interlaminar strength calculation, and be able to support maximum load levels and fatigue dynamic loads without total failure. Good knowledge of interlaminar fracture behaviour can facilitate reliable and efficient design criteria to prevent the final failure of the component.

Carbon fibre reinforced woven textile laminates are widely used in aeronautics, automotive or sport equipment applications due to their excellent performance and low weight. One of the reasons is that as the drapability of these textiles is high compared to unidirectional laminates, curved shapes can be manufactured easily. Due to the yarn alignment in orthotropic directions, woven structures show good in-plane mechanical behaviour, but low delamination resistance because of poor through-thickness properties. Many authors have seen in their experimental tests that fracture toughness and surface geometry can be affected because of textile structure geometry characteristics; the inner structure of the woven material has an impact on the delamination damage evolution in the laminate. The nesting effect, for example, which is the interaction between neighbouring layers of a textile composite laminate, can be strongly linked to the fracture surface geometry and the delamination behaviour. Current manufacturing processes do not take into account the shifting between textile layers, and consequently the obtained nesting values are random over the entire area and thickness of a panel. The variability in the nesting value can result in the increase in the uncertainty of the delamination behaviour of the laminate. The introduction of a suitable nesting value in the analysis of delamination is a first step in a sensitivity study. In the subsequent step of the manufacturing process the effect of nesting may be taken into account for optimum delamination behaviour of the composite panel.

1.2 PROBLEM STATEMENT

During the design of a textile composite part, all measures should be taken to avoid delamination failure. The lack of knowledge about the static and dynamic behaviour of delaminated surfaces makes the final design heavier than it should be. Safety

requirements impose the “crack no-growth” design criteria, and this restriction reduces considerably the possibility of obtaining an optimal final part. The lack of awareness of material´s delamination mechanics results in a non-efficient design of the components. Different knowledge areas should be reviewed in order to design efficiently the components in means of avoidance of delamination. Next points are the key to understand the presented problem:

- Textile´s internal structure does not follow an ideal and repetitive pattern. There is a lack of experimental data on the geometry of the layers interfaces.
- The size effect (unit cell size dimension) is another issue to be considered as a design parameter. The textile geometry scale effect on mechanical properties has not been analysed.
- There is no standard for measuring static fracture toughness values for textile materials. The actual standards for static mode I and mode II only deal with unidirectional fibre reinforced composite materials.
- There is no standard for measuring the delamination fatigue onset and growth considering mode I fracture toughness values for textile materials. In 2008 a standard for measuring the onset was issued, but only for unidirectional fibre reinforced composite materials.
- The interrelationship between the delaminated surface geometry and the fracture toughness values are still not studied in depth. The nesting effect has not been linked yet to the fracture toughness properties.

This research will cover all aspects necessary to improve the design process of composite materials made of textile structures.

1.3 RESEARCH OBJETIVES

The objective of this thesis is to investigate delamination phenomena of textile composites, trying to understand the influence of the delaminated surface´s geometry. The presented research links the geometrical structure of carbon fibre reinforced woven laminates with its effect on the quasi-static and fatigue delamination behaviour (Figure 1).

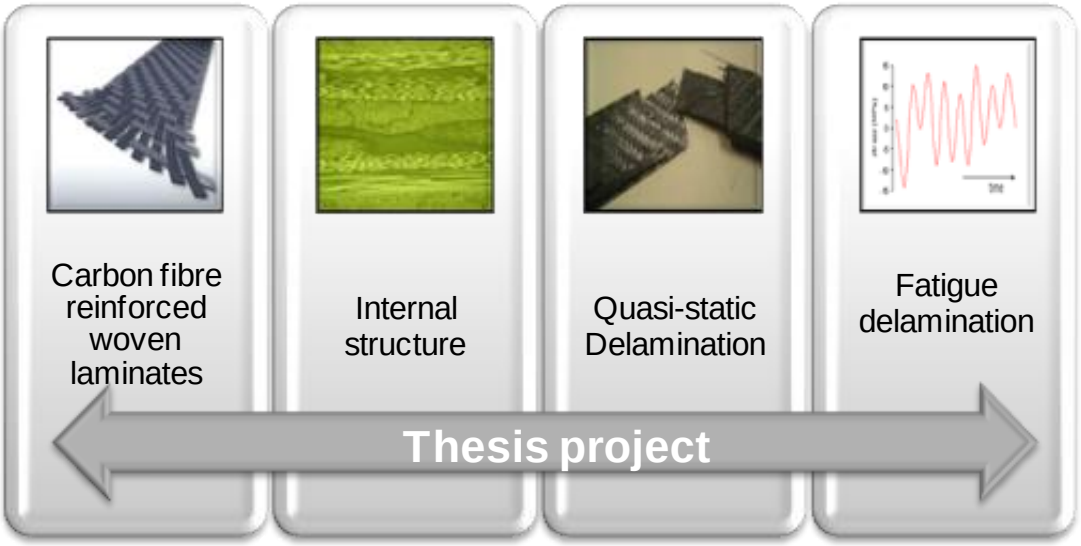

Figure 1: The areas analyzed in this research work

In order to obtain answers to the presented problems, the questions defined in Figure 2 must be solved.

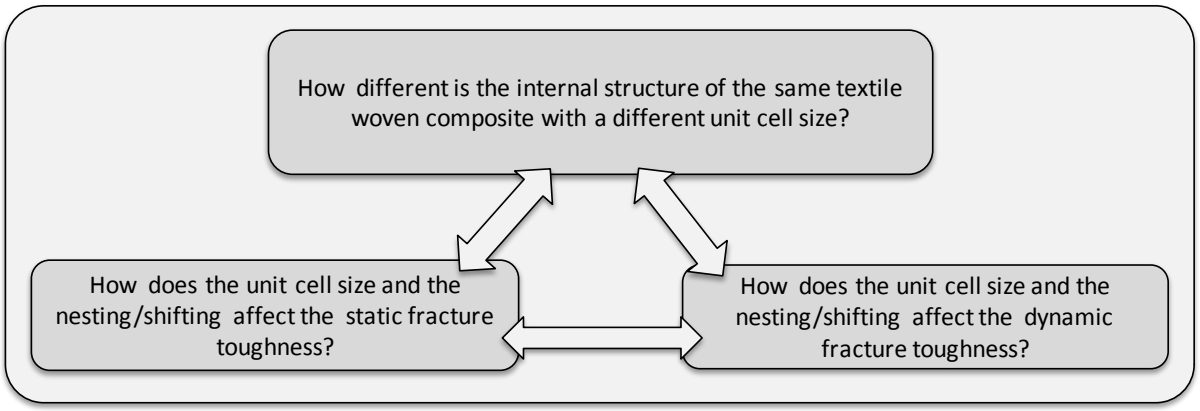

Figure 2: Questions that must be solved during this research

The research objectives are divided in three main areas of interest, each one related to different experimental and technical issues:

a) ***Experimental analysis of the geometrical structure of textile materials.*** The internal variability of geometrical properties of textile materials is evaluated. The effect of this variability is linked to the mechanical properties measured experimentally.

b) ***Static facture toughness measurements of textile materials and the effect of the internal geometry.*** The impediment of not having a standard for measuring mode I and mode II fracture toughness values has to be overcome. Modifications

to existing test procedures are proposed in order to obtain reliable values. Geometrical parameters are linked to static fracture values, obtaining the relation between the controlled input parameters and the results from experimental measurements.

c) ***Dynamic fracture toughness measurements and the effect of the internal geometry***. Standards for fatigue delamination onset and growth in mode I for textiles materials are not available. As for static fracture toughness measurements, modified test procedures are used. Geometrical parameters are linked to dynamic fracture values, obtaining the relation between the controlled input parameters and the results from experimental measurements.

1.4 OUTLINE OF THE DISSERTATION

The thesis manuscript is divided into nine different parts. The first chapter describes the problem statement and the research objectives. The second part explains the state of the art and reviews the literature. The third part reviews the critical analysis of the literature, summarises the thesis phases and describes the preliminary work done before stating the main topic of the research. This preliminary work studies the size effect on the internal geometry and mechanical property variability of woven composites.

In the fourth chapter the internal geometry measurement of two woven composites is analyzed: cross section of the yarns, fiber volume fraction, crimp, misalignment of the samples, thickness of the plates, nesting value, etc. The chosen textile composites are produced using the same resin reinforcement and same architecture, but have different yarn size (3K and 12K). The dispersion of measured geometrical parameters is introduced in a numerical multi-scale modeling approach to evaluate the macroscopic stiffness values. A sensitivity analysis is performed for each geometrical parameter and laminate stiffnesses are derived. These are linked to the experimentally obtained elastic properties by tensile tests. Finally the unit cell size scale effect for measured geometry variability and experimentally obtained elastic properties are evaluated.

The fifth chapter evaluates the fracture toughness of two woven laminates for different nesting/shifting values between advanced layers. The analysed woven composites are manufactured using the same resin-reinforcement and same architecture, but have a

different tow size (3K/12K). Three different nesting/shifting configurations are applied to the plies at the fracture surface: zero shifting, middle shifting and maximum shifting. Before being tested, the internal geometry of the material is evaluated and any shifting error is measured. For all these configurations Mode I fracture tests are carried out. The differences obtained between 3K and 12K cases can be explained by fibre bridging, but not the differences between the nesting configurations. Depending on the nesting/shifting value the delaminated surface waviness is different, and consequently the fracture toughness is also influenced.

The sixth chapter evaluates the mode II fracture toughness for the same material using the end notch flexure set-up. Corrected Beam Theory with effective crack length method (CBTE) and Beam Theory including Bending rotations effects method (BTBE) are evaluated for obtaining mode II fracture toughness. During data post-processing, the importance of the bending angle of rotation and the test configuration is observed to be important. The results show that crack propagation under mode II is more stable if the matrix is evenly distributed on the surface. The nesting does not significantly affect mode II fracture toughness values, although a greater presence of matrix on the delaminated area increases its value.

The seventh chapter investigates the mode I fatigue delamination onset and growth for the same material. The nesting differences show little effect on the delamination onset fracture energy threshold limits, but normalised results show higher values for the smaller unit cell size. Analyzing the normalised Paris diagrams it is concluded that the unit cell size and the nesting configuration does not affect the slopes for the Paris plot. However a smaller unit cell size shifts the normalised Paris diagram to the right. The non-homogeneity of the delaminated surfaces of textile materials leads to irregular slopes.

Finally, in the last two chapters the main conclusions and future works are discussed.

2. CHAPTER 2: LITERATURE REVIEW

The first part describes composite structure types, their classification based on matrix/reinforcement type and a deeper description of textile reinforced composite materials. The second part introduces a detailed description of woven structures, their internal geometry and mechanical properties. The third part details the delamination damage mechanism in quasi-static and fatigue load conditions. And finally the fourth part resumes the behaviour of woven materials when delamination takes place.

2.1 COMPOSITES STRUCTURES

A composite material is a system created by combining two or more materials, mixed or bonded, on a macroscopic scale. The purpose of a composite material is to optimally utilise the properties of the individual constituents obtaining enhanced mechanical, physical or chemical behaviour. Literature provides many definitions for composite materials, but the description by Chawla [1] covers all possible aspects. Chawla considers that a composite material must fulfil next conditions:

- A composite material is manufactured by an artificial process.
- A composite material is composed by two or more phases or physically and/or chemically different, separated by a defined interface.

- The properties of the composite material cannot be achieved by the materials used alone.

2.1.1 Composites classification

In the literature there are many classifications of composite materials depending on the property analysed [2, 3]. Figure 3 shows the classification based on the reinforcement type and

Figure 4 shows the classification based on the matrix material. Three reinforced types are distinguished in composite materials: fibre-reinforced (classified depending on the length and positioning of the fibres), particle-reinforced (classified depending on the size and dispersion in the composite) and structural (where the properties of the composite are obtained from the stacking sequence of the materials). For fibre or particle reinforced composites organic or inorganic matrices can be used. In structural sandwich materials, the core material can be made of a honeycomb structure, balsa wood or foam, among others.

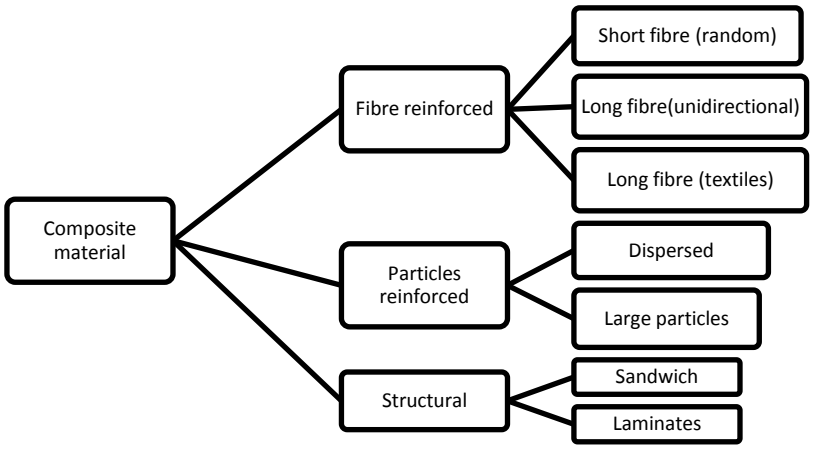

Figure 3: Classification of composite materials depending on the reinforce type

The reason why composite materials are widely used in different applications is that they display competitive advantages with respect to other types of materials. The lightness, corrosion resistance and high specific stiffness/strength values make them suitable for many applications, including automotive, aeronautical, railway transportation, wind energy or building industry. Although considerable improvements

have been made in the analysis of damage and long-life behaviour, researchers need to understand and control all possible failure mechanisms in composite materials.

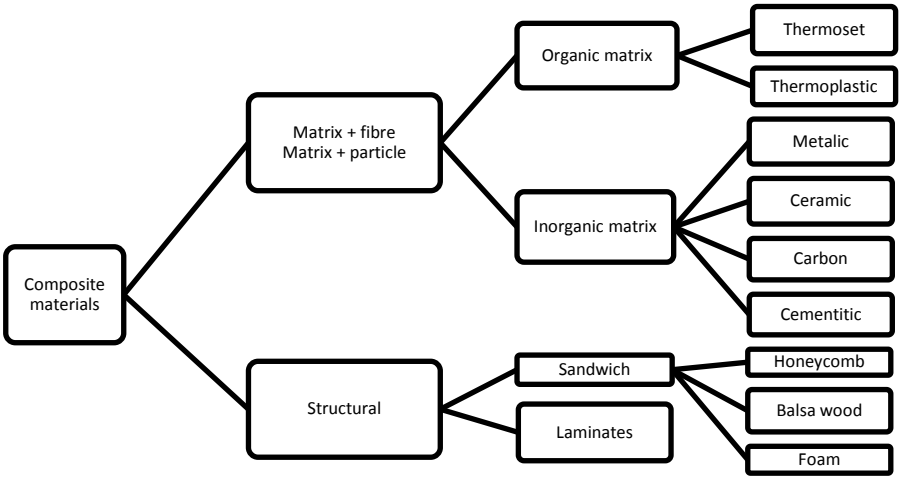

Figure 4: Classification of composite materials depending on the matrix type

For high stiffness/strength requirements, for instance in aircraft structures, the most widely used composite-reinforced material is carbon fibre. The Boeing 787 [4] aircraft is composed of 50% composite, 20% aluminium, 15% titanium, 10% steel and the rest of other materials (Figure 5). Carbon composites are used on the fuselage, wings, tail, doors, and interior parts. The Boeing 787 craft is 80% composite by volume, making it possible to create a lighter aircraft.

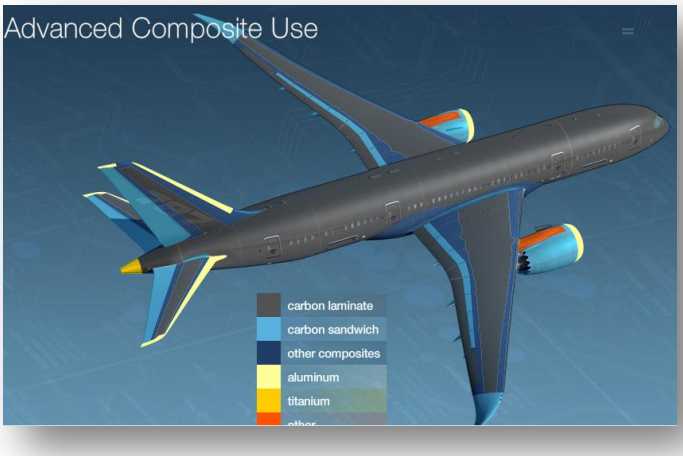

Figure 5: Composite content of the New Boeing 787 [4]

Historically, small and medium size wind turbine blades have been made using fibreglass/epoxy prepegs. Each blade is made of two shell sections, which are bonded

onto a precured spar. As wind turbine manufacturers are building larger turbines (above 5 MW) and new turbine concepts are being launched onto the market (e.g. offshore), they need to explore new materials and designs in order to optimise the weight of the components. The LM [5] blade manufacturing company, for example, is currently creating a new design concept based on a combination of glass fibre and carbon fibre, which can be defined as a hybrid composite concept. Although carbon fibre cost is higher than glass fibre, the lightness obtained helps to minimise the loads on the nacelle and the tower, thus improving efficiency. The high specific stiffness/strength of carbon fibre compared to glass, aramid or natural fibres makes them suitable in many applications. The carbon fibre properties are characterised by:

+ Low density.
+ High specific stiffness/strength, with very little plastic deformation.
+ High fatigue strength.
+ High temperature resistance (mechanical properties at 100ºC remain the same).
+ Moisture resistance.
– Low impact resistance.
– Low wear resistance.
– High cost.

Carbon fibres can be embedded in a thermoset or thermoplastic matrix. In most cases, thermosets are in a liquid or semi-liquid state at room temperature, and a curing process is needed in order to solidify them (this process is irreversible). Thermoset matrices do not melt at high temperatures, the material would degrade. Thermoplastic matrices are usually tougher, easier to recycle and lighter than thermosets, but a high viscosity hampers good impregnation with the fibres.

The classification diagram in Figure 3 shows that fibres can have different structures inside the composite material: short fibres, long unidirectional fibres or long textile fibres (Figure 6). For randomly placed short fibres, the composite material displays a quasi-isotropic behaviour and the mechanical properties obtained are lower than for other structures (unidirectional or textile) made of the same kind of fibres. In unidirectional (UD) composite materials the fibre longitudinal direction shows much higher stiffness and strength value than the transversal direction. UD composite materials are in most cases stacked in laminates, where the lower transversal properties can be improved by applying UD layers in different orientations ($\pm\theta$).

A laminate is constructed by adding two or more layers of material together (UD, textiles or random fibre layers). The laminates, for example, can be manufactured by means of hand lay-up of the layers in an open mould, by curing prepeg layers in an autoclave, or by applying pressure on a hot press.

The textile reinforcement creates a hierarchical structure in which the fibres are grouped into strands (yarn) forming a periodic configuration. Depending on the textile structure and repetitive pattern specified for the composite material, the properties obtained could be isotropic, orthotropic or anisotropic. One of the characteristics of textile composites that differentiate their behaviour from UD laminates is the crimp of the yarns. The advantages over UD composites are better drapability, impact and delamination strength, although the waviness of the fibers in the textile results in a lower in-plane stiffness and strength.

This thesis project focuses on textile fibre-reinforced composite.

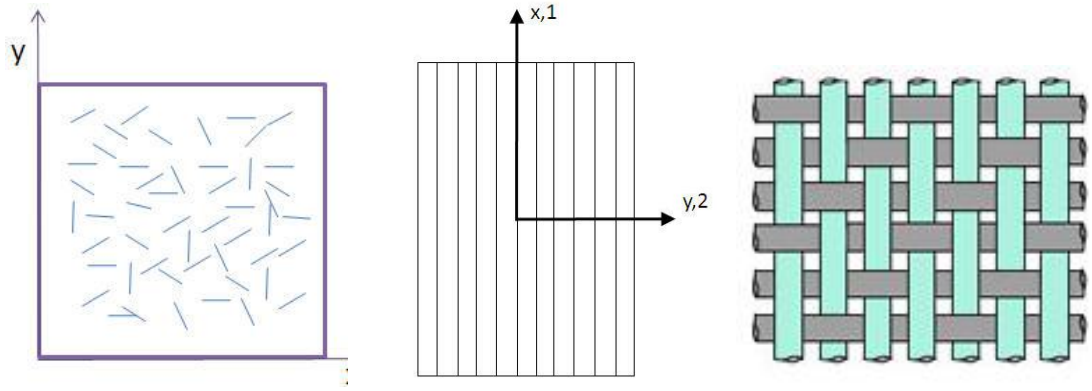

Figure 6: Short fibres, long unidirectional fibres and long textile fibres

2.1.2 Textile-reinforced composite materials

Textiles are characterised by a unit cell, which is the smallest repetitive pattern that can be distinguished inside the structure. The squares in Figure 7 represent the unit cell for each different type of woven material.

Textile technologies allow three-dimensional reinforcements to be manufactured, in which the fibres are distributed along three main directions.

Textile architectures are also distinguished by the number of main dimensions in which the textile stretches. When the yarns (bunch of fibres) are extended only in the plane, this is known as two-dimensional or 2D architecture. When the fabric has yarns in the direction perpendicular to the main plane, the textile architecture is known as three-

dimensional. 3D textile composites can achieve better stiffness and strength out of the plane than textile laminated composites, where delamination damage can affect the overall behaviour of the component [6].

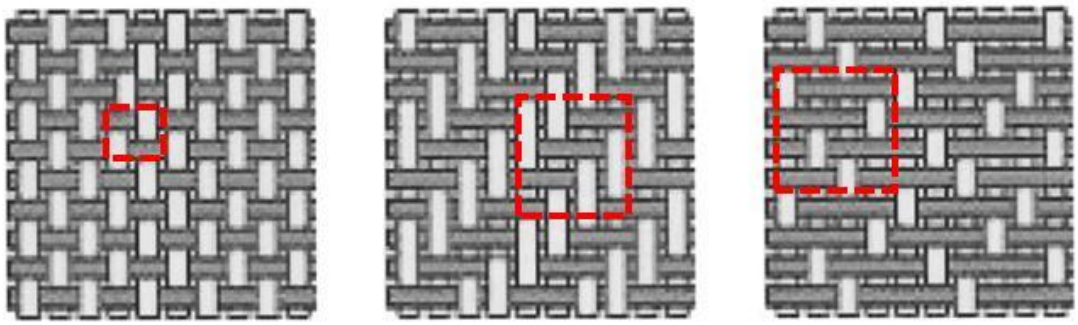

a) Plain **b) Twill** **c) Satin**

Figure 7: Three types of woven structures and the repetitive unit cells.

Textiles are built from these basic manufacturing techniques: weaving, braiding, knitting and stitching.

Weaving: A weave is the architecture in which two types of threads, called warp and weft, are intertwined. The yarns oriented in the manufacturing direction are called the warp and the yarns that run across from side to side are the weft or filling. The vast majority of two-dimensional woven fibreglass and carbon fibre that are used as reinforcement in the textile composite material industry are made using this technique [7]. Figure 8 shows the main sub-architectures in 2D weaving structures, which are distinguished in the sequence used to weave the warp and weft. This sequence has a clear influence on the mechanical properties of the finished part in service and in the drapability or deformation during processing of composite material. The plain woven textile reinforcement is most commonly used each warp passes over the first frame and below repeatedly (Figure 7a).

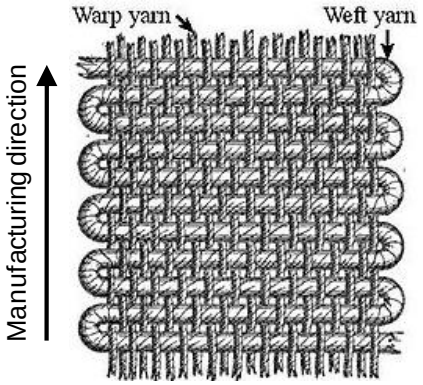

Figure 8: Woven structure

3D woven architectures have additional strands in the direction away from the main plane. There are a variety of sub-architectures. The main ones are the angle-interlock followed by orthogonal weaving (Figure 9).

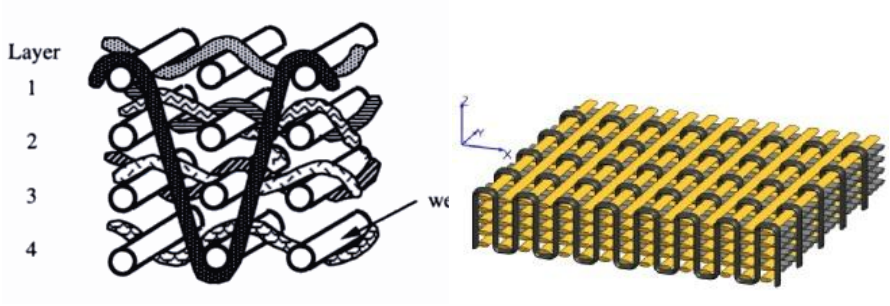

(a) Angle interlock (b) Orthogonal 3D weaving

Figure 9: 3D Weaving

In general, the mechanical properties of woven architecture are governed by [7]:

- Textile structure parameters: type of architecture, thread size, space between the fibres, fibre orientation, volume fraction of fibres, etc.
- Global parameters: the orientation of the fibres or fibre volume fraction and matrix in the composite.

Woven fabrics exhibit good stability in the direction of the warp and weft and they offer a high fibre volume ratio.

Braiding: Braiding is a process created by intertwined twisted coils from numerically controlled movements. The yarns are interlaced at angles ranging between 10º and 80 º, fibres at 0 ° can also be included.

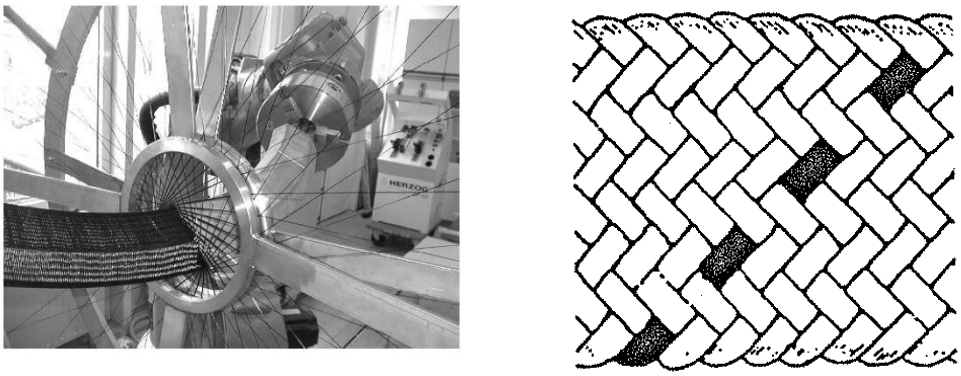

(a) (b)

Figure 10: (a) 2D Braiding architecture manufacturing, (b) a detail of the yarn displacement

As shown in Figure 10a, the textile pattern is manufactured on a mandrel. Depending on the geometry of the mandrel, different tubular preforms can be obtained. Figure 10b shows a typical pattern of 2D braiding architecture. This type of architecture has been used for some time to strengthen golf clubs, aircraft propellers, and masts of ships or bridges [8]. The 3D braided architecture is mainly used to manufacture preforms for reinforcing beam-type profiles [6]. Braided architecture is particularly suited to torsion resistance, shear deformation and impact [7]. However, these architectures offer a poor performance against tension or compression in the manufacturing direction.

Knitting: There are two variations: warp knitting (Figure 11a) and weft knitting (Figure 11b). Weft-knitting is created from a single yarn that is formed in successive curves with the movement of the needle in the transverse direction row by row. In warp knitting, unlike weft knitting, the fabric consists of multiple yarns, so the manufacturing process is more complex. However, warp knitting achieves superior mechanical properties to those of weft knitting [2]. In knitting, the threads take a much larger degree of curvature than in other textile architectures; as a result, this architecture usually has a lower stiffness at rest (weaving and braiding). However, it has the advantage that it is highly conformable. Therefore, it is ideal for preforms having a structural function that is not too demanding when it is adapted to very complex shapes during the process of forming and consolidation.

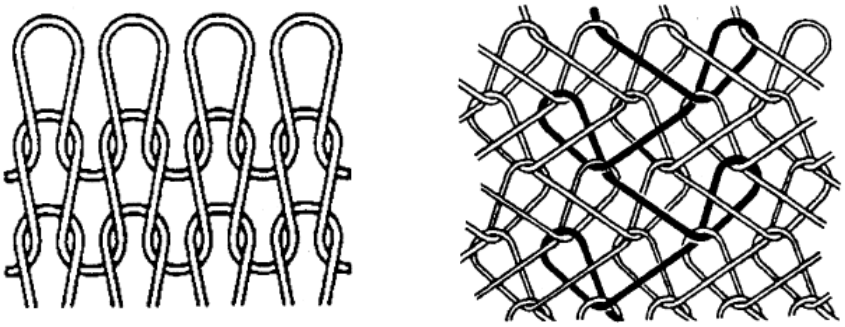

(a) Weft knitting (b) Warp knitting

Figure 11: Knitting types depending on the manufacturing process

Stitching: The stitching process is the simplest and cheapest of all the basic weaving techniques. Roughly, it consists of sewing, using a needle and thread, a stack of two-dimensional textiles to obtain a three-dimensional structure. The stitching has certain advantages over other architectures. The possibility of using standard two-dimensional fabrics that are commonly used in the composite industry allows greater flexibility in component manufacture. The process is highly automated and therefore relatively fast, economic production processes can be developed. However, the stitching also has its disadvantages compared to other 3D architectures. The main one is the reduction of mechanical properties in the plane of the preform. When the needle punctures different tissues, local damage is generated in the fibres that changes mechanical architecture. This reduction may be exacerbated further by the bends and through the interstices produced by this technique in two-dimensional tissue. After impregnating and consolidating the reinforcement with the matrix, these gaps produce concentrations of resin which are potentially prone to crack initiation [6].

2.2 WOVEN STRUCTURE

This section investigates woven laminate structures. The properties that are studied are divided into three main parts: specification of the structure's geometry variables, mechanical behaviour and damage in woven laminates.

2.2.1 Woven structure geometry

Woven structure properties are highly dependent on the waviness of the yarns in the material. The crimp percentage of the yarns is specified by the ratio of the yarn's length (curved shape) to the length of fabric ($crimp[\%] = \frac{L_f - L_0}{L_0}$ Eq.

1). The crimp depends on fabric thickness, mechanical and fibre volume fraction. In turn, the performance of the fabric depends on crimp (Figure 12).

$$crimp[\%] = \frac{L_f - L_0}{L_0} \quad \text{Eq. 1}$$

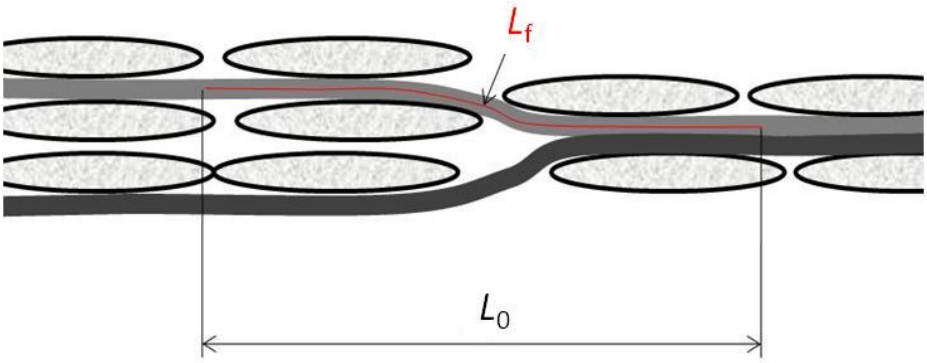

Figure 12: Crimp percentage is obtained by L_f and L_0 measurement.

Crimp value depends on the nesting effect between advanced layers; the accommodation of yarns between each other can lead to a repositioning of the yarns in the other direction. Yarn thickness, yarn width and spacing length between advanced yarns are also important for specifying the nesting effect in the woven structure (Figure 13).

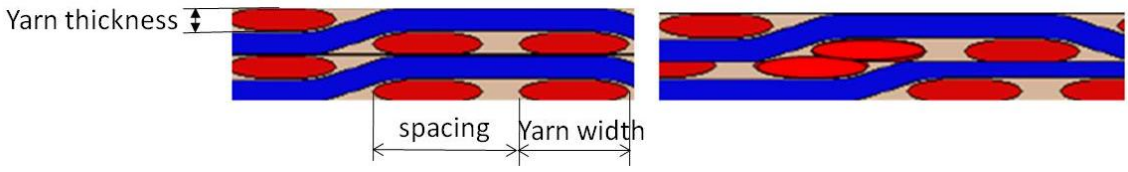

Figure 13: Geometry properties of the woven structure

Lomov [9] specifies the nested position using the variable h^*, which is calculated from the minimum distance between centre planes of the layers. Lomov considers two identical layers, with one layer shifted relative to the other. When there is no nesting between layers, the nesting distance is equal to the layer thickness (Z). The distance (δ) between the face surface of the botton layer and the back surface of the top layer is calculated by , Eq.2, Eq. 3 and Eq. 4 (Figure 14). The dx and dy parameters represent the shifting between layer position in both directions (x, y).

$$\delta(x, y; h) = h - Z + h_f(x, y) + h_b(x - dx, y - dy) \quad \text{Eq. 2}$$

$$h_f(x, y) = \frac{Z}{2} - z_f(x, y) \quad \text{Eq. 3}$$

$$h_b(x,y) = z_b(x,y) + \frac{Z}{2} \quad \text{Eq. 4}$$

h_f, h_b= Face and back surface of the fabric.

z_f, z_b= Face and back surface coordinate.

The nesting distance (h^*) is the value that minimizes the distance δ (Eq. 5).

$$\delta^*(h) = 0 \quad \text{Eq. 5}$$

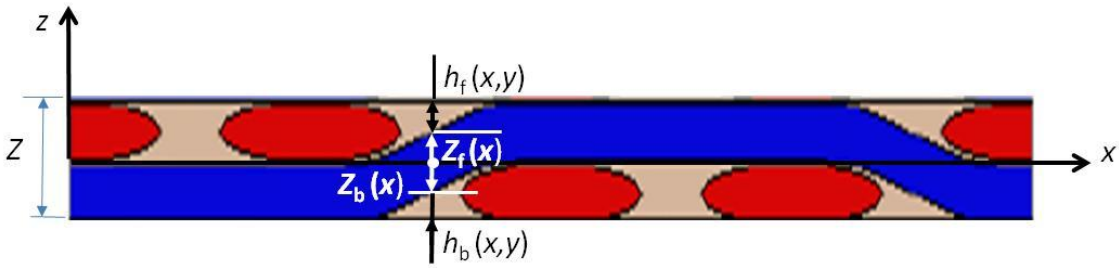

Figure 14: Face and back surface distances at position (*x*)

2.2.2 Woven structures´ internal variability

The importance of the internal geometry of the structure is crucial when analysing the behaviour of the material during loading conditions. The scatter of the geometrical structure in textile composite materials can lead also to a scatter of physical properties. This is the reason why the knowledge of the correlation between the source of variability and the resulting behaviour is essential for controlling the manufacturing process and consequently the final material properties. Significant features such as mechanical elastic properties, formability, permeability, initial failure and damage progression are very sensitive to the variability of the internal geometry structure. Many authors [10-13] found a direct relation between fabric structure and material permeability values. As an example Hoes [10] defined the nesting of layers as the major source of variations in permeability values for fabric composite materials. Endruweit et al. [11] investigated the influence of variability of reinforcement geometry (for example, variation of fiber orientations, fiber angle variation in a non-crimp fabric) on permeability measurements. Related to other properties, Skordos [14] found significant variations in the formability due to the effect of misalignment of yarns and local unit cell size in pre-impregnated woven textiles.

In most of the mathematical models an ideal repetitive unit cell for mechanical characterisation is used, without realising how important the difference between the real structure and a model can be. Variables such as fibre volume fraction, defects related to the manufacturing process or misalignment of fibres with respect to the load application axis create scatter in the mechanical properties that are measured experimentally. Directionality and misalignment is the paramount factor for the scatter in the properties on the loading direction. John et al. [15] pointed to the orientation of the yarn relative to the loading axis as the most critical variable while calculating the tensile properties. When there is an unintentional misalignment of small angles between the applied load and the sample orientation, the stiffness and strength properties are affected. Vallons [16] found stiffness and strength changes for a biaxial non-crimp fabric composite at small off-axis angles (below 5°). The observed changes were higher for the strength property than for stiffness values. Pinho [17] concluded that in advanced composites, local micro-structural defects, such as fibre misalignments seem to be initiation of kinking. From the normally distributed fibre angle variations, Endruweit [11] calculated the permeability changes in textile materials. Increasing fibre angle variations for resin injection simulations, times for complete filling of the mould increase. Loendersloot [18] found that the impregnation and mechanical behaviour are affected by the misalignment of the fibre bundles, those initial misalignments can be up to 7–8º. Liu [19] evaluated the average and standard deviation of the misalignment angles in carbon-epoxy pultrusions for different fibre volume fraction values. Depending on the fibre volume fraction and the size of the mould used during the manufacturing process the mean value of the average misalignment angle reaches values up to 3.5° and the standard deviation varied from 1.2° to 4.3° respect to the desired orientation.

The internal geometry variability has been studied by several authors using mainly optical methods. Desplentere [20] compared the suitability of two methods, an optical microscopy and X-ray micro-CT, for measuring stochastic parameters of the geometry for 2D and 3D woven textile preforms. The conclusions showed no significant differences between both methods. The standard deviations found were close to 16% while measuring yarn thickness, width and spacing.

Charmpis [21] et al. defined the lack of micromechanical data measurements as a big problem while evaluating the results for stochastic finite element methods. This work is

an attempt to overcome the problem examining and evaluating the micromechanical characteristics of the material. The main objective of the present research is to analyse the variability of the internal geometry of two woven structures and to evaluate how this scatter affects the macroscopic mechanical properties. First the measurements of geometrical parameters are analysed by means of optical microscopy. The evaluation of how different an ideal geometrical model of a textile woven unit cell can be from the real inner structure is described. Then the elastic properties are evaluated from a numerical multi-scale model simulation having as input data the measurements carried out in the first part and taking into account their identified variability. The properties obtained are compared to the values obtained experimentally during tensile tests.

2.2.3 Woven structure mechanical and damage behaviour

Static behaviour and degradation of woven structures had been studied by many authors [22-24], showing a repetitive damage evolution pattern. In woven laminates at low applied strains, damage starts as fibre-matrix debonding, and progresses creating transverse intra-yarn cracks. When these cracks develop until they reach an edge, delaminations between orthogonal yarn interfaces take place. In woven composite materials, three damage levels are linked to the global mechanical behaviour of the structure: micro level (fibre-matrix debonding), meso level (transverse cracking of the fibre bundle or crack in the matrix) (Figure 15) and macro level (delamination at the fibre bundle boundaries) [25-28]. In order to evaluate the properties of woven materials, different authors [26, 28-30] have developed analytical and numerical methods to calculate the mechanical properties and final strength values of woven structures.

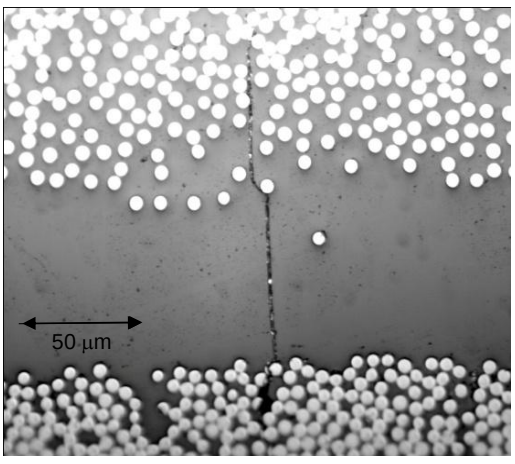

Figure 15: Intra yarn and matrix crack in a woven structure (IKERLAN)

The importance of the internal geometry of the structure is crucial while analysing the behaviour of the material during loading condition. Main features, such as mechanical elastic properties, formability, initial failure and damage progression are very sensitive to the variability of the internal geometry structure [15]. Variables, such as fibre volume fraction, defects related to the manufacturing process, nesting between layers or misalignment of fibres with respect to the load application axis, create a scatter in the mechanical properties measured. John et.al., for example, pointed to the orientation of the tow relative to the loading axis as the most critical variable when calculating the tensile properties.

The nesting of reinforcements in textile laminates, for instance, is linked to permeability and mechanical properties and influences laminate thickness and fibre volume fraction. Lomov [9] observed that when the number of layers in a laminate is increased, the thickness per layer decreases, increasing the fibre volume fraction for the given pressure for larger numbers of layers stacked together. Nesting has different behaviour in phase or out of phase configurations, showing differences in laminate stiffness depending on the positioning of the nested layers. Lomov also analyzed the wide scatter of permeability due to random nesting in woven laminates. Woo and Suh [31] obtained non-symmetrical scatter distributions of the elastic moduli (10-20%) having the same sample width but with nesting variations. Naik et.al. [30] found that the shifting creates an increase in strength of %10. Vaidya et. al. [32] found that nesting creates bridging between the laminate layers that prevents the delamination damage mechanism from functioning. This delamination delay creates better strength properties in the material.

2.3 DELAMINATION

2.3.1 Delamination mechanisms

Delamination is a failure mode where, due to cyclic, impact or thermal/chemical shrinkage stresses, the layers of a structure separate, creating a loss of mechanical properties [33]. Delamination failure can also be arise during manufacturing; the shrinkage of the matrix during the curing process can lead to shear stresses in the interlayer. Structural discontinuities can also be a source of delamination; stress concentrations near holes, notches or ply-drop areas can produce an initial crack.

Bolotin defined two kinds of delaminations (Figure 16, Figure 17): internal delamination and external delamination.

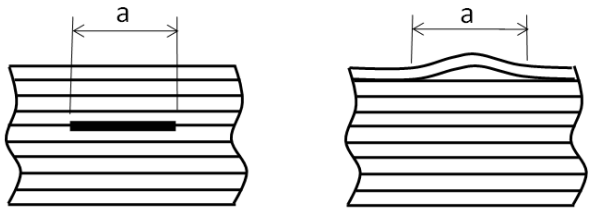

Figure 16: Internal and external delamination

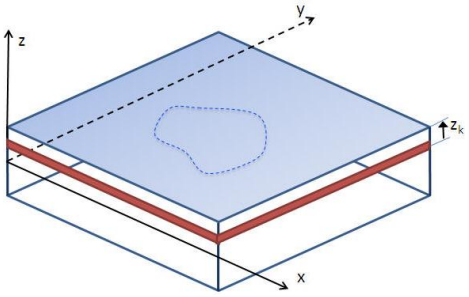

Figure 17: Internal delamination in a laminate at z_k distance to the surface

Internal delamination takes place in the inner plies of the laminate, far from the surface layers, and tries to separate the laminate into two parts. Although the strength of the laminate is considerably affected, there is still an interaction between the deformations of the parts that are separated by delamination. External delamination takes place near the surface layer. Contrary to what happens in internal delaminations, deformation of the rest of the laminate does not affect the behaviour of the separated layer.

Depending on the acceptable damage value specified for a delamination, the design of composite structures can be divided in terms of two strategies [34]:

- No-growth design criteria (safe life): the loading does not exceed crack growth threshold.
- Damage tolerant design criteria (fail safe): the loading can exceed crack growth threshold, but without a catastrophic failure.

Both design criteria need a good understanding of the damage behaviour in the material, although the second one requires more accurate knowledge of damage evolution to obtain a reliable design. In order to acquire this knowledge, the delamination damage mechanism in plastics and reinforced materials has been studied since early 20th

century because of its big influence on the behaviour and final failure of the structures [35-40].

Depending on the deformation zone on the crack tip and the state of stress, 3 types of crack propagation modes are distinguished (Figure 18): Mode I (opening mode), Model II (Sliding mode) and Mode III (tearing mode). Fractures in which two or more modes are operative are called mixed-mode fractures.

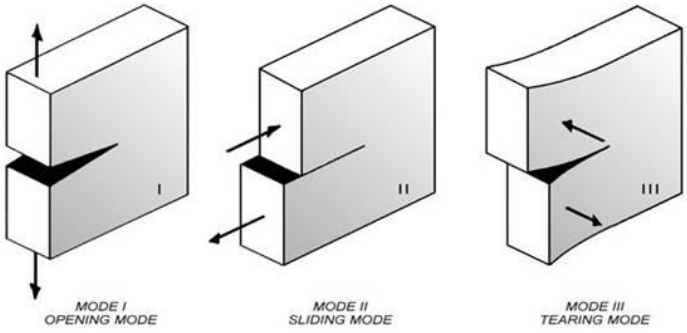

Figure 18: Mode propagation types

2.3.2 Experimental measurements

The tests needed to characterise delamination in laminated structures are reviewed in this chapter. The delamination initiation and growth measurement techniques are also analysed. Standard tests and alternative set-up will be explained for mode I, mode II and mixed modes (I/II). Tests for mode III are not analysed in this chapter due to the experimental difficulties in introducing pure mode III loading [41]. Brunner [42] reviewed fracture toughness measurement standard tests for fibre-reinforced polymer-matrix composite and analyze also new developments for new standard test procedures.

Mode I

The opening (mode I) test method is accepted by the international standard organisations ASTM and ISO [43, 44]. There is no specific standard for mode I test for textile or non-unidirectional materials. The common specimen shape is the Double Cantilever Beam (DCB) (Figure 19), where a non-sticking thin film (below 13μm) is inserted as starter of the crack (Figure 20). When the machine starts loading the specimen, the crack starts opening and crack length development is measured optically. These standard tests are limited to quasi-static measurements. For mode I, sometimes fibre bridging and fibre breakage is observed in fibre reinforced composite materials.

For fatigue tests, an ASTM procedure for mode I dynamic loading is defined for crack initiation measurement [45]. Tension-tension loading is applied to the specimen having constant amplitude and for different G values. The procedure does not take into account fatigue propagation of the crack, but these aspects were measured by other authors [46-48].

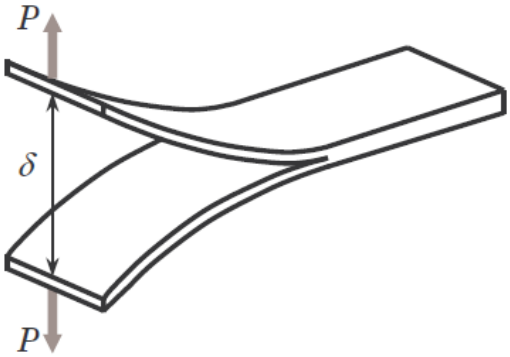

Figure 19: DCB test loading condition [49]

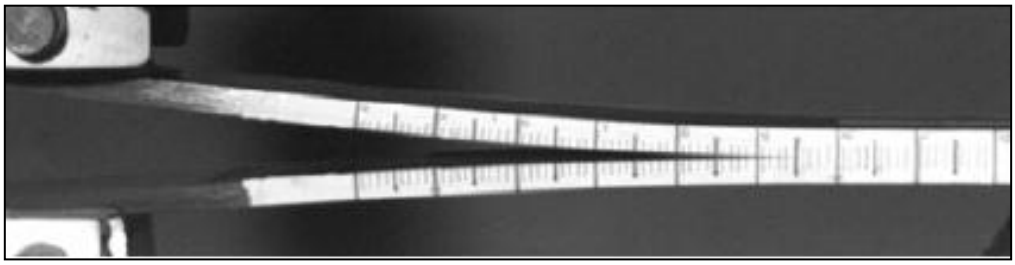

Figure 20: Mode I DCB test detail from one side [50]

Mode II

For measuring mode II fracture toughness there are different test configurations: end notch flexure (ENF), four point end notch flexure (4ENF) or end loaded split test (ELS) (Figure 21) are used [50, 51]. An international standard [52] was developed for determining mode II fracture toughness of unidirectional fibre reinforced materials based on ENF configuration. Another new standard [53] using the calibrated end-loaded split (C-ELS) test was established simultaneously. The instability of ENF and the fact that there is not enough knowledge about the effect of friction during the test makes difficult to conceive an international standard. For mode II fracture toughness measurement four point end notch flexure (4ENF) test was defined by Martin and Davidson [54]. The test can overcome the difficulties during ENF test. For fatigue tests

on mode II ENF was used by Beguini [55], but more recent works are using 4ENF [56, 57].

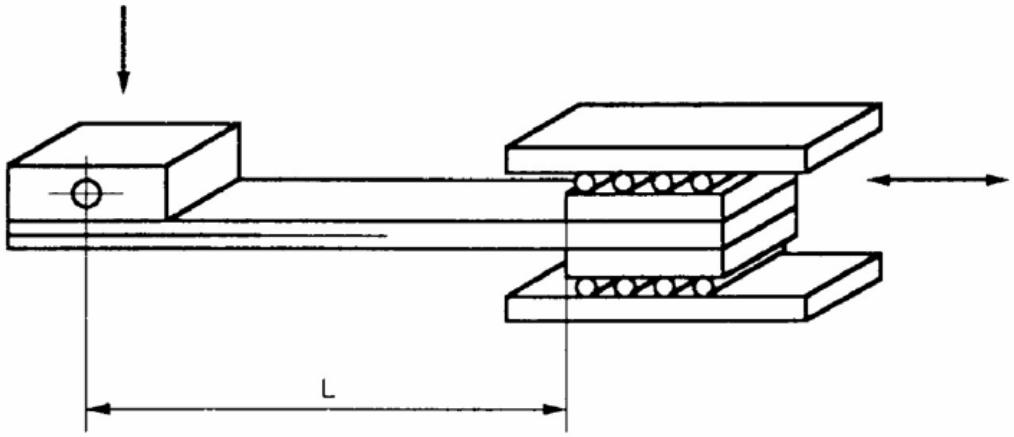

Figure 21: End loaded test set-up [50]

Mixed mode I/II

A widely used test in determining the fracture toughness of mixed mode (I+II) is called MMB and DMMB (Double) Mixed Mode Bending, which is included as a standard test method [49, 58]. This test combines the double cantilever beam (DCB) test loading mode I and the end-notch flexure test loading mode II (Figure 22).

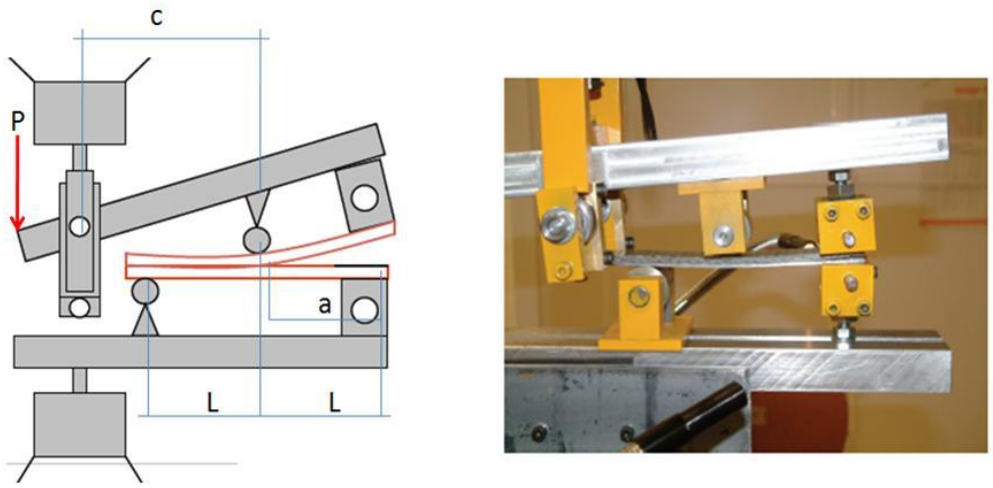

Figure 22: DMMB test for obtaining fracture toughness under mode I and II.

Delamination initiation and growth measurement under mode I fatigue

In the last few years different authors have carried out delamination evolution measurements using techniques that were not used before for this purpose. The most

common way of analysing crack propagation is by visual definition of crack front or measuring the compliance changes during the fatigue tests.

The better understanding of the initiation mechanism can lead to an improvement in the material and, as a result, increased strength against crack initiation. Davijani [59] studied the initiation of delamination using Acoustic emission (AE) techniques [60, 61]. The source of AE events depends on the material and energy release phenomena that are taking place at the particular moment. The materials analysed for interlaminar fracture toughness behaviour measurement are 0º/0º and woven/woven (with different patterns). The test carried out was a Double Cantilever Beam (DCB), one sensor is near the pre-delaminated area and the other at a more distant location (50mm further away). He considered the sentry function, which is the logarithmic ratio between the strain energy and the acoustic energy. Stutz [62] used an embedded optical fibre in the delaminated surface to quantify the fibre bridging contribution to the delamination fracture toughness during static and fatigue double cantilever beam test (DCB) [63]. The embedded optical fibre measures strain distribution in the delamination front tip and along the surface, which is used to calculate the energy release rate (ERR). The fibre bridging effect observed in tests is included in a cohesive element model by a traction-separation law. The model shows two different parts when the propagation has ocurred at the interface: the first part with the fracture of the polymer matrix that corresponds to the initial ERR, and a second part related to the fibre bridging effect following the maximum stress of the bridging tractions. Long Fiber Bragg Grating (FBG) are suitable tools for detecting the crack tip position in composite samples under Mixed Mode Bending [64]

2.4 DELAMINATION IN WOVEN MATERIAL

The failure mode of delamination in composites creates a loss of stiffness and strength that leads to an accelerated degradation of the material. In laminated materials, the application of repeated cyclic stresses (fatigue loading) can drastically decrease the capability of carrying load forces.

The relationship between the textile structure of the layers in a laminate and fracture toughness has been studied by many authors. Briscoe [65] for example analysed the influence of fabric weave and fabric surface texture for mode I interlaminar toughness

in aramid/epoxy laminates. The results of tests carried out by Briscoe showed higher fracture toughness for coarse fabric than for fine fabrics. He pointed out that the fracture performance can be linked to local fibre-resin distribution at the interface. The delamination damage behaviour of woven laminates is affected by matrix-rich areas and the migration of fibres to resin zones. The lack of matrix rich areas at fracture surfaces reduces matrix contribution to composite toughness. On the other hand, an increase in fibre migration to resin-rich areas increases the toughness as fibre bridging formation takes place. Alif [66] also found that fibre bridging was happening in fracture surfaces of twill and satin weave, but he did not come across this effect in plain weave structures. Alif analysed the interaction between weave pattern structure and fracture behaviour in plain, twill, 8H-satin and 5H-satin carbon/epoxy composite. For transversely oriented yarns (from the delamination front), higher fracture resistance was observed, while resistance in longitudinally oriented yarns was lower. Fracture surfaces of debonded fibres were observed by Optical and SEM micrographs, where differences between crack propagation direction and surface structures were distinguished.

The manufacturing process can also be a source of variability in the delamination behaviour of a woven laminate. Hunston [40] analysed the fracture toughness of two identical materials but manufactured in different places; one by Hexel and the other by NASA. Data obtained showed that Nasa samples were 40%-100% tougher than Hexcel samples. The geometry evaluation could demonstrate that in NASA material the fibre nesting between advanced layers was much higher than in Hexel material.

Kim [67] linked delamination failure mechanisms taking place in woven materials to angle-ply prepeg tapes. He pointed out that propagation fracture toughness for 0º/0º interface in an angle-ply laminate is much lower than for 0º/90º interfaces or woven-fabric laminates. In the fabric material, the delamination crack interacts with matrix-rich areas and the woven structure increasing fracture resistance. The delaminated wavy surfaces for woven structures were analysed using Scanning Acoustic Microscopy (SAM) (Figure 23). In a similar way, Gill [68] also saw that the toughness was higher when there were more 90º oriented tows in the direction of the propagation in 5HS woven structures, due to the 0º/90º interfaces created on the surface. He found that the fibre volume fraction variation had an effect on mode I delamination behaviour in 5HS woven materials, as the fibre content increased, the mode I toughness increased.

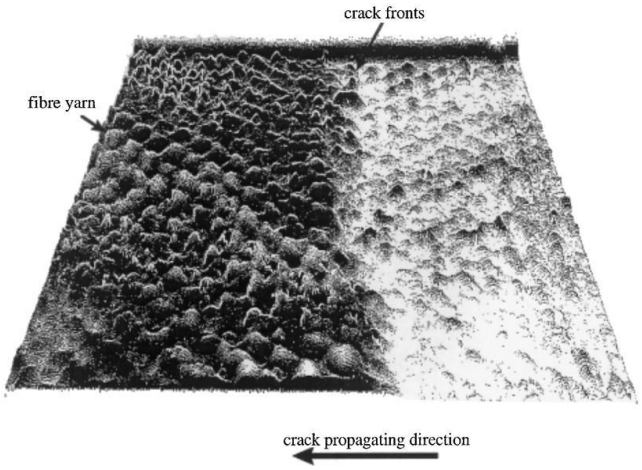

Figure 23: 3D perspective for a delaminated plane [Kim00]

Some authors realised that a wavy surface is obtained in the fractured surface in textile laminates [56, 67, 69]. Shindo [56, 57] pointed to the heterogeneity of the woven materials as the reason why a non smooth delamination surface is obtained with a 4-5 times higher toughness value than for a smooth delamination surface. The resin-rich regions between the fabric increase this value. Espinosa [69] used cohesive elements to analyse an impact-induced delamination in woven materials, taking into account the heterogeneity of the material leading to wave dispersion. The heterogeneity of the composite materials leads to dispersion and scattering of stress waves during impact, which is why he modelled interfaces with flat and different types of waviness. Fracture interfaces are modelled flat and wavy to simulate differences between surface structures. The interface waviness introduces a degree of coupling of mode I and mode II failure during delamination.

The effect of wavy fracture surfaces has been studied numerically mainly using cohesive elements. Zavattieri [70, 71], for example, simulated a sinusoidal interface morphology by cohesive elements. He pointed out that crack propagation along interfaces is affected by the roughness profile of the interface topography, as previous works also showed [72]. Applying a remote mode I loading to sixteen different surface interfaces, crack initiation and propagation were compared. His research focused on the idea that the manipulation of the surface roughness in a material (by hot rolling, grit blasting, etc) increases interface toughness (the topography of the surfaces affected the value). The surfaces created are patterned sinusoidal interface morphology. To evaluate the effects of the sinusoidal morphology on the macroscopic fracture toughness at the interface, the behaviour of the crack is observed when a remote mode I loading is

applied. The models of the materials used are elasto–plastic or perfectly elastic materials. Crack propagation is modelled as a cohesive traction separation law in ABAQUS/Standard. Previous works also studied the mixed mode effects due to the sinusoidal interfacial delamination curvature [72]. Gao et al. [73] also used cohesive elements to study the crack propagation under mode I with sinusoidal waviness between two semi-infinite models. They concluded that the waviness had a positive effect on the surface toughening value.

In a recent piece of work Li [74] investigated the effects of hierarchical wavy morphology of a delaminated surface on the interfacial fracture toughness under mode I and mode II using a cohesive zone model (ABAQUS). The proposed wavy morphologies displayed a better interfacial fracture toughness than an interface with a flat surface. He modelled the surface with a sinusoidal shape, and this surface is also modelled with a smaller scale sinusoidal wavy shape (Figure 24). Interfacial friction also plays an important role in mode II fracture toughness, increasing mode II fracture toughness for the same sinusoidal interfacial delamination. Li pointed out that the quantitative relation between delaminated surface geometry and fracture toughness had not been investigated.

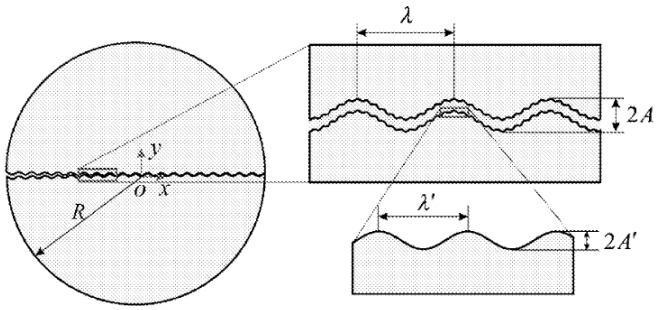

Figure 24: Double sinusoidal fracture surface defined by Li.

Although most of the authors used cohesive elements for modelling the delamination surface, some researchers found other alternatives. Benzerga for instance [75] did not use cohesive elements for modelling the fracture surface, he specified the interface by means of 1D elements (springs) covering the whole surface. Benzerga developed a model based on a mixed-mode failure criterion using an elastic and damageable surface for analysing the delamination growth in woven composite laminates. Those elements follow a non-linear force deformation rule that can support a damage variable when the maximum stress criterion is exceeded.

Most recent works introduce new variables into the fracture toughness behaviour in woven laminates, such as environmental conditions. Shindo [56] described the correlation between energy releases and temperature effect (cryogenic temperatures) under mode II delamination fatigue loading for woven glass fibre-reinforced polymer composites. The experimental set-up used was a four-point bend end-notched flexure (4ENF). The results showed that the delamination rate is lower at lower temperatures and that in static and fatigue the delamination growth is governed by the same mechanism. The fracture surfaces analysed had a wavy route due to the woven fabric architecture. In order to correlate the experimental data with a numerical model, a Virtual Crack closure technique (VCCT) was used for determining energy release rate. In a later piece of work Shindo [57] investigated the mixed-mode I/II delamination fatigue loading for woven glass fibre-reinforced polymer composites at different temperatures, and the experimental set-up used in this case was a mixed-mode bending test (MMB). The solution obtained for mode II is similar to the solution obtained for mixed mode; the cryogenic temperatures increases fracture toughness between layers.

2.5 CONCLUSIONS

In this chapter a literature review has been done. The subjects related to the thesis proposal are analysed: composite material classification, textile-reinforced composites, woven structures´ internal geometry and delamination mechanisms. Finally the works dealing with the delamination in woven structures are described.

3. CHAPTER 3: THESIS PROPOSAL

3.1 CRITICAL ANALYSIS OF THE LITERATURE

Delamination between textile layers is a common damage mechanism that tends to occur in woven laminate structures, where the layers are bonded without any reinforcement in the out of plane direction. Most of the authors have analysed the delamination behaviour experimentally, trying to link the textile geometry with the fracture toughness value. In woven structures the nesting value has been shown to exert a great effect on fracture toughness value and on the fracture surface geometry, but nobody has evaluated this phenomenon in depth. As current textile laminate manufacturing processes do not monitor the shifting between layers, the nesting values in the laminates are unknown. The variability of the nesting introduces an uncertainty into the fracture toughness behaviour of the material and this aspect has not been studied in the literature.

The fracture surface in woven laminates has a wavy geometry, which can be different depending on the textile's geometry structure. Some pieces of work simulate wavy fracture morphologies numerically using cohesive elements, and orient the delamination phenomena to the fracture geometries obtained by surface treatment techniques. However nobody has introduced geometrical characteristics of woven laminates, such

as nesting or woven size, into numerical simulations of the fracture surface. And it is further observed that experimental investigation of the fatigue delamination behaviour is less developed than the static delamination behaviour.

These are the reasons why 2D woven laminate structures are studied in greater detail in this thesis proposal due to the need to understand the delamination failure that affects their overall mechanical behaviour. As a short conclusion of the textile types described in this chapter, 2D woven composites offer less design flexibility than knitted or braided structures. The properties in the warp (0º) and weft (90º) directions due to better fibre alignment and higher fibre volume fractions provide 2D woven structures with superior mechanical properties. However, as mentioned previously, the difficulty to overcome is the low delamination resistance because of poor through-thickness properties when the 2D woven structure is stacked in a laminate.

The experimental relationship between nesting in woven laminates and static fracture toughness has been slightly studied by some authors, showing tougher values as the nesting increases. In contrast, the fatigue delamination behaviour linked with the nesting in woven structures has not yet been studied. For static fracture toughness measurements there are more standardised procedures than for fatigue fracture toughness measurements. Each author tries to overcome the difficulties of measuring fatigue delamination by applying the set up, loading conditions and techniques most suitable for the purposes in each case.

The main contribution of this work is the analysis of the effect of nesting value in static and dynamic toughness for a carbon-reinforced woven material using the same structure with different tow size. Nesting and the structure's scale factor (related to the tow size) is related with interlaminar fracture surface waviness. The wavy surface geometry linked to the interlaminar fracture toughness for woven materials. The variability of nesting values introduced by current manufacturing processes is measured in order to evaluate the real fracture toughness dispersion in real woven textile laminates.

The final aim of this thesis proposal is the introduction of a new design parameter, the nesting, into the design and manufacturing process. With the introduction of the nesting value as a new design criteria and a new modelling parameter, the following advantages can be obtained: in areas which are sensitive to damage, the most suitable nesting value

can be selected by increasing fracture toughness values and directly avoiding catastrophic damage. As a result, the reliability of the components improves.

3.2 THESIS PHASES

The phases of the thesis can be divided into four stages:

i. ***Preliminary work***: Geometry and mechanical property variability measurements in two woven structures. The controlled input parameters are the unit cell size of the woven twill structure: 3K and 12K.

ii. ***Internal geometry variability***: internal properties are measured and the results are linked to the tensile mechanical properties.

iii. ***Static fracture toughness measurement taking into account the nesting effect***: Experimental characterisation of quasi-static fracture toughness for woven laminates with different conditions of nesting are carried out. A specific manufacturing concept has been set up for accurate production of samples.

   → Manufacturing the material with different fracture surface geometries.

   → Static fracture toughness measurements in Mode I.

   → Static fracture toughness measurements in Mode II.

iv. ***Dynamic fracture toughness***: Experimental characterisation of mode I fatigue fracture toughness for woven laminates with different nesting values (onset and growth).

3.3 PRELIMINARY WORK: Size effect on the internal geometry and mechanical property variability of woven composites

This preliminary work tries to understand the effect that introduces the size effect in textile materials. The analytical and numerical models presented in the literature deal with textile materials in a similar way even when the size is completely different. The materials used in this research only differ in the unit cell size, having all other properties in both materials as close as possible. The most difficult issue at this point is to really

compare only the size effect, having in all other parameters and tests conditions similar requisites and properties. The questions that are answered in this preliminary work are:

- Does unit cell size affect the tensile mechanical properties and internal damage?
- How different is the internal structure of the same textile woven composite with a different unit cell size?

The assumption that the unit cell size of woven materials can lead to differences in the internal geometry and properties is analysed next. This first stage also helped to learn about the manufacturing process, tensile/fatigue tests and damage inspection techniques in composite materials. Figure 25 shows the steps that will be explained in this chapter.

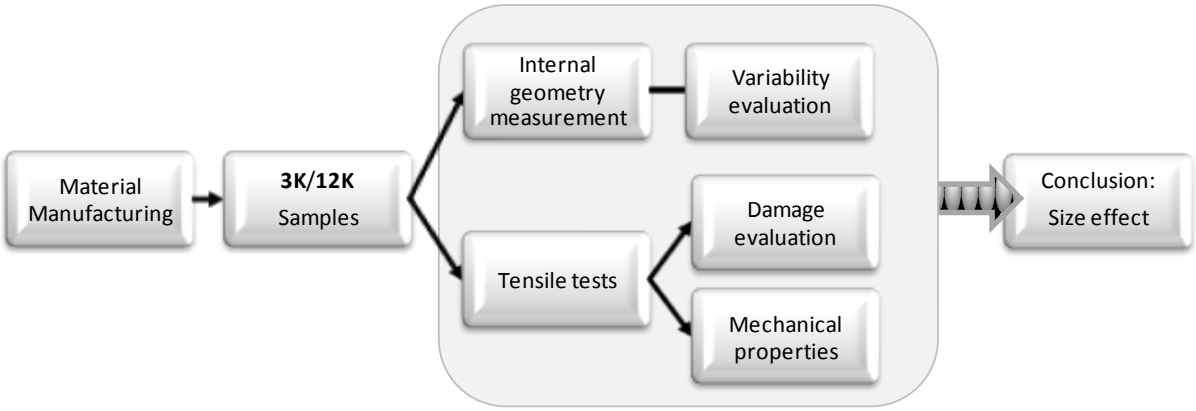

Figure 25: Scope of this chapter

3.3.1 Materials and experimental methodology

The material used is made using HexPly® M10.1 prepregs [76] with T700S carbon fibers. Prepreg material, which is stored in a freezer at -17ºC, is cut with 300x300mm measure. The layers are stacked without taking into account the shifting between the textile geometry: a random nesting structure is applied to the material. The conditions defined in the autoclave for the curing process are 5 bar of pressure, at 120°C for 1 hour. The complete cycle lasts 2 hours, half an hour to reach the required temperature, one hour at 120°C and half an hour for cooling. The selected textile composites are manufactured using the same resin, the same fibres and the same twill 2/2 woven architecture, but having different yarn size (Figure 26). One fabric has 3000 filaments per yarn (3K) and the other 12000 filaments per yarn (12K). The linear dimension of the repetitive unit cell for 12K material is more than two times larger than the repetitive unit cell for 3K. The reason why two structures are chosen is that we want to analyse the scale effect on the variability of the geometrical properties of the measured inner

structure. 3K material has 13 layers and 12K material 9 layers. The approximate thickness value from the specifications of the supplier is 3mm. The fibre volume fraction is measured using a burn-out test. The fibre content is calculated measuring the weight of the samples just before and after removing the matrix using sulphuric acid (Figure 27).

The specimens for cross sectional observations are cut out of the composite plate using a diamond saw with the 0º cut plane orientation (warp direction). The samples are polished using sandpaper with roughnesses from 320 to 4000 in the automatic polishing machine (TF250). The prepared cross sections are observed under an optical camera (Microscopio Leica). The images are post-processed and analysed using the image manager software of the microscope and in-house developed programs.

In most cases the number of measurements of the internal geometry parameters (yarn cross section dimensions etc) carried out for 12K material is lower than for 3K material. The main reason is the unit cell geometry scale difference between both structures; the number of unit cells suitable for measuring is more than two times lower at the same specimen dimension for 12K than for 3K.

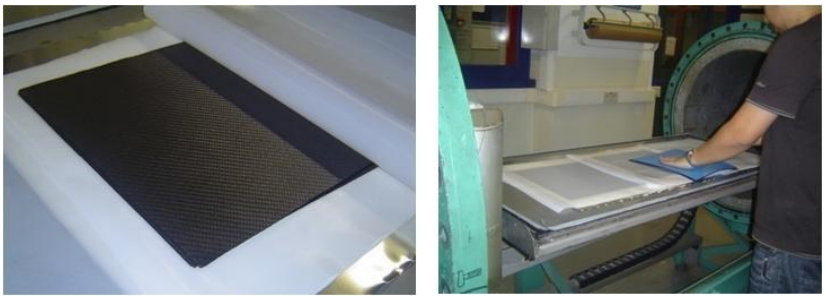

Figure 26: Manufacturing process in the autoclave in KU Leuven facilities

Figure 27: Sample with the acid for at least 20 minutes on the sand oven for removing the matrix

3.3.2 Mechanical properties: Tensile tests

Tensile tests are done using a standard INSTRON machine (INSTRON 4505) at 1mm/min test speed. The dimensions of the specimens are 25 mm width, 135 mm gauge length and 2.6 mm thickness. Strain measurement is done by strain mapping, which is based on a digital image correlation technique (LIMESS). Due to the high variability in the mechanical properties that may appear on composite materials, 9 samples are tested for 12K structure and 14 samples for 3K (the number of samples is different just because of the availability of the material was different at this moment). During loading, acoustic emission sensors are mounted on the sample´s surface (Figure 29). The acoustic events are recorded for each test and afterwards damage evolution is evaluated from the data obtained. The set-up required for the test is defined in Figure 28. Figure 30 shows stress versus strain curves for both materials plotted together and experimental results are summarised in Table 1.

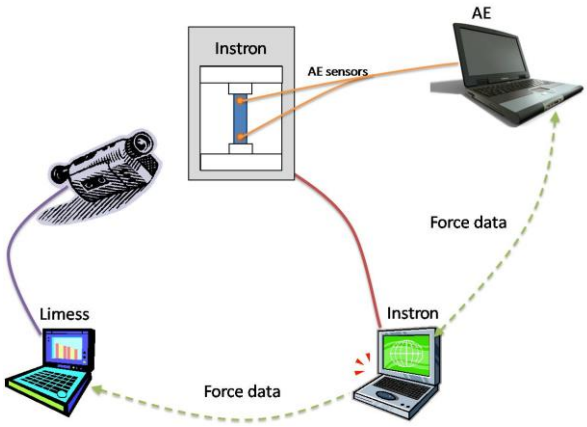

Figure 28 : Image correlation technique and AE data recording set up during tensile test

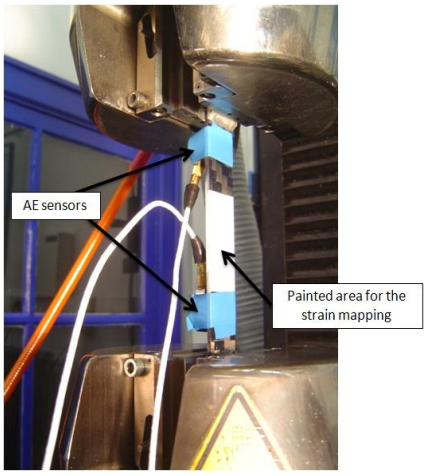

Figure 29: AE sensors on the samples

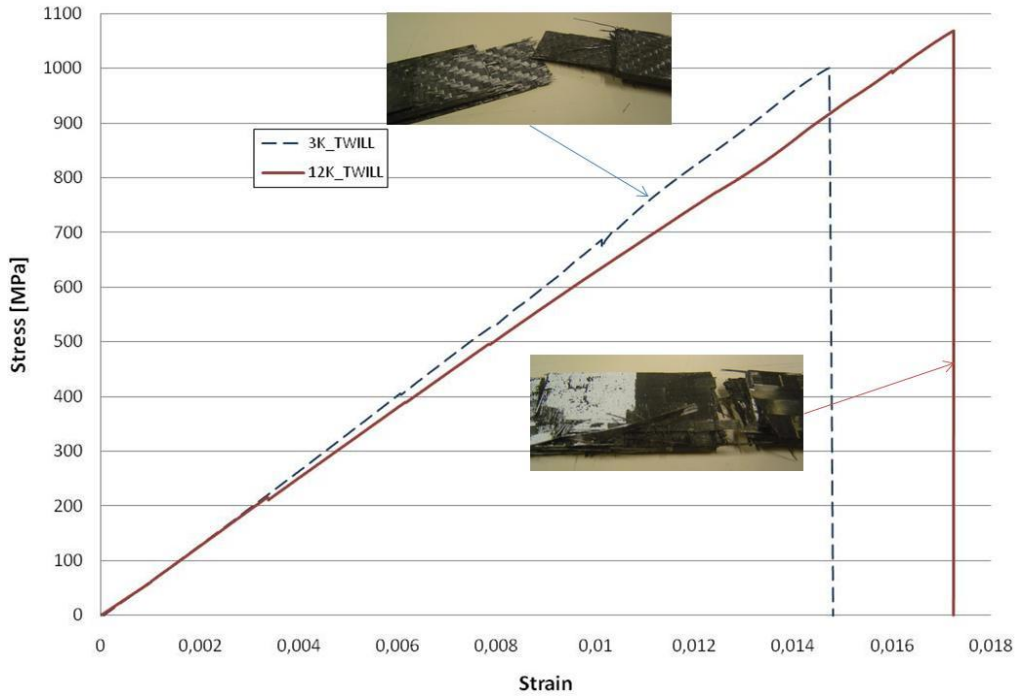

Figure 30: Stress versus strain curves for 3K and 12K.

Table 1: properties obtained in the tensile test (values normalized to 55% fibre volume fraction)

	3K	12K
	Experimental	**Experimental**
Initial modulus (0-0,1%) [Gpa]	68,49 ± 2,9	61,54 ± 1,84
Modulus (0,1%-0,3%) [Gpa]	69,94 ± 2,6	65,3 ± 2,6
Modulus (0,3%-1%) [Gpa]	70,9 ± 3	66,27 ± 2,06
Strength [MPa]	959,87 ± 42	1131,93 ± 22,05
Strain [%]	1,45 ± 0,057	1,8 ± 0,076
Supplier´s data (HEXCEL) Elastic modulus [GPa]	71	65
Supplier´s data (HEXCEL) Strength [MPa]	900	1220

The dispersion of the elastic modulus results are below 5%. The variability is related to the sample geometry variability (previous chapter) and other effects are related to the testing of the samples. During the test, as the strain is applied to the samples, the elastic modulus increases by 3% for 3K and 7% for 12K. This effect is due to the crimping of the textile, the inherent stiffening of the carbon and the misalignment of the samples that tried to straight the yarns.

In Figure 31 punctual elastic modulus is plotted against during the tensile test. Each plotted point represents the value of the elastic modulus at the applied strain value. The tendency of the elastic modulus is the increasing during the loading at the beginning, and decreasing after reaching a maximum value.

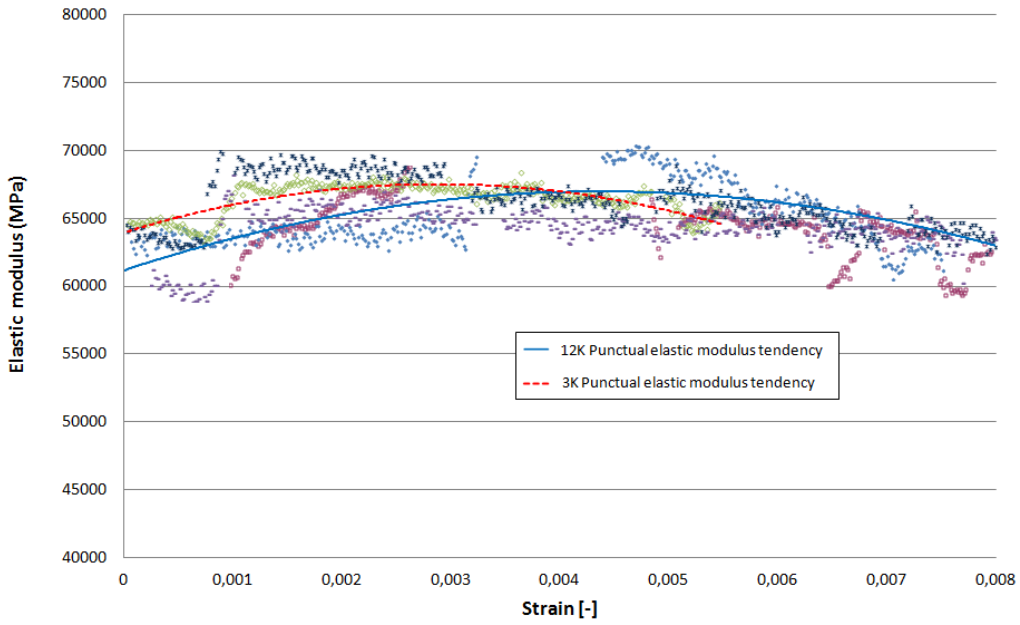

Figure 31: Punctual elastic modulus during tensile test

3.3.3 Acoustic events measurement

During the tensile tests AE sensors are mounted on the sample to register the acoustic events density and energy levels at each strain value applied on it. The purpose of this analysis is making a correlation between the energy changes and damage mechanism working inside the composite material. Two AE sensors are situated at the boundaries of the gauge length region (Figure 29). Signals that occur outside of the sensors are filtered out by the system. The energy of AE events is registered and the dependency of cumulative energy of AE events versus tensile strain is plotted (Figure 32). After the acoustic threshold (35 dB) strain, low energy events start to occur with low frequency. During the loading of the sample, the density and energy lease of these events start increasing until the sensors are removed from the sample.

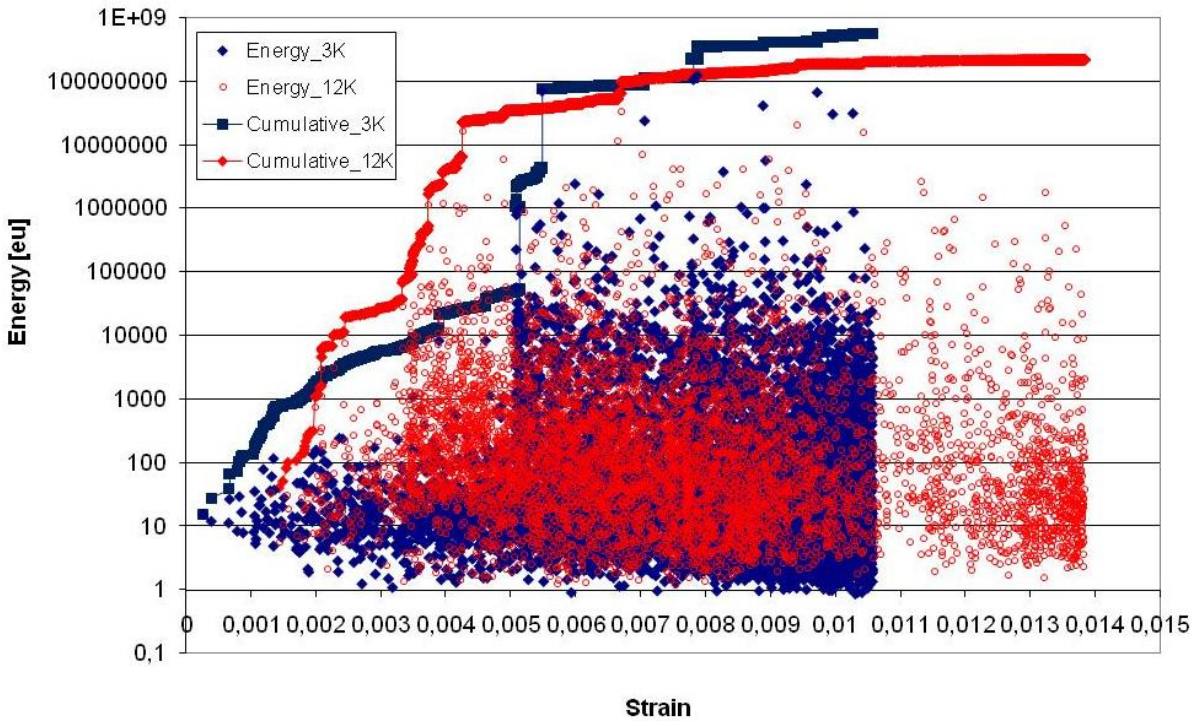

Figure 32: AE measurements for 12K and 3K materials

Both materials show a similar first event strain value around 0,18%, but the increase of the energy is different in each one: for 12K material, the acoustic energy accumulation increases faster than for 3K material due to higher energy level events at low strains (Table 2). It seems that the damage creation inside 12K material creates more sudden and abrupt changes than in 3K. The first transition strain happens at a higher strain value for 3K than for 12K, showing a delay of the damage mechanism from 0,32% to 0,47%.

Table 2: Strain transitions defined by the acoustic events

	3K Experimental	**12K Experimental**
First transition strain ε_1	0,22 ± 0,04	0,18 ± 0,005
Second transition strain ε_2	0,47 ± 0,05	0,32 ± 0,024

3.3.4 Damage inspection

For microscopy inspection some samples are removed from the tensile test at a certain percentage of the final strength value. The microscopic analysis allows for the visual observation of damage at different strain levels and at different locations (inside the width of the specimen and near the edges, Figure 33). For 12K (Figure 34), intra-yarn,

inter laminar and matrix cracks in resin rich areas are observed at 0,844% strain value. For 3K material the amount of cracks is less at similar strain levels. Although acoustic measurements show that there are damage events inside 3K material, the cracks do not propagate as easy as in the 12K material, and cannot be visually seen.

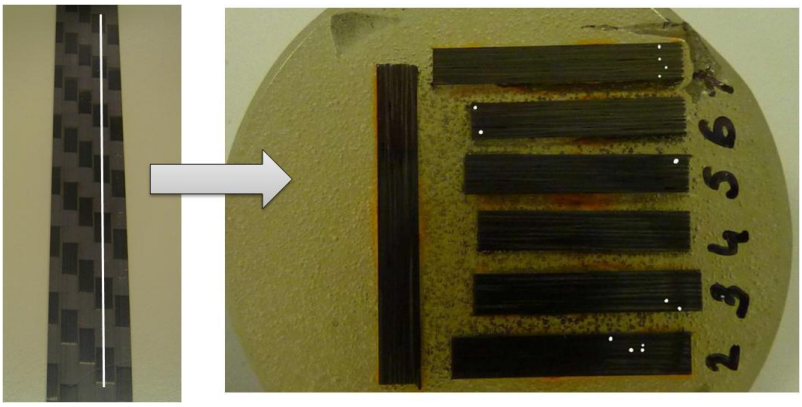

Figure 33: The line on the sample represents the position of the inspected area and the white points on the right the position of the damage

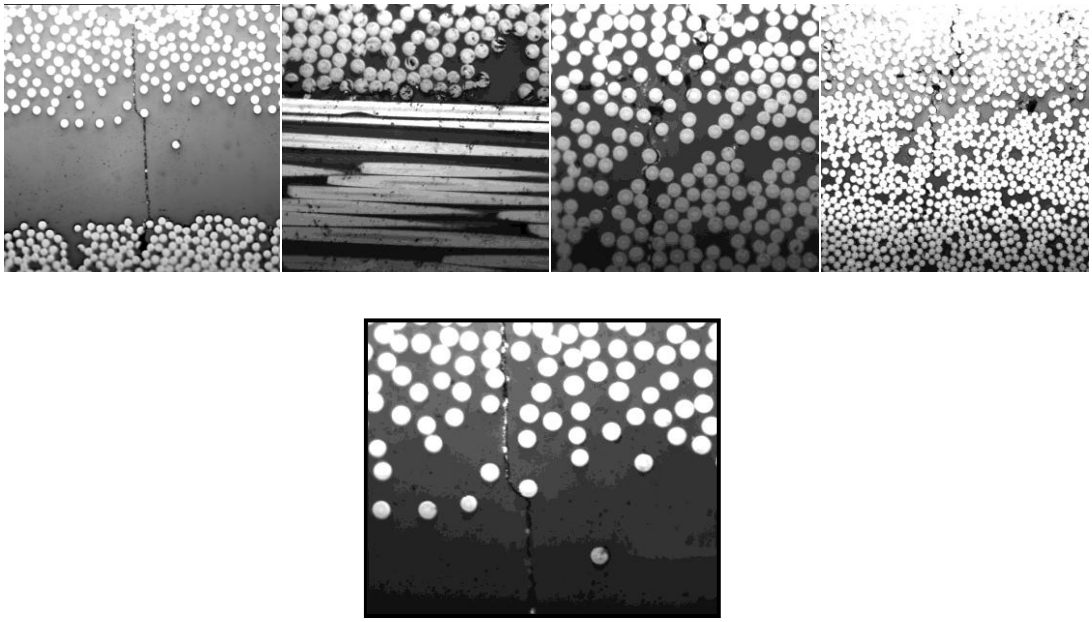

Figure 34: Microscopy for 12K specimens loaded 0,844%

For the X-radiography analysis, the loaded specimens are submerged in a penetrant bath for some hours and afterwards they are exposed to soft X-rays to obtain the radiographs. Only cracks which extend to the outer surface can be seen using this method. In Figure 35 and Figure 36 some cracks can be seen for 0,844 % and 1,14 % strains in 12K material (from the front and lateral view of the samples). For lower strains it is not possible to see any crack. For 3K material we do not see any cracks at strains below

1%; that means that the amount of cracks developed until the surface is much lower than for 12K material.

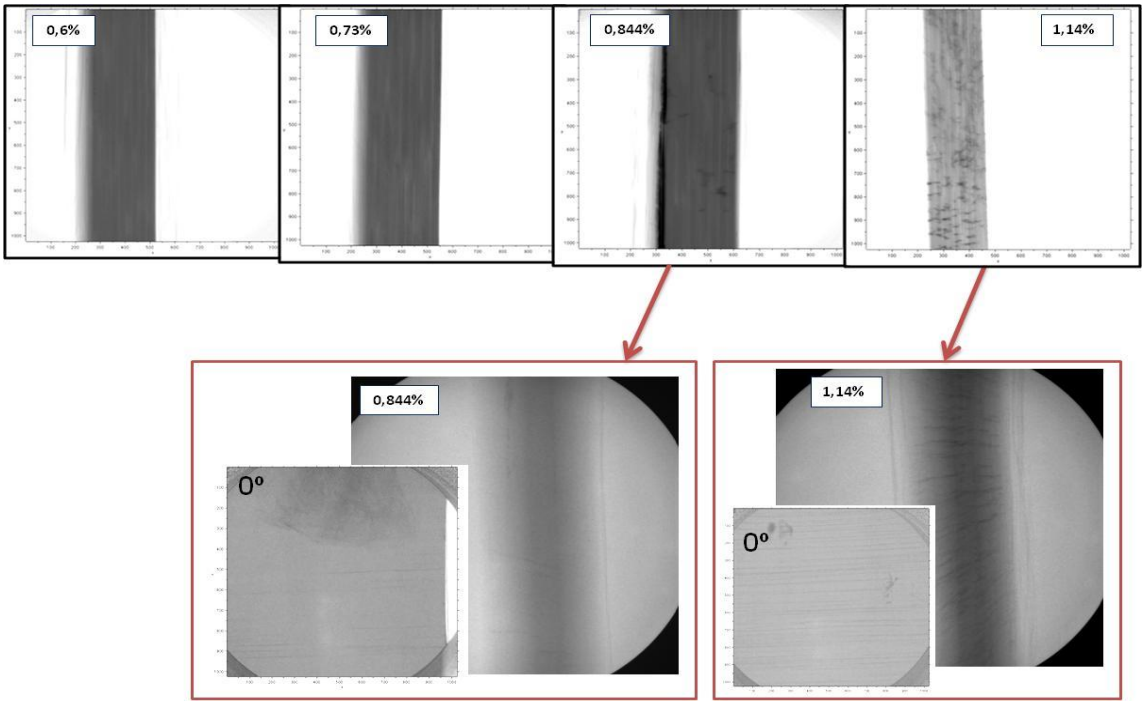

Figure 35: X-ray pictures for the 12K material at different load values.

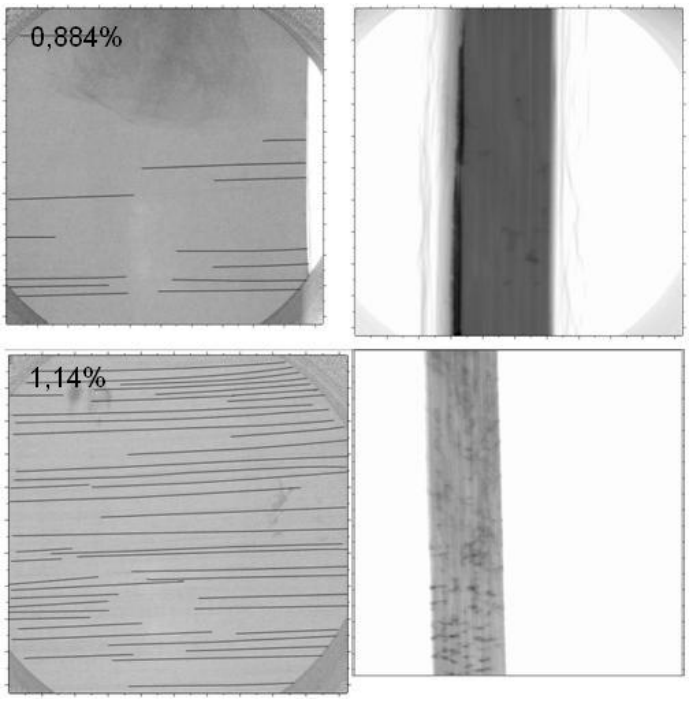

Figure 36: Highlighted cracks at high strain levels

3.3.5 Conclusions for preliminary work

Tensile tests on two different materials with random nesting (same architecture, but having a different tow size) are carried out using AE sensors and strain mapping. For damage analysis after the specimen loading at different strain levels, microscopy and X-radiography are used. From the AE measurements we conclude that 3K material delays the first strain transition and that damage creation inside 12K material creates more sudden and abrupt changes. Using microscopy we can see that 12K material has more cracks than 3K material at the same load levels. The radiography results also show more damage for 12K material. In short, the behaviour of the material is not only related to the architecture of the composite material, the tow size exerts a significant influence on the mechanical properties.

4. CHAPTER 4: INTERNAL GEOMETRY VARIABILITY OF TWO WOVEN COMPOSITES AND RELATED VARIABILITY OF THE STIFFNESS

4.1 INTRODUCTION

The main objective of the research presented in this chapter is to analyze the variability of the internal geometry of two woven structures and to evaluate how this scatter affects the macroscopic mechanical properties. First the measurements of geometrical parameters are analyzed by means of optical microscopy. The evaluation of how different an ideal geometrical model of a textile woven unit cell can be from the real inner structure is described. The dispersion of measured geometrical parameters is introduced in a numerical multi-scale modeling approach to evaluate the macroscopic stiffness values. A sensitivity analysis is performed for each geometrical parameter and laminate stiffnesses are derived. These are linked to the experimentally obtained elastic properties by tensile tests. Finally the unit cell size scale effect for measured geometry variability and experimentally obtained elastic properties are evaluated.

4.2 MATERIALS AND EXPERIMENTAL METHODOLOGY

The material used in this research is made using HexPly® M10.1 prepregs [76] with T700S carbon fibers, curing them in an autoclave based on the conditions defined by the

supplier: pressure 5 bar at 120°C for 1 hour (the same material defined previously in section 3.3.1). The unit cell sizes for 3K and 12K twill structures are defined in Figure 37 and the properties of the reinforcements are summarized in Table 3.

Table 3 : Properties of the reinforcements

	Areal density*	Filaments per yarn*	Unit cell	Fibre volume fraction**
3K	200 g/m^2	3000	~ 8x8 mm	53 ± 0.08%
12K	285 g/m^2	12000	~ 22x22 mm	55 ± 0.17 %

* specifications of the supplier

** measured by burn-out test

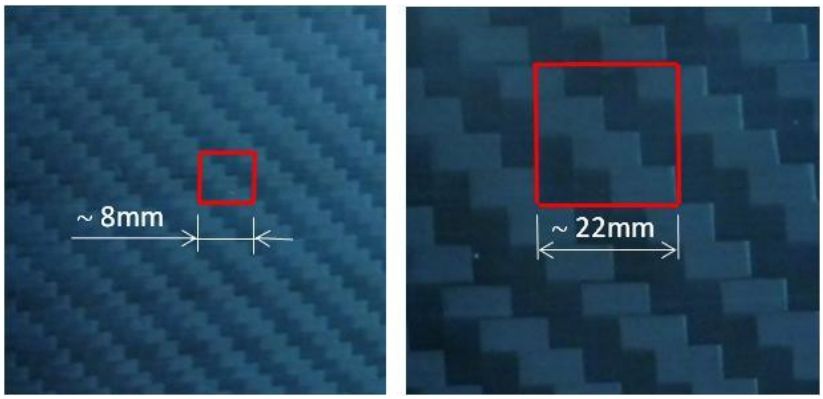

Figure 37: Surface scans of the prepregs: left 3K, right 12K. The square designates a unit cell of twill 2/2 weave

The specimens for cross section observations are cut out of the composite plate using a diamond saw with the 0º cut plane orientation (warp direction). The samples are polished using sandpapers with roughnesses from 320 to 4000 in the automatic polishing machine (TF250). The prepared cross sections are observed under an optical camera (Microscopio Leica). The images are post-processed and analyzed using image manager software of the microscope and in-house developed programs. In most cases the number of measurements of the internal geometry parameters (yarn cross section dimensions etc) carried out for 12K material is lower than for 3K material. The main reason is the unit cell geometry scale difference between both structures; the number of unit cells suitable for measuring is more than two times lower at the same specimen dimension for 12K than for 3K.

4.3 GEOMETRY VARIABILITY MEASUREMENT

The parameters measured in two textile structures are specimen thickness, yarn cross section shape and dimensions, fiber volume fraction, crimp, nesting value,

misalignment of the samples and spacing between yarns. Warp direction is the loading direction during tensile test and the perpendicular direction is the nominal weft direction. Tensile tests are aligned respect to the warp direction of the outer and visible textile layer in the composite material. Cross section of the yarns and fiber volume fraction parameters are measured for the weft yarns, while crimp, misalignment and spacing between yarns are measured for yarns in warp direction. As the structure of the fabric is symmetric, we assume that the geometry variability is the same in both directions. For assuring this assumption the comparison between ends/picks in weft and warp directions is done, showing differences close to 1%. All data measured are summarized in Table 4, presented at the end of this section.

Table 4 : Measured parameters of the internal geometry variabilities for 12K and 3K

	3K				**12K**			
	Value	***Std. dev.***	***Coefficient of variation [%]***	***Number of measurements***	***Value***	***Std. dev.***	***Coefficient of variation [%]***	***Number of measure-ments***
Spacing warp (mm)	1.99	0.04	2.4	40	5.47	0.07	1.3	40
Spacing weft (mm)	2.00	0.02	1.4	40	5.54	0.06	1.1	40
End/pics warp (1/cm)	5.01	0.12	2.5	40	1.82	0.02	1.3	40
End/pics weft (1/cm)	4.98	0.07	1.4	40	1.80	0.02	1.1	40
Crimp (%)	0.22	0.11	50.4	14	0.13	0.06	51.8	10
Yarn thickness (mm)	0.116	0.01	11.2	72	0.177	0.03	17.5	22
Yarn width (mm)	2.07	0,11	5.3	72	5.65	0.38	6.7	22
Yarn area a) method (mm2)	0.188	0.02	11.7	72	0.8	0.1	12.5	22
Yarn Fibre volume fraction a) method	62	7.3	11.7	72	58.1	7.4	12.7	22
Yarn area b) method (mm2)	0.191	0.01	9.4	72	0.83	0.1	12,6	22
Yarn Fibre volume fraction b) method	60.8	5.9	9.7	72	56.3	7.2	12.7	22
Misalignment (º)	1.71	0.69	40.3	38	2.88	1.23	42	32
Nesting value	1.16	---	---	---	1.24	---	---	---

4.3.1 Thickness of the plates

The manufacturing process is the major source of variability of the thickness in the samples. In our samples the thickness for 12K is 2.55±0.2 mm and for 3K 2.6±0.22 mm (200 measurements per material in several samples); the autoclave process gives a standard deviation of about 0.2 mm to our woven material. Coleman [77] defined the

variance of ±7% to the thickness of graphite/epoxy woven fabric materials for autoclave curing manufacturing process. This value is close to the values obtained for the 12K (7.8%) and for 3K (8.4%). Karahan et al in [78] defined a deviation in the thickness of the composite material around 0.11 mm for a similar average thickness carbon/epoxy non-crimp 3D woven composite manufactured using VARTM under pressure; the lower variation can be explained by the more stable structure of the 3D woven reinforcement.

In any case the thickness variability measured for 12K and 3K materials manufactured in the autoclave seems high in comparison to other manufacturing processes. In order to evaluate the real thickness distribution on the plates manufactured in the autoclave the thickness is measured on the plates with a dial gauge every 30 mm (dimension of the plates: 300x300mm). Figure 38 shows a concave geometry for both materials with a thicker value in the middle and thinner values on the edges (differences from 800 to 900 μm). In the autoclave process the layers were positioned without using a frame, the lack of this element made possible the movement of the resin from the edges to the outside.

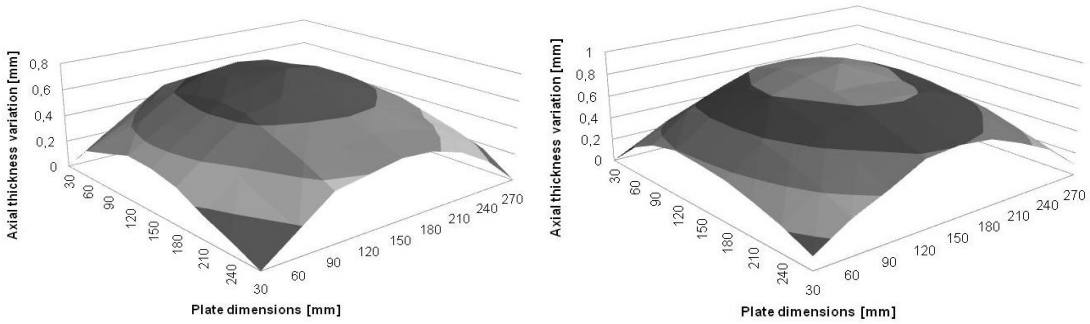

a) b)

Figure 38: Thickness variation on a) 3K and b) 12K plates

4.3.2 Yarn cross section area and fiber volume fraction inside the yarns

In most of the numerical models of woven structures cross sections of the yarns are modeled as symmetrical shapes (elliptical or lenticular), they remain constant along the fabric [79]. The more advanced recent models introduce more a complex shape description [80, 81]. The analysis of several yarns inside the two woven structures (12K and 3K) shows that they have not an elliptical cross section as expected in an ideal structure. Most of the yarn cross sections are not symmetric about their horizontal and vertical axes. The measurements take into account the wider and thicker dimensions of

obtained yarn´s envelopes (Figure 39, Figure 40). Yarn thickness for 12K is 0.177±0.031 mm and for 3K it is 0.116±0.013 mm. Yarn width for 12K is 5.65±0.38 mm and for 3K it is 2.07±0.11 mm (number of yarns measured: 72 yarns for 3K, and 22 yarns for 12K). The geometry variability between different yarns is quite high, the shape from one yarn to the other changes considerably. The same conclusion was found by Hivet [80] analyzing the geometry of carbon twill yarns using optical methods. The yarns in observation did not show lenticular shapes and depending on the situation of the yarn (in contact or not with other yarns) the cross section was different. Lomov [82] measured the variability of a woven glass/ PP (Twintex ®) material sample using optical microscopy of the cross-sections for the woven fabrics and the results showed lower scatter in yarn dimension than the ones measured in our material. For the woven glass/ PP material, deviation in yarn width in warp direction is 0.6%, and 2.6% in weft direction. For thickness values, the deviation is 4.9% in warp direction and 6.8% in weft direction. In our materials the yarn width deviation is 6.7%-5.3% and yarn thickness deviation 17.5%-11.2% (12K-3K). Although 12K and 3K show higher scatter in the measurements, the common tendency is for the thickness in all measurements to be more variable than the width. Saunders [83] found 13% of difference between the minimum and the maximum measured yarn width value and 22% for yarn height measurements in a plain weave glass fabric.

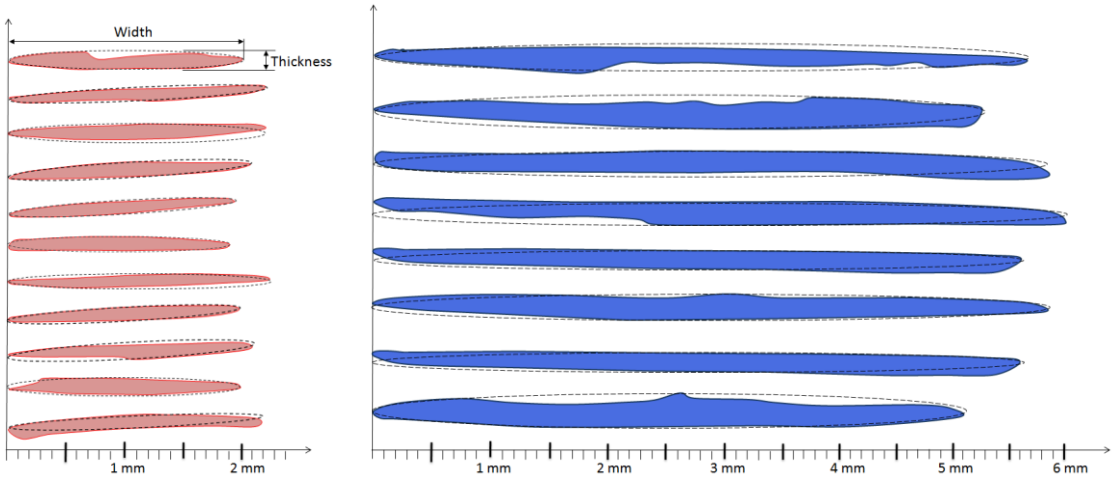

a) **b)**

Figure 39: Yarn geometry differences between the real and ideal elliptical areas, a) 3K b) 12K.

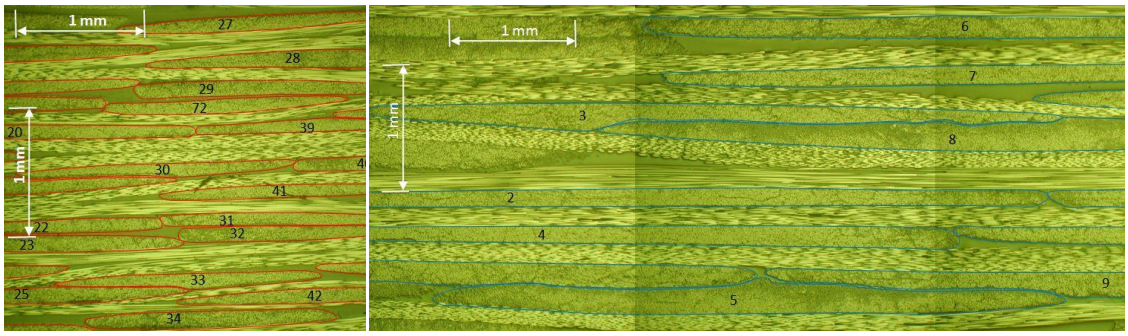

a) **b)**

Figure 40: Numbered yarns for the geometry measurements, a) 3K, b) 12K.

The volume fraction in the yarn is obtained by dividing the cross section of the fibers by the yarn area. The supplier gives 7 μm as the average value of the fibers and we assume this value is the average diameter. Multiplying the fiber area by the fiber number per yarn, the total area of fibers is calculated. The yarn cross section area *A* is obtained by two methods:

a) By applying the ellipse formula with yarn width and thickness values (Eq.6).

$$A_{elipse} = \frac{\pi \times width \times thickness}{4} \quad \text{Eq. 6}$$

b) By measuring yarn areas using *CoCreare ME10 (*2D CAD software system). Surface contour is reproduced point by point and area is evaluated by the software.

In both materials the ellipse-approximated yarn cross section area is bigger when the area is obtained using the *CoCreare ME10* 2D CAD software, which takes into account the real contour of the yarn. As the area is bigger, the fiber volume fraction is lower. Measured area for 3K is 0.191 mm^2 and the calculated elliptical area is 0.188 mm^2 (1.5% lower). Measured area for 12K is 0.83 mm^2 and calculated elliptical area is 0.8 mm^2 (3.75% lower). Desplentere [20] measured a variation of 15% for the yarn cross section value. In our material the variation is lower for the yarn area, 12.5-12.6% for 12K and 9.4-11.7% for 3K (a-b methods). The obtained yarn volume fractions are proportional to yarn areas, for 3K they are 62%-60.8% and for 12K 58.1%-56.3% (method a-method b).

The difference between the values obtained by an ellipse approximation and actual shape measurement is small compared with the coefficient of variation. This leads to a

conclusion, that for the similar materials the ellipse approximation can be cautiously used for estimation of fiber volume fraction inside the yarns.

Looking into the fiber distribution inside the yarns in detail, we can clearly observe important in-homogeneities in most of the yarn cross sections. Karahan [78] analyzed this scatter and found differences of between 58% and 74% in yarn volume fractions in a non-crimp 3D orthogonal woven fabric. In 3K and 12K materials the measured fiber volume fraction varies between 20% and 75% (Figure 41). Very low fiber density areas (20%-40%) are found near yarn boundary zones, which are more common in 12K than in 3K. Other authors as Summerscales [84] also found highly non-uniform fiber distribution within a yarn of a plain woven composite. Koissin [85] found fiber distribution reductions of 15% at yarn edges for tri-axial carbon-fiber braid material.

4.3.3 Average Waviness of the yarn centre line

Crimp (waviness) of the yarn is measured from the microscope images using *CoCreare ME10* 2D CAD software. The applied formula is:

$$crimp[\%] = \frac{L_f - L_0}{L_0} \qquad \text{Eq.7}$$

where L_f is the curved length of the yarn centre line, L_0 is the corresponding distance along the mid-plane of the fabric (Figure 42). These values must be obtained for several zones inside the microstructure to ensure that we obtain the global average value from the samples.

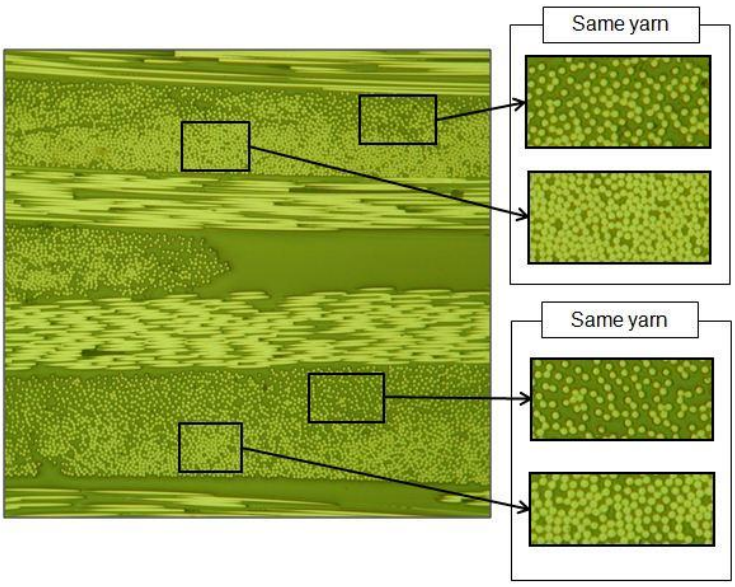

Figure 41: Uneven local fiber volume fraction inside yarn in 12K, variations of between 20% and 75%.

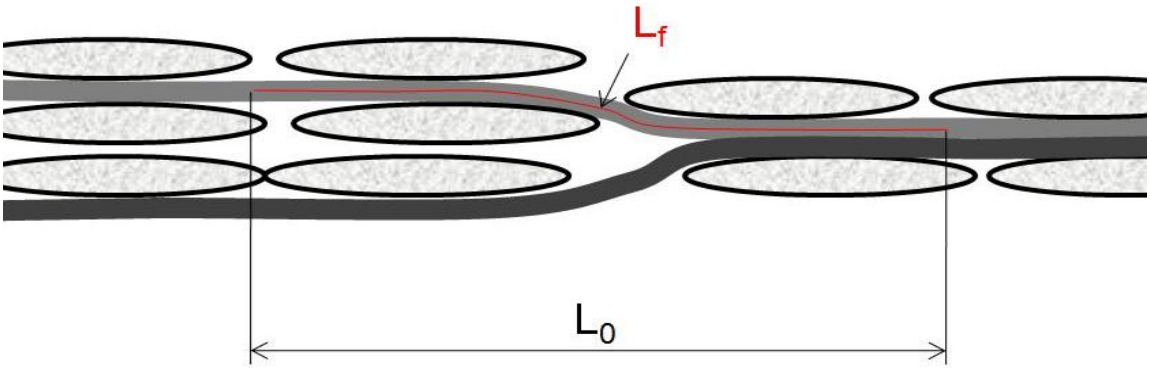

Figure 42: Crimp percentage is obtained by L_f and L_0 measurement.

For 12K, average crimp of the yarn is 0.13%±0.067% and for 3K it is 0.22±0.11%. The 3K woven structure shows higher crimp percentage than the 12K.

4.3.4 Orientation and Misalignment

The layer orientation is measured using microscopic images to evaluate the misalignment of the fiber bundles with respect to a reference direction along which the load is applied. Several authors have evaluated the fiber orientation measuring the geometry of fibers from the cross section of the specimens [86, 87]. The studies are divided into two areas: some dealing with continuous fibers and others dealing with short fibers. Mlekusch [88] described a methodology for measuring fiber orientation in short fiber reinforced thermoplastics. The method proposes to cut the samples using a section that forms an angle for about 30º to overcome the problems coming from angle orientation ambiguities (positive or negative angles from the expected average orientation). After polishing the cross sections, elliptical cross sections of the fibers are evaluated with an image analysis system. The average misalignments for continuous fibers have usually smaller angles than the fiber alignment in short fiber materials. Many times it is not possible to identify the direction in which angle deviations occur. For overcoming this problem Yurgatis [86] evaluated the samples sectioning the specimen such the average misalignment angle is 5º, in order to avoid the definition of the misalignment angle error between positive and negative angle values.

For the evaluation of the misalignment in the 3K and 12K specimens, the samples are cut in warp direction (load direction) and we analyze cross section of fibers in warp direction (Figure 43). When the textile composite material is well oriented, the cross

sections show a line along the longitudinal dimension of the sample. By contrast, when an elliptical cross section shape is observed, a misalignment angle (θ_m) can be calculated between the load applied direction and the orientation of warp yarns (Eq 8).

$$\theta_m = 90º - \text{acos}\left(\frac{fiber\ \ diameter}{cut\ \ fibre\ \ widt\,h}\right) \quad \text{Eq. 8}$$

When a 2D optical microscopy is used for the orientation measurement it is not possible to assure if the angle is positioned with a positive angle or with a negative angle respect to the cutting surface. The procedure proposed by Yurgatis [86], cutting the samples at 5 degrees instead of in the direction of the applied load, would overcome this problem without the need of applying any assumption.

At this point it is necessary to distinguish two types of misalignment variability: misalignment scatter between layers (MSBL) and sample misalignment (SM). The MSBL can find its way into the material during the manufacturing process. When the prepreg layers are cut for the lay-up preparation before the autoclave process, the positioning of the layers is carried out manually. At this step a direction misalignment is introduced between layers. During the autoclave process the pressure and temperature can change the orientation of the fibers in some places. For our material this effect is not very significant, because the epoxy has already been impregnated into the fibers and resin flow is not expected to take place inside the layers during curing process. The resin flow might have more effect in other manufacturing processes such as RTM. SM is a consequence of cutting samples from the manufactured plate with the only reference being the outer layer geometry. The samples to be tested are cut from the plate without any clear reference as to the best orientation. For our measurements it will be assumed that the cutting misalignment error (SM) is bigger than the lay-up misalignment error (MSBL) and all measured angles will be defined at the same side with the same positive sign for obtaining the mean value and the deviation (from these measurements it is not possible to identify the direction in which deviations occur).

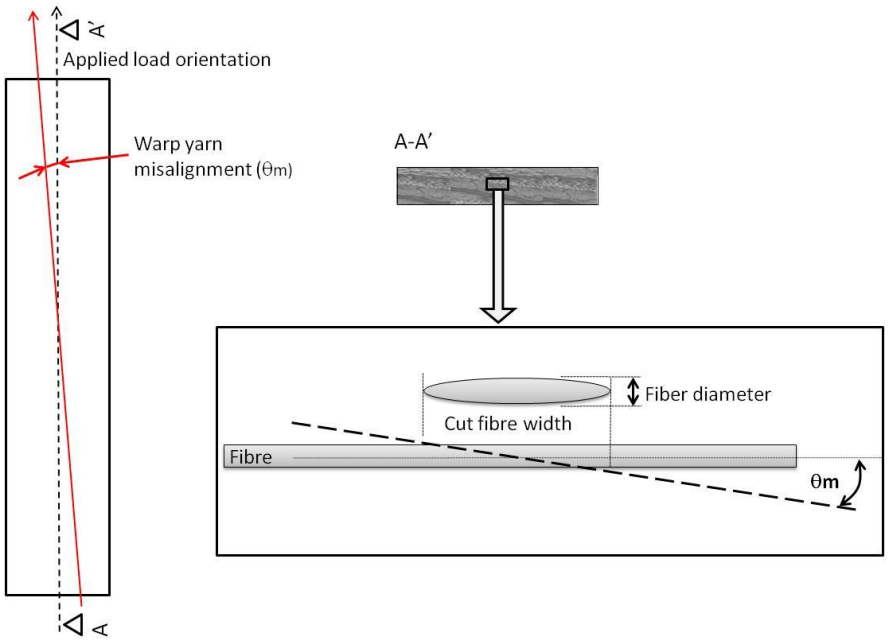

Figure 43: Misalignment of warp yarns to the load orientation.

For variability characterisation 38 cut fibers are measured for 3K and 32 fibers for 12K. The measured average misalignment is 2.88º±1.23 for 12K and 1.71º±0.69 for 3K material. The misalignment mean value may be mainly related to the cutting of the samples from the plates (SM). The deviation value may be related to the MSBL.

4.3.5 Warp and fill yarn spacing

The spacing of yarns in the woven structure is measured from the outer layer: the widths of 10 end/pics are measured and the yarn spacing is obtained by dividing the width by 10. Yarn spacing is 5.47±0.07 mm for 12K and 1.99±0.04 mm for 3K. Another way of showing the spacing is by means of the number of end/picks per cm: for 12K this is 1.82±0.02 end-pics/cm and for 3K 5.01±0.12 end-pics/cm. Desplentere [20] found a 5% variation coefficient for the spacing within a 3D textile. In a Woven Glass/PP (Twintex ®) Lomov [82] measured deviations of between 1.4% and 4.8%, depending on the direction (warp or weft). In our materials the variations are lower than in Desplentere´s data and similar to the data obtained by Lomov, 1.3% for 12K and 2.4% for 3K.

4.3.6 Nesting

Crimp, spacing and other geometrical property values can be affected by the nesting effect between advanced layers; the accommodation of yarns between each other can lead to a repositioning of the yarns in the other direction. Yarn thickness, yarn width

and spacing length between advanced yarns are also important for specifying the nesting effect in the woven structure (Figure 44). Lomov [9] specifies the nested position using a dimensional parameter, which is calculated from the minimum distance between centre planes of the layers. Lomov considers two identical layers, with one layer shifted relative to the other. When there is no nesting between layers, the nesting distance is equal to the layer thickness. The maximum nesting value is the one that gives the minimum thickness of the laminate. The formula used by Lomov for the calculation of the nested position defines the repetitive unit cells between advanced layers as equal, but the measurements made for the 3K and 12K show differences between the yarn and spacing dimensions. For this reason a new definition for the nesting percentage will be used in experimental measurements. The nominal thickness of the ply is assumed to be the double of the average thickness of the yarn. The nesting value (N_e) between two layers is obtained dividing the real thickness ($s_{R,i}$) of two layers by the nominal thickness (s_I) of both layers (Eq.9).

$$\boldsymbol{N_e} = \frac{\boldsymbol{2*s_I}}{(\boldsymbol{s_{R,1}+s_{R,1}})} \qquad \text{Eq. 9}$$

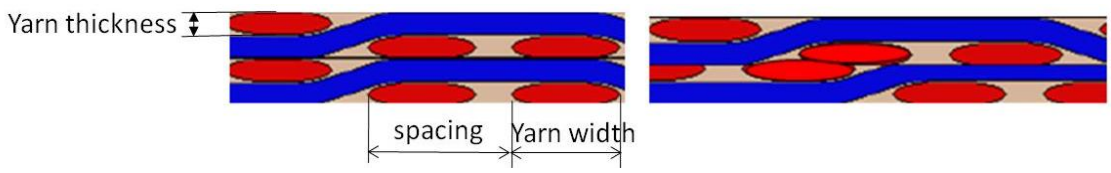

Figure 44: Non-nested woven laminate and a nested laminate.

The nominal thickness of a laminate can be obtained by multiplying the nominal layer thickness with the number of layers (n). The nesting percentage obtained ($N_{e,lam}$) is related to the whole laminate thickness (t) (Eq.5). As the nesting value is higher, there is more nesting effect on the laminate, but at lower values the nesting is lower (when the value is 1 there is no nesting).

$$\boldsymbol{N_{e,lam}} = \frac{\boldsymbol{n*s_I}}{\boldsymbol{t}} \qquad \text{Eq. 10}$$

The nominal thickness of the layer for 3K is 0.232 mm and 0.354mm for 12K (obtained from average thickness values of yarns measured). For 3K material the nesting value is 1.16 and for 12K 1.24. The nesting value is larger for 12K material than for 3K.

Distribution typesTable 5 **summarized the geometrical property variability using the standard deviation and consequently assuming that the data are normally distributed. In order to evaluate the distribution types of the internal geometry parameters, histograms are drawn and skewness and curtosis values are evaluated using Eq.11 and Eq 12 (**Figure 45**,** Figure 46**,**Figure 47**,**Figure 48**,** Table 5).

$$skewness = \frac{\sum_{i=1}^{N}(Y_i - \bar{Y})^3}{(N-1)s^3} \quad \text{Eq. 11}$$

$$kurtosis = \frac{\sum_{i=1}^{N}(Y_i - \bar{Y})^4}{(N-1)s^4} \quad \text{Eq. 12}$$

Y_i= data

$\bar{Y}$= Mean value

s= standard deviation

N= number of data points

Table 5 : Skewness and curtosis values for 3K and 12K measurements

	3K		12K	
	Skewness	**Curtosis**	**Skewness**	**Curtosis**
Yarn thickness	0.13	2.43	-0.70	2.16
Yarn width	0.25	3.84	0.71	2.89
Real area of the yarn measured by a CAD software	0.13	2.66	0.01	1.85
Laminate thickness	-0.63	2.28	-0.47	2.33

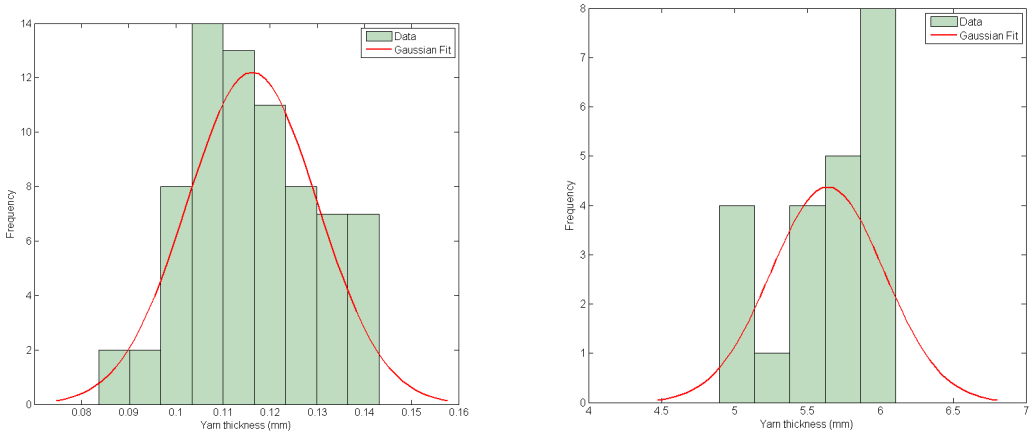

a) b)

Figure 45: Yarn thickness distribution, a) 3K, b)12K

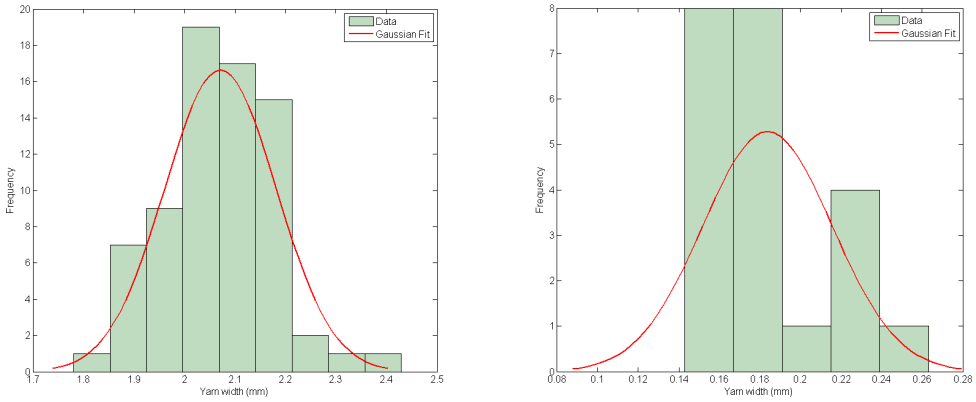

a) b)

Figure 46: Yarn width distribution, a) 3K, b)12K

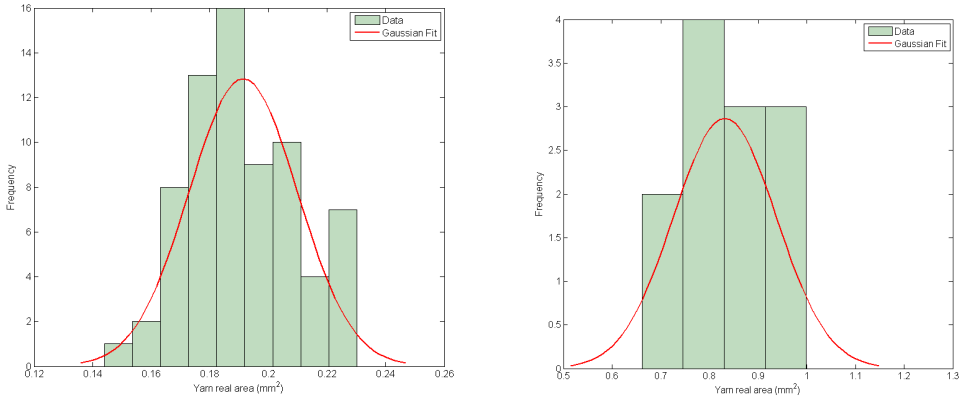

a) b)

Figure 47: Real yarn area distribution, a) 3K, b)12K

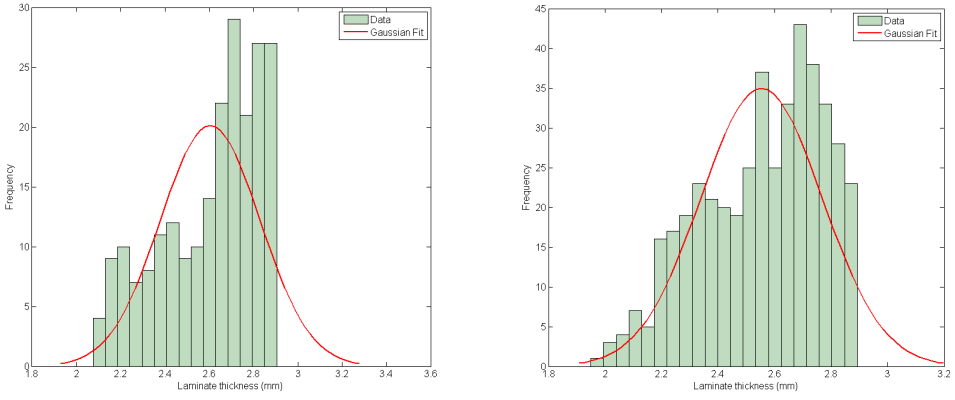

a) b)

Figure 48: Laminate thickness distribution, a) 3K, b)12K

A normal distribution shows 0 as skewness value (evaluates the asymmetry of the probability distribution) and 3 as curtosis value (evaluates the flatness of the probability distribution). The yarn thickness, yarn width and yarn area distributions are closer to a normal distribution for 3K material than for 12K material. The reason might be the data population, for 3K material more measurements are done than for the 12K. As the number of measurement is increased, the distribution might be closer to a normal distribution. For the laminate thickness the distribution shows a tendency of having higher probability for thicker laminates than for thinner values in both materials.

4.4 STIFFNESS EVALUATION BY MULTI-SCALE MODELLING APPROACH

A numerical model is proposed to quantify the macro-level stiffness variation due to geometrical variability. Results of the Young's modulus statistics are presented with a sensitivity analysis in order to identify the structural parameters which have a dominant effect on the resulting macroscopic stiffness values. The section concludes with a critical view on the uncertainty in sampling parameters.

Multi-scale modeling methodology

The developed methodology is illustrated by Figure 49. The composite plate is simplified as a laminate where each ply consists of identical unit cells. The overall build up of the laminate can be outlined by the following consecutive procedures: (i) random construction of distinct unit cells at meso-scale, (ii) homogenization of each unit cell from meso- to macro-scale and (iii) construction of the structural laminate based on unit cell randomness with additional randomness at the macro-scale. In-house developed software and programmed Matlab® routines are applied for this analysis. The procedures are elaborated in detail below with the assumption of perfect impregnation of the matrix material without any void formation or defects. Bonding between plies is considered to be perfect. The Classical Laminate Theory [89] is used to derive the mechanical properties of the orthotropic composite plate, which is in a plane stress condition.

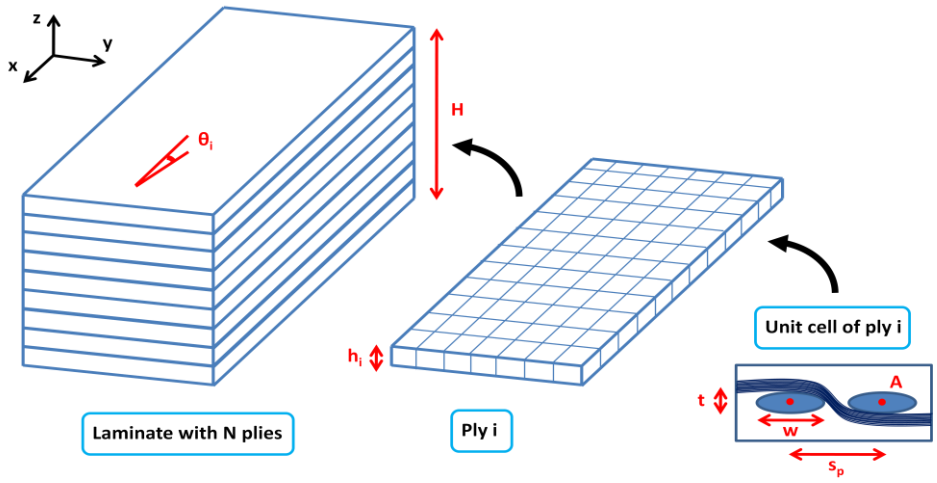

Figure 49: Methodology of the stiffness evaluation by multi-scale modelling

Random unit cell description

A unit cell model is constructed with random parameters yarn width ***w***, thickness ***t*** and spacing s_p. The WiseTex software [79] computes this generalized description of the internal structure of the textile reinforcement on the unit cell level based on the random parameters. Figure 50 shows the WiseTex model for the considered topology; the cross sections are assumed to be elliptical.

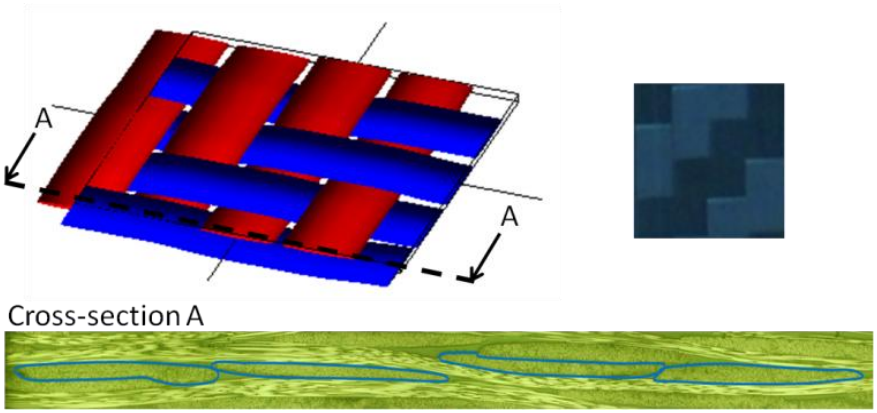

Figure 50: WiseTex model of the twill woven unit cell compared with optical view of surface and cross-section.

A set of these random meso-scale parameters is obtained by sampling parameters yarn width ***w***, yarn area A_{wt} and yarn spacing s_p from its experimental statistical distributions, of which the statistical parameters are presented in Table 4.

The yarn thickness is determined from the dependency relation between randomly sampled yarn width $\boldsymbol{w}$ and thickness $\boldsymbol{t}$. The estimated elliptical area $\boldsymbol{A_{wt}}$ of both parameters must equal the prescribed randomly sampled elliptical yarn area.

$$A_{wt} = \pi \cdot \frac{t}{2} \cdot \frac{w}{2} \Leftrightarrow t = \frac{4 \cdot A_{wt}}{\pi \cdot w} \qquad \text{Eq.13}$$

In a nominal weave structure a dependency exists between the yarn spacing $\boldsymbol{s_p}$ and the yarn cross sectional variables. The dataset is however insufficient to establish a relation between yarn spacing on the one hand and cross sectional area, with corresponding yarn width and thickness, on the other hand. Although, the sampling distribution is truncated in a way to account for that consecutive yarn tips at least touch each other or overlaps.

A total of 100 unit cells are constructed using the WiseTex software, based on 100 random sets of meso-structural parameters. These unit cell models are stored and used as database for the random laminate build-up.

Homogenization technique

A multi-inclusion Eshelby approach (Mori-Tanaka method) [90], is applied to derive the macroscopic stiffness value $\boldsymbol{E_i}$, corresponding to the lower scale random structure of a unit cell $\boldsymbol{UC_i}$.

Random laminate build-up

A simulated laminate (one random realization) is described by its thickness $\boldsymbol{H}$, ply unit cells $\boldsymbol{UC_i}$, ply thicknesses $\boldsymbol{h_i}$ and ply orientations $\boldsymbol{\theta_i}$. An arbitrary unit cell, from the constructed unit cell database, is randomly appointed to each ply in the laminate. The effective stiffness $\boldsymbol{E_i}$ is normalized to the corresponding ply fiber volume fraction $\boldsymbol{V_{f,i}}$ to obtain $\boldsymbol{E_{i,n}}$. The other structural laminate parameter values are obtained as follows:

- ***Laminate thickness :*** The laminate thickness $\boldsymbol{H}$ histogram presents a high variability due to the spatially distributed local dimension fluctuations resulting from the autoclave curing process. To sample a feasible unique value of thickness $\boldsymbol{H}$, a volume-averaged thickness interval is proposed which is indirectly derived from measurement data of $\boldsymbol{V_{f,L}}$. The latter data is obtained by burn-out experiments and is related to $\boldsymbol{H}$ by:

$$V_{f,L} = \sum_{layer\ i} \frac{V_{f,i}}{N_{layers}} = \frac{1}{N_{laye\ rs}} \cdot \sum_{layer\ i} \frac{\rho_A}{\rho_f \cdot h_i}$$

Eq.14

With $\boldsymbol{\rho_A}$ the areal density, $\boldsymbol{\rho_f}$ the carbon fiber density and $\boldsymbol{h_i}$ the ply thickness. This adapted thickness interval ensures that the generated composite laminate will have a realistic fiber volume fraction.

- ***Ply thickness :*** The ply thicknesses $\boldsymbol{h_i}$ are randomly sampled, with the only restriction that the sum of ply thicknesses must comply with the prescribed laminate thickness: $\Sigma \boldsymbol{h_i} = \boldsymbol{H}$. The sampled values are used to quantify the $\boldsymbol{V_{f,i}}$ of each ply by the relation given in eq. 9.

- ***Ply orientation :*** The ply orientation $\boldsymbol{\theta_i}$ is sampled from an adapted database of measured orientations, since the sign of measured angles cannot be determined from the images (section 4.4). In the original database orientation angles are arbitrarily switched between positive and negative values using a random generator.

Interdependencies are present between the laminate structural parameters and the unit cell geometrical parameters: e.g. the ply thickness value depends on the yarn thicknesses within a unit cell due to compression in the production step. Due to a lack of a large dataset, these dependencies cannot be determined for application in the numerical model. However, the sensitivity analysis in the next section will show that the correct representation of the laminate parameter values is more important than the unit cell parameters. Omission of this interdependency is thus expected to have a low influence on the resulting stiffness values.

Statistical analysis strategy

Monte Carlo simulation is used as stochastic solver to derive the laminate Young's modulus mean value and zero-mean variation. Each deterministic run calculates the stiffness value of the generated random panel using the methodology described in the previous section 5.1.

Young's modulus statistics

A Monte Carlo sequence of 500 deterministic runs is performed for (i) each single random parameter as a sensitivity analysis and for (ii) a case where all parameters are random. The effect of uncertainty on evaluated stiffness values in the present methodology is discussed in section 5.3.3.

Sensitivity analysis of the considered parameters on the stiffness values

A sensitivity analysis is performed for each random parameter:

- the general unit cell ***UC*** (effect of yarn spacing and cross-section),
- thickness of the laminate ***H***
- thickness of the laminate ***H***, including the ply thicknesses h_i
- orientation of each ply θ_i

All other parameters are maintained at their mean value during each parameter analysis.

Table 6 presents the result of the analysis on the laminate Young's modulus in the x-direction. Since the fabric is balanced in warp and weft, the y-direction has similar results which are not shown here. The presented values are non-normalized with respect to the overall fiber volume fraction.

Table 6: Sensitivity analysis of geometrical parameters on the stiffness values

	Laminate with 3K yarn		**Laminate with 12K yarn**	
	Exx mean [GPa]	**Exx COV** [%]	**Exx mean** [GPa]	**Exx COV** [%]
Nominal	65.11	-	68.75	-
UC	65.10	0.18	68.81	0.09
H	65.14	0.78	68.76	0.72
H, h_i	65.11	0.80	68.69	0.74
θ_i	64.91	0.19	67.96	0.78

The mean value of the laminate stiffness decreases only slightly with a different ply orientation, when compared to the mean value of the nominal case and other cases. The distribution of orientation is the only structural parameter, in opposite to the laminate height and the general unit cell parameters, where a lower or higher parameter value than the mean evolve in a reduction of the stiffness value in the x-direction. The random sampling in both sides of the distribution in the Monte Carlo analysis, will give an

overall lower mean value. Due to the symmetric fabric, this also means a reduction in the y-direction of the laminate.

The dispersion of the stiffness values, here described by the coefficient of variation (COV), is largely influenced by the random laminate thickness. The orientation variation for the 12K yarn also results in a large COV on the stiffness value. This is due to the sampling interval of the 12K which is larger than the 3K orientation. The random unit cell and random ply thicknesses are less important for the resulting stiffness statistics.

Laminate stiffness values based on random structural parameters

Table 7 shows results of the stiffness value statistics when the randomness of all structural parameters is taken into account. The stiffness distribution parameters describe the scatter due to inherent variability in the geometry. Comparison of the mean value of stiffness for the non-normalized result with the nominal value, indicates that the deviation between both mean values is small.

Table 7: Laminate stiffness variability for different normalization approaches

	Laminate with 3K yarn		**Laminate with 12K yarn**	
	Exx mean [GPa]	**Exx COV** [%]	**Exx mean** [GPa]	**Exx COV** [%]
Nominal case	65.11	-	68.75	-
Non-normalized	64.89	0.84	67.94	1.11
Normalization to $V_{f,L}$=55% approach 1	66.55	0.26	67.73	0.81
Normalization to $V_{f,L}$=55% approach 2	66.55	0.84	67.73	1.11

The COV-value shows that the dispersion of $\boldsymbol{E_x}$ is significant, and dependent on the normalization approach:

- ***Normalization approach 1 :*** Each value of the dataset $\boldsymbol{E_x}$ is normalized to a $\boldsymbol{V_{f,L}}$ =55% with a specific normalization factor. This factor is constructed using the apparent laminate fiber volume fraction.

- ***Normalization approach 2 :*** All values of the dataset $\boldsymbol{E_x}$ are normalized to a $\boldsymbol{V_{f,L}}$ =55% using a single normalization factor. In this approach, the mean value of $\boldsymbol{V_{f,L}}$ of all laminates is used as the apparent laminate fiber volume fraction.

The experimentally obtained COV, due to variability on geometry, will have an intermediate value. The reason can be found in the average value of $\boldsymbol{V_{f,L}}$, which is given to distinct tensile specimen cut from a certain composite plate.

Comparison with Table 6 also demonstrates that the COV can be estimated from the sensitivity analysis. The COV must be larger than the influence as if the largest contributor to the COV stiffness value (here the thickness or orientation) is the only variability source, but smaller than the addition of each COV to the stiffness as if each single variability source is influencing the stiffness independently.

The presented result of this statistical analysis does not explicitly take into account the randomness in geometry due to nesting and crimp of a woven fabric. Nevertheless, these effects are implicitly taken into account by tuning the fiber volume fraction of the nominal (average) WiseTex model to the measured one.

Effect of uncertainties on evaluated stiffness values

The stochastic analysis is performed with variable input parameters of which some are inevitably uncertain. The strongest assumption is the chosen normal truncated distribution type for each random variable. Nevertheless the histograms in section 4.7 show that this assumption can be adopted for the yarn thickness and width; this is not a valid condition for the laminate thickness and ply orientation for the considered dataset which are both the most sensitive parameters for the resulting laminate stiffness. Uncertainty also exists in the correlations assumed between distinct parameters. This effect is difficult to quantify and is the topic of ongoing research of which results will be presented in future publications.

- ***Uncertainty in laminate thickness values:***

  The histograms in Figure 45 of the laminate thickness show a large spread, resulting in a high coefficient of variation. The large uncertainty in defining an appropriate mean value impedes the determination of one representative value for the total laminate thickness. Another approach can be chosen to filter out a part of this uncertainty by using the thickness specification of the ASTM norm D3039. This standard for tensile tests of composite samples prescribes an allowable thickness tolerance of ± 4%. If this tolerance is used as sampling interval of possible laminate thickness values $\boldsymbol{H}$, a comparison can be made

based on practical limits which cancels the uncertainty present in the standard deviation from the mean value of the thickness. Table 8 shows the obtained stiffness values with this new ***H*** interval. The larger sampling interval results in a high COV.

- ***Uncertainty in ply orientations within the laminate:***

The orientation data are uncertain due to the sign of measured ply angle, which cannot be determined from the optical cross-sectional images. To quantify the influence due to this uncertainty, the sensitivity analysis to the laminate stiffness is repeated for the extreme combination of orientation from the statistics of the dataset. From the results shown in Table 8 it is concluded that the mean value decreases by 7.5% with respect to the nominal value.

Table 8: Sensitivity analysis for a new laminate thickness sampling interval and extreme orientation positions

	Laminate with 3K yarn		**Laminate with 12K yarn**	
	Exx mean [GPa]	**Exx COV** [%]	**Exx mean** [GPa]	**Exx COV** [%]
Nominal	65.11	-	68.75	-
H,h_i ASTM	65.26	2.31	68.76	2.22
Stiffness ASTM	65.05	2.32	68.03	2.36
θ_i extremes	60.33	-	55.59	-

4.5 EXPERIMENTAL MECHANICAL PROPERTY MEASUREMENTS

9 samples are tested for 12K structure and 14 samples for 3K (previously explained in 3.3.2). The results are listed in Table 1. The deviation of elastic properties varies between 2.9-3.1% in 12K material and between 3.7-4.2% in 3K material. For the strength values the deviation is 1.95% for 12K and 4.4% for 3K.

Three elastic moduli at different strain values are obtained from the tests: the initial elastic modulus from 0 to 0.1% strain value, the second modulus from 0.1% to 0.3% and the third elastic modulus from 0.3% to 1%. The initial increase in the elastic modulus up to 1% of applied strain is 7% for 12K, and 3% for the 3K material. This initial elastic modulus increase may be related to the effect of crimp, the inherent

stiffening of carbon fibers or layer misalignment straightening (MSBL and SM). The higher misalignment and scatter value on the orientation of the layer for 12K material may be the reason why the increase in the elastic modulus is more pronounced in these samples. The effect of the stiffening of carbon fibers at strains below 1% was already investigated by Curtis [91]. Increasing values up to 20% were evaluated being independent to the strain rate. This effect also can be the reason why the modulus changes, but the percentages obtained are much lower than the ones obtained by Curtis. The strength is sensitive to crimp percentages; a higher crimp value leads to a lower strength of the woven textile material.

By way of guidance, Hexcel [76] gives some mechanical property values normalized to 55% of fiber volume fraction of the material used for this research: an overall elastic modulus of 65 GPa for 12K and 71 GPa for 3K and a strength value of 1220 MPa for 12K and 900 MPa for 3K. These values are very close to the values obtained in the measurements carried out in this paper.

4.6 DISCUSSION

The variability of measured geometrical values is higher for 12K material than for 3K material. A possible reason for this is the scale factor. The linear dimension of the unit cell for 12K is 2.7 times bigger than for the 3K having the same thickness. As Table 4 shows, there is a significant variation in the average fiber volume fraction among different yarns using two different methods for the area measurement. A difference of 12.7% for 12K and 11.2% for 3K is evaluated between average volume fractions. The fiber density inhomogeneity inside the yarn is very high in both materials, but for 12K it is more substantial.

Table 9 summarizes the obtained stiffness values with statistics from the numerical and experimental procedures. The second normalization approach (normalization of 55% with a single normalization factor is applied to the result of the numerical model, since this corresponds best to the post-processing procedure applied to the experimental data. The main reason that the mean value of Young's modulus differs from the manufacturer's value is the higher fiber volume fraction of the tested plates. Table 3 shows a higher fiber volume fraction for the 12K material. The numerical model is based on these target volume fractions, which flattens out the differences between

mechanical properties of 3K and 12K. The trend of higher variation for the 12K is however still present.

Table 9: Stiffness values obtained by numerical and experimental procedures

	3K		12K	
	Mean value	Deviation	Mean value	Deviation
Manufacturer [GPa]	71.00	-	65.00	-
Initial modulus (0-0.1%) [GPa]	68.49	4.2%	61,54	2.9%
Modulus (0.1%-0.3%) [GPa]	69.94	3.7%	65,3	3.9%
Modulus (0.3%-1%) [GPa]	70.9	4.2%	66,27	3.1%
WiseTex Average normalized to V_{fL}=55% - approach 2	66.5	0.83%	67.7	1.11%

The experimental variability is higher than the geometrical variability obtained by numerical simulations. This implies that there must be other sources of variability that contribute to the resulting randomness of an experimentally obtained stiffness value and that are not included in the current analysis. An additional reason can be that the correlations between the yarn parameters and spatially distributed are not modeled correctly. Correlations between parameters, except for the yarn thickness and yarn width, are not considered since the experimental data do not allow the derivation of this relationship. Future work will tackle this problem to obtain a more realistic model. Among the former uncertainty sources are variations acquired by the (i) experimental preparation, set-up and/or testing conditions, (ii) post-processing computations on the dataset and (iii) manual errors. The effect of the normalization approach on the results in Table 7 is an example of the post-processing variability source. At last, it is important to consider the step of manual, or even automated, measurement of each geometrical entity also as a source of variability. The measurement of each random parameter in the above analysis is influenced by this bias. This is a non-negligible factor, which is difficult to quantify but must be kept in mind throughout the analysis.

Results from the numerical model exhibit an inherent bias with the real value due to the uncertainty in the input parameters which are based on the measured data where for each parameter a normal distribution is proposed as the traditionally most obvious representation. The data set is however too small to confirm that the normal distribution is a realistic representation. More data would allow the derivation of the most realistic distribution (which can still be the normal distribution) and may also establish correlations between the parameters.

Using the characterization of the unit cell in WiseTex (applying an overall composite volume fraction of 55%) the volume fraction inside the yarn is 68.4% for 3K and 69.9% for 12K, higher values than the ones obtained from the experimental measurements. The reason may be the way the textile geometry is modeled. The calculations do not take into account possible nesting effects between advanced weft and/or warp yarns. This effect softens the crimp of the yarns and reduces matrix rich areas, showing lower yarn volume fraction at the same overall volume fraction of textile composite.

4.7 CONCLUSIONS

The internal geometry measurements carried out in carbon reinforced woven materials show high scatter values. The internal geometrical variability in the material is higher as the unit cell size increases due to the scale effect. 12K geometrical measurements statistics show a larger scatter for yarn thickness, width and yarn fiber volume fraction than 3K statistics. The nesting effect between layers is also more pronounced for 12K than for 3K composite material.

These geometrical deviations are afterwards introduced in the WiseTex software to generate a database of numerical models. The obtained modeling results also show the size effect, as the 12K statistics are higher than 3K statistics. Sensitivity analysis shows that the laminate thickness and orientation are the largest contributors to the stiffness dispersion.

The stiffness values derived from the statistical numerical analysis show a lower scatter compared to the experimental stiffness. This comparison reveals that the variability in experimental stiffness is not only linked to the internal geometry, but also to other parameters. Geometrical variation is only a small contributor to the total experimentally obtained variability. The uncertainty during the manufacturing and experimental tests must be taking into account during stiffness evaluation.

5. CHAPTER 5: NESTING EFFECT ON THE MODE I FRACTURE TOUGHNESS OF WOVEN LAMINATES

5.1 INTRODUCTION

In this chapter the fracture toughness of two woven laminates is evaluated for different nesting/shifting values between advanced layers. The analysed woven composites are manufactured using the same resin-reinforcement and same architecture, but have a different tow size (3K/12K). Three different nesting/shifting configurations are applied to the plies at the fracture surface: zero shifting, middle shifting and maximum shifting. Before being tested, the internal geometry of the material is evaluated and any shifting error is measured. For all these configurations Mode I fracture tests are carried out. The differences obtained between 3K and 12K cases can be explained by fibre bridging, but not the differences between the nesting configurations. Depending on the nesting/shifting value the delaminated surface waviness is different, and consequently the fracture toughness is also influenced.

5.2 MANUFACTURING OF DIFFERENT DELAMINATED SURFACES

The material selected for this research is the carbon fibre (T700)-epoxy reinforced woven laminate made of 2/2 twill woven layers and manufactured from prepreg sheets in an autoclave (described in chapter 3.3.1). The elastic and geometrical properties of

the material are described in previous work carried out by the author [92] (Table 1,Figure 37). The standards for fracture mode tests [93, 94] define the required thickness in the range 3-5 mm. To obtain average values of 3 mm, even numbers of layers are applied per material: 14 layers for 3K (thickness ~ 3.26mm) and 10 layers for 12K (thickness~ 3.32mm).

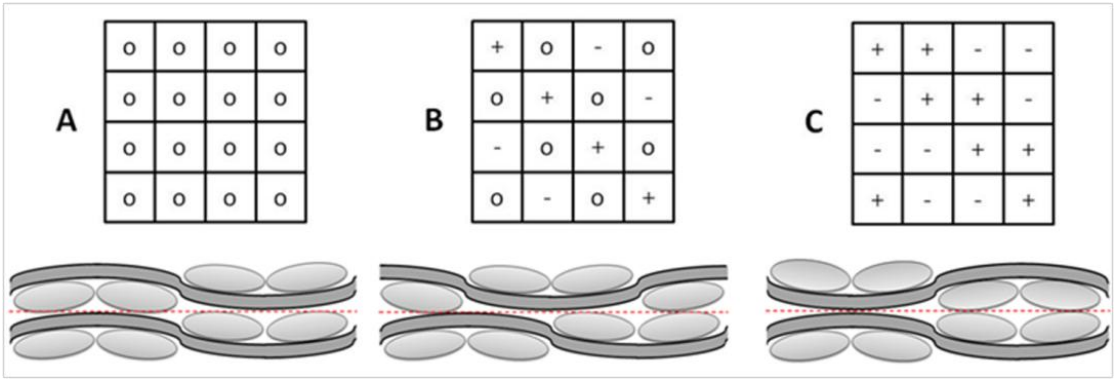

Figure 51: Three configurations at the delamination area, A, B and C.

In this work the shifting control between advanced layers is included during the manufacturing process, controlling the positioning of the prepreg layer at the delaminated surface. In a commonly produced material (without layer shifting control), the probability of having a repetitive delaminated surface geometry is low. Three different fracture surface configurations are manufactured by carefully controlled shifting of the textile in the middle layers. The delaminated area´s configuration patterns are described in Figure 51; the obtained configurations are defined as A, B and C. The shifting distance is related to the length of the unit cell. In configuration A, the shifting distance is zero, in configuration B, the shifting distance is one quarter of the unit cell length, and in configuration C, the shifting distance is one half of the unit cell length. The symbols used for describing the configuration are related to the fibre angles between layers (Table 10). 0º corresponds to the warp direction and 90º corresponds to the weft direction. The warp is the delamination crack propagation direction. The manufacturing process is divided in the following steps.

Table 10: Notation for the fibre configurations

Symbol	Fibre angle configuration in the adjacent layers (θ_1/θ_2)
o	0/90 or 90/0
+	0/0
-	90/90

- **Step 1**: Prepreg layers are cut (plate dimensions 300*300 mm). During the cutting of the prepreg layers the manipulation of the textile must be done carefully, because the cutting can be the source of the distortion on the textile.
- **Step 2**: Half of prepreg layers are stacked up randomly (3K: 7 layers/ 12K: 5 layers). The random positioning of the layers above and below the middle ones is related to nesting (shifting) between layers and does not influence much in the fracture toughness values. Until the next layers are applied the material is vacuum packed.
- **Step 3**: In the crack front a Teflon layer is positioned. The Teflon must start at a unit cell boundary line.
- **Step 4**: Using a thread or other kind of mark, the shifting position of the next prepreg layer is marked (A, B or C). The layers are shifted according to the applicable criterion not only in the crack propagation direction, but also in the direction of the sample width. The Teflon layer is positioned as accurately as possible by two persons, in order to reduce errors. Afterwards the mark that is used for helping during the positioning of the layer is removed.
- **Step 5**: The upper layers (9-14 in 13K, 7-10 in 12K) are positioned randomly and the material is vacuum packed.
- **Step 6**: The plates are placed in an autoclave for 2 hours, 120ºC and 5 bars.

After the samples are made, the final real shifting on the material is measured. Manual positioning of the layers, vacuum application and autoclave process can also lead to a repositioning of the layers (at step 2 and 6), which may alter the intended shift. It is known from previous measurements that there is a variation between 1.3 and 2.5 % in the ends/picks distances in woven textile materials [92, 95], hence the unit cell dimensions may vary. The final real shifting on the material is measured from optical images of the laminates edges. The shifting error defined between layers for all material types is between 0.4 to 1 mm, below the yarn thickness (~2mm for 3K and ~5 mm for 12K). This positioning error does not change the configuration type. From these results it is concluded that the configurations obtained in the material are the ones defined during the manufacturing process.

5.3 DOUBLE CANTILEVER BEAM (DCB) TEST

5.3.1 Test procedure

There is no specific standard for mode I test for textile or non-unidirectional materials; that is why special attention is taken in this work to the test protocol. Mode I opening test is performed following the international standard ASTM-D5528 [93] defined for unidirectional (UD) fibre reinforced polymer matrix composites (similar to the ISO [94] standard). The standard explains how the delamination can branch away from the midplane in non-unidirectional DCB configurations. In these cases the obtained fracture toughness may not be pure Mode I fracture values, as the delaminated surface is not straight. It is explained also that for woven composites the scatter can be greater, as the resin pockets can appear at the interface. Different authors [8, 50] followed the ASTM and ISO standard for carrying out the mode I test for textile materials. As the textile materials show unstable crack propagation, an incremental test method for mode I fracture testing (loading-crack propagation-unloading sequence) was also used by Alif [66]. Davies [96], Dharmawan [97] and Blake [98] defined a run-arrest behaviour in textile materials having three different situations: INST where the sudden crack growth starts, ARREST where the crack propagation is stopped after load reduction and STABLE where a stable crack growth is observed. The fracture toughness values are obtained at INST and STABLE positions. In the woven material used for this research, it is not possible to determine any STABLE zone in the load/displacement curve. Almost all the delaminated area is created by sudden jumps after reaching a maximum load for each delaminated position. De Baere [99] introduces a procedure to obtain an estimated fracture toughness value by fitting a model based on elastic fracture toughness. He reproduces the DCB test by applying a monotonic opening of the samples to a carbon fibre 5-harness satin weave reinforced PPS composite. One of those samples was tested applying an incremental test method, in order to crush and buckle most of the fibre bridging created along the delaminated area. The results show a reduction on the fracture toughness propagation value when a loading-crack propagation-unloading sequence is applied.

In this work the opening displacement is applied in a monotonic way without loading and unloading the sample at each jump of the crack. The reason why a monotonic loading is applied is that as in fibre reinforced composites the fibre bridging is an

intrinsic mechanism in the material, the elimination of this effect may reduce the real fracture toughness value. In the test bench the opening forces are applied to the specimen using blocksglued to the sample. A load cell of 200 N records the force evolution. The opening displacement is measured by a laser device that records the displacement of a metallic part that overhangs from the load cell. One lateral side of the specimen is painted in white and position marks are defined every 5 mm. Crack front evolution is recorded with a video camera and analysed during the post-process step. The samples are pre-cracked (3 to 5mm) and the crack front location is again defined and the new crack front position marks are created. The test is carried out with a displacement speed of 3 mm/min and it ends when the crack front reaches 50mm. The unloading path is also recorded for data evaluation afterwards. As the material fracture surface geometry is non-homogeneous, load and crack jumps appear during the test; crack front may suddenly increase more than 3-5 mm.

5.3.2 Data post-processing

Six samples per material type are tested and the data are post-processed using three different methods for obtaining fracture toughness values in mode I. The initiation values in textile materials show high scatter (20-40% for standard deviation of initiation fracture toughness, six specimens per material) because of the non-heterogeneity of the material and the fact that the crack front position is not controlled during the tests. The crack at the beginning of the delamination (after the initial precrack) might be located anywhere on the surface. In the present work only the crack propagation mechanism is investigated.

ASTM standard method [93] (Method 1): The Modified beam theory method with the correction for the rotation is used as a data reduction method for calculating G_{IC}. The Fracture toughness values are obtained at maximum loads, before sudden crack propagation occurs and load reduction happens. If the fracture values are not obtained at INST positions and other non-critical positions (ARREST positions) are also included, fracture toughness can be underestimated [96-98] (Figure 52). In order to confirm this assumption, one sample is tested and two G values are calculated from the same force/displacement curve: in the first R curve all points are taken into account (INST and other positions as ARREST) and in the second R curve only the critical points where the crack is bound to propagate (INST values) (Figure 53). The average value

obtained for the first R curve is 11% lower than the value obtained in the second one. For calculating the average fracture toughness, first values obtained at the initial crack evolution are not taken. These points are related to crack initiation instead of crack propagation, and they can distort the final values.

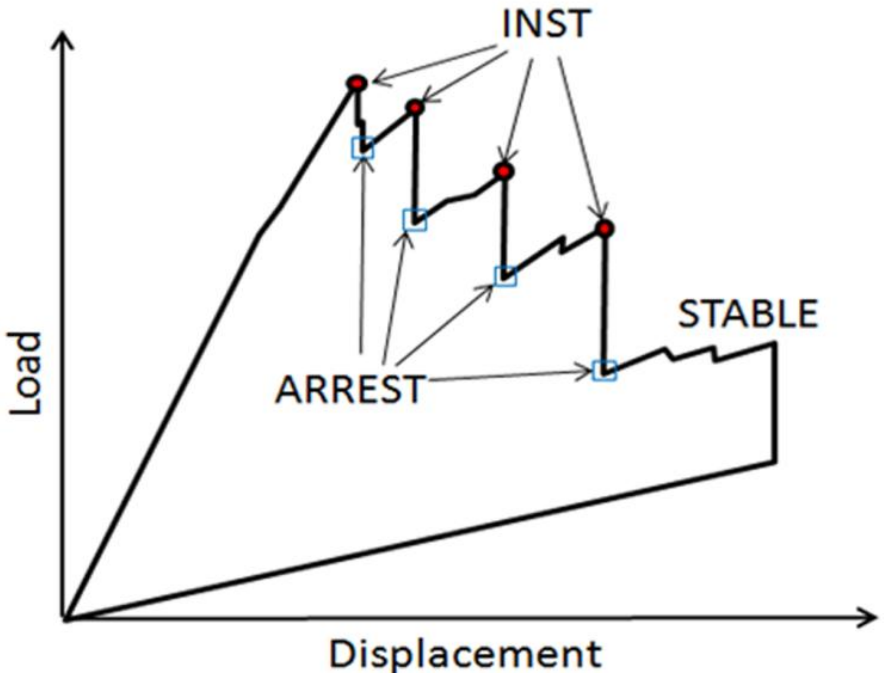

Figure 52: Load-displacement chart for a no stable crack propagation

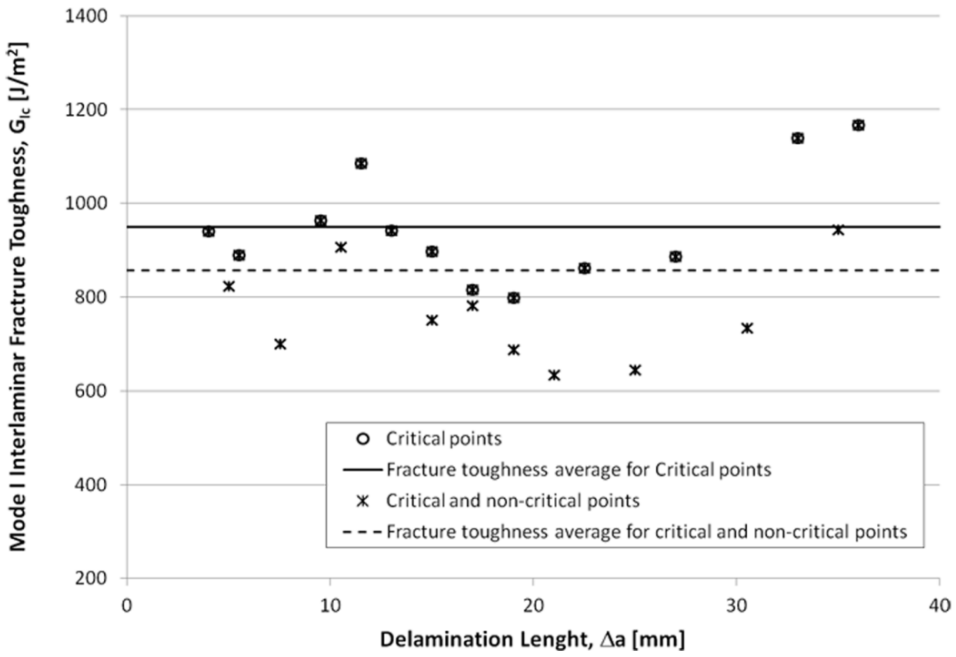

Figure 53: R curve for the same sample (12K-A) but different data post-processing

Curve Fitting method [99] (Method 2): The method calculates a curve fitting value from the force peaks (except the first peak, which is related to the fracture toughness initiation) obtained in the force/displacement curve (Figure 54). The analytical model is based on a linear elastic fracture mechanics formula, where the load and the displacement during the test are linked by the fracture energy value (without the delaminated length value). Fracture toughness is obtained by fitting the force (F) reduction law with an exponent of -0,5 (Eq.15).

$$F = \sqrt{8}\left(\frac{G_{IC}}{12}\right)^{3/4}\frac{1}{\sqrt{\delta}}b(h^3E_{11})^{1/4} = f(G_{IC})\delta^{-0.5} \quad \text{Eq. 15}$$

b= width

h= half of the thickness

E_{11}= longitudinal modulus

δ= displacement

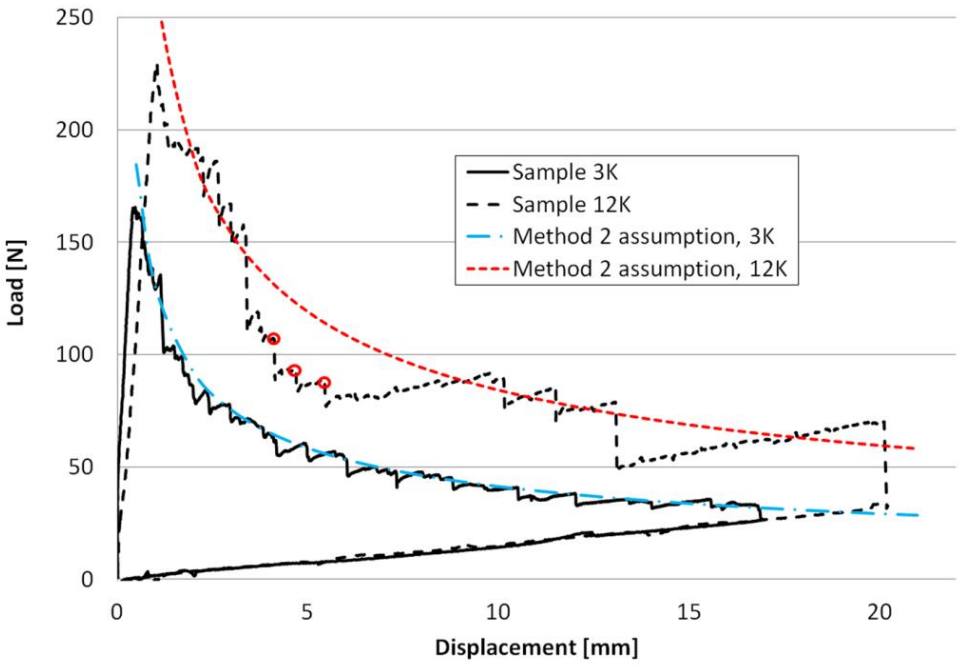

Figure 54: Method 2 for 3K and 12K material and the fitting curves obtained

Area method [100] (method 3): This method was proposed by Airbus and the main advantage is the simplicity of the formula. The only data required is the load/displacement value from the test bench (the unloading data is also required for the area calculation) and the initial/final delamination length. The procedure defines a minimum delaminated length of 100 mm and an opening speed value of 10mm/min. In

this work the delamination length (50 mm) and the speed (3 mm/min) are lower because of the requirement for method 1. The area from the load/displacement chart is calculated and fracture toughness is obtained by dividing this value by the delaminated area (a is the crack length and b is the sample width) (Eq. 16).

$$G_{\mathrm{IC}} = \frac{Area}{a*b} \qquad \text{Eq.16}$$

Table 11: Fracture toughness in mode I using Method 1, Method 2 and Method 3.

		3K			12K		
		A	B	C	A	B	C
Method 1	Average [J/m^2]	591	574	468	1172	1116	1013
	Standard dev. [J/m^2]	71	54	53	137	50	134
	Standard dev. [%]	12%	9,4%	11,4%	11,6%	4,5%	13,2%
	Median [J/m^2]	572	555	484	1146	1125	1080
Method 2	Average [J/m^2]	557	550	462	1159	966	851
	Standard dev. [J/m^2]	63	74,7	63	162	71	92
	Standard dev. [%]	11,3%	13,6%	13,7%	14%	7,3%	10,8%
	Median [J/m^2]	541	548	461	1150	970	817
Method 3	Average [J/m^2]	549	549	442	1042	1022	870
	Standard dev. [J/m^2]	65	62	55	124	80	153
	Standard dev. [%]	11,8%	11,4%	12,4%	11,9%	7,9%	17,6%
	Median [J/m^2]	549	542	432	1050	978	799

5.3.3 Mode I test results

Table 11 shows the average results for the three methods per material size and configuration. From the recorded load-displacement charts and images it is possible to verify that the crack front jumps (INST positions) do not follow any tow size pattern and the size of the jumps is not stable along the sample. The differences obtained between the three methods for the same material are below 8% for 3K and 12-19% for 12K. Method 1 shows the maximum average fracture value for all material types. For 3K the tendency is repetitive; method 3 shows the lowest average value, method 2 the medium value and method 1 the maximum. For 12K material the tendency is not always the same for method 2 and 3. Analyzing method 2 more in detail, the estimated power law obtained from the peak points does not fit properly the force/displacement curve for 12K. Crack jumps create high load reductions, creating less and non-continuous critical points than 3K material. These small load drops occur almost in all 12K samples. The maximum load peaks highlighted by circles in Figure 54 displace the estimated power law line. On the contrary, the line for 3K material fits the force/displacement curve

better. This effect is consistent for all material configurations. The assumption that the delamination follows a linear elastic fracture behaviour is wrong for 12K, but it works for 3K. On the other hand, the area method averages the fracture toughness value and underestimates the critical fracture toughness of these textiles composites.

The analysis of the differences between materials is done using method 1 (Table 11). The size effect on the fracture toughness value in mode I is noticeable; for 12K fracture toughness values are almost twice than for 3K material. The results also show differences between configurations. In both sizes, A configuration shows the maximum average values, B configuration shows a 3-5% reduction with respect to A, and C configuration a 16-26% reduction with respect to A. The standard deviation obtained for mode I fracture tests (4.5-13.2%) are higher than the deviations obtained for elastic modulus (4.2% for 3K and 3.1% for12K) and tensile strength (4.3% for 3K and 1.9% for 12K) using the same material [92]. One of the reasons is that fracture toughness depends strongly on what is happening in just few unit cells. The delamination length is 50 mm, two unit cells for 12K material and six unit cells for 3K. Although the delaminated surface was controlled in order to create a similar waviness pattern for three configurations, the variability on the position of the crack front, the inclusions, matrix pockets, the non-stable crack propagation and other variability inherent to the material create a dispersion on the results. Argüelles [101] tested five specimens made of UD carbon fibre reinforced epoxy material in mode I. The standard deviation obtained using the ASTM D5528 was 9,6%, close to the values obtained in this research.

For 3K/12K material the range of fracture values and the median value for A and B configurations is similar (12K-A configuration shows higher dispersion). The probability of obtaining a better fracture toughness in A configuration than in B configuration is not high. On the contrary, as the fracture values obtained are higher for A and B configurations, the probability of obtaining a better result using A or B configuration instead of C configuration is higher.

5.3.4 Delaminated surface

Delaminated areas are analysed after testing the samples using an optical camera (Microscopio Leica) and the images are post processed with the image manager software of the microscope. On all materials bright matrix pockets can be seen between

yarn transitions (Figure 55, Figure 56). The surface for 12K shows more broken fibres than for 3K, where almost no fibre is seen.

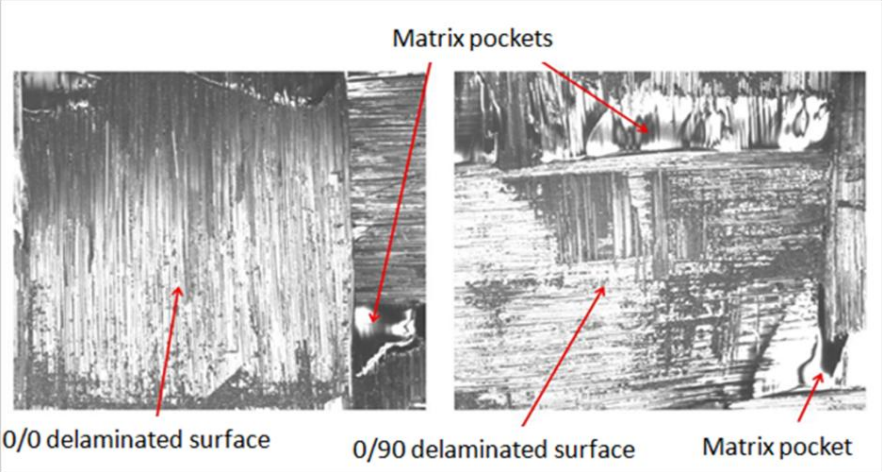

Figure 55: Delaminated surfaces 3K for 0°/0° and 0°/90°

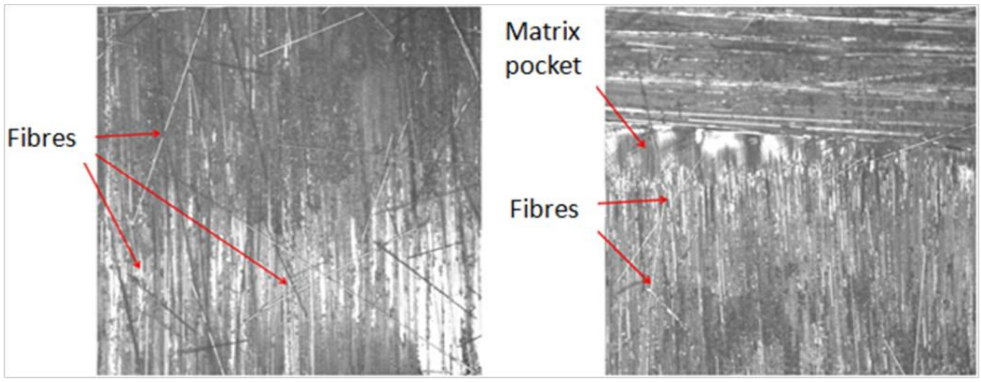

Figure 56: Delaminated surfaces 12K for 0°/0° and 0°/90°

5.4 DISCUSSION AND TESTS FOR UNDERSTANDING DELAMINATION MECHANISMS

The results show that the scale effect in woven laminates is high for fracture toughness in mode I. The size of the unit cell in woven material increases the fibre-bridging mechanism in a positive way. The general tendency shows a slightly higher fracture energy for A configuration than for B configuration and a higher reduction (16-26%) for C material. The difference on fracture toughness values between 3K and 12K can be explained by the amount of fibre bridging on the surface. But the mechanism taking part on the differences between configurations is not clear. Is the fibre bridging also

responsible for the increase of fracture toughness in A/B configurations? Are there any other mechanisms involved? Does fibre bridging exist in a small percentage on 3K samples?

New DCB tests were made to quantify the mode I fracture toughness percentage increase produced by the fibre bridging. Two tests are performed on the same specimen per material type (one specimen per unit cell size and configuration) (Figure 57). By using the same sample for both tests the scatter due to the manufacturing process and the variability between specimens is reduced.

i. Test 1: Monotonic DCB test
ii. Test 2: Loading-unloading DCB test (Figure 58)

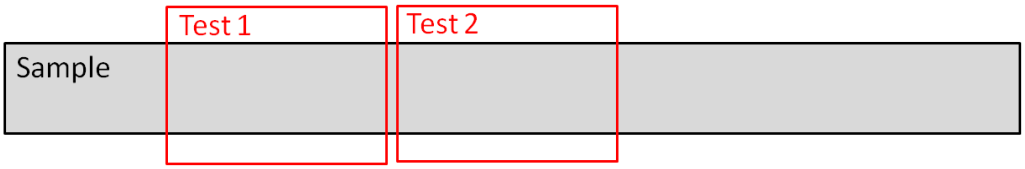

Figure 57: Test 1 and Test 2 are carried out on the same sample.

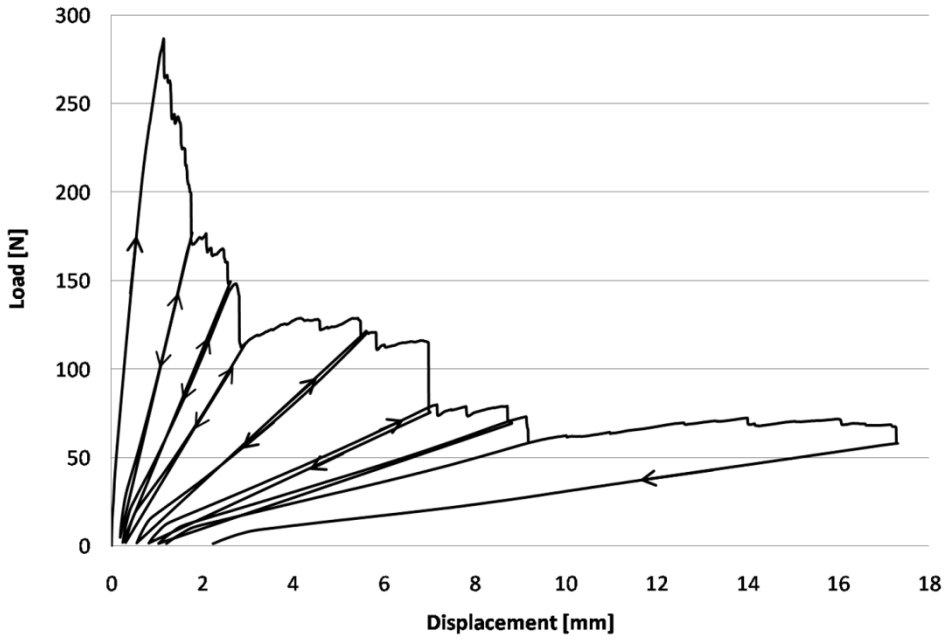

Figure 58: Loading and unloading DCB test (12K-A)

The monotonic test yields the fracture toughness result without changing the fibre bridging amount at the crack front, whilst the loading-unloading test breaks the fibre bridges. If the fibre bridging is the reason why A/B configurations show higher fracture toughness value, the reduction percentage after loading-unloading test should be higher

for these configurations. The obtained results are summarized in Table 12. For 3K, the loading/unloading tests do not change significantly the fracture toughness, the effect even increases slightly for 3KA material. For 12K, the loading/unloading tests reduce the fracture toughness in a range of 6-9%. The conclusion obtained is that 3K does not have significant fibre bridging on the crack tip. On the other hand 12K shows a higher fibre bridging effect, with a reduction of the fracture toughness in the order of 6-9%, similar for all configurations. At this point it is assumed that the largest part of the variability obtained in Table 12 is due to the differences between specimens, and not due to the scatter introduced carrying out the tests. If the scatter due to the test set up would be significant, the expected scatter for 3K would be similar to the scatter for 12K.

Table 12: Results for DCB tests

	Test 1: Monotonic G_{IC} [J/m2]	Test 2: Loading/unloading GIC [J/m2]	Difference
3KA	572	583	1,9%
3KB	572	570	-0,4%
3KC	623	615	-1,2%
12KA	1288	1205	-6,5%
12KB	1333	1208	-9,4%
12KC	1297	1194	-7,9%

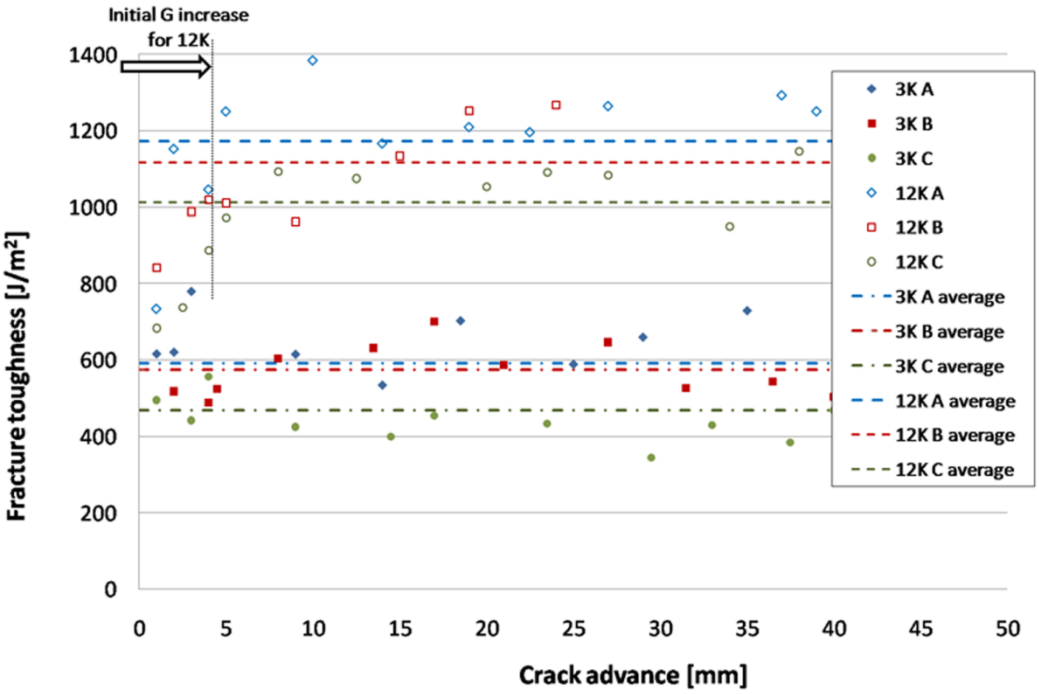

Figure 59: R curves for six material types and fracture toughness average values

The absence of fibre bridging in 3K material is also possible to ratify analyzing R curves obtained from previous samples when they are loaded in a monotonic way (Figure 59). 3K materials do not show an increase on the toughness value at the beginning of the crack advance; but for 12K an increase is observed before 5mm of crack advance. These results confirm that 3K material almost does not have fibre bridging at the crack front and that 12K material does have it. The fibre bridging does not seem to be responsible for the differences between configurations. As the characteristic controlled during manufacturing process is the nesting/shifting value, the differences between configurations may be dependent on it.

5.5 CONCLUSIONS

This research investigates the effect of the unit cell size and the nesting/shifting values between advanced layers on the fracture toughness in mode I. For this purpose, special samples have been prepared in which the layer is precisely positioned over the next one. A crack is initiated in between both layers. Although maximum efforts have been done for perfect positioning of the two neighbouring layers, some error occurred. The shifting error applied to the samples respect to the unit cell size is bigger for 3K material than for the 12K material. The reason is the unit cell size; for the same dimensional error (manual positioning of the upper layer creates always a similar error) the percentage is bigger for 3K than for 12K.

The DCB test is used for performing the mode I test and three post-processing methods are compared to evaluate the most suitable for the woven textile materials tested. The method proposed by de Baere (method 2) seems suitable for 3K material, but it does not fit the force/displacement curve for 12K material. Due to the high instability of crack propagation and sudden load reductions, the force/displacement curve does not follow a linear elastic fracture mechanics formula. The reason may be that only the length for two unit cells is delaminated for 12K material. For future tests longer delamination lengths are recommended. The area method (method 3) is the easiest way of obtaining a fracture average energy in mode I, because it does not need any control of the crack tip during the test. As the requirements of minimum delamination length and opening speed for method 3 are not fulfil in the test carried out, it is not possible to evaluate the suitability of using it. For future work new experiments should be performed following

the methodology proposed in method 3 for obtaining reliable conclusions. The proposed method for post-processing the materials analysed in this research is the ASTM (method 1). Only critical points (just before sudden crack propagation) on the force-displacement curve must be taken into consideration. The standard deviation obtained for fracture tests in mode I are higher than the values obtained for the same material in tensile tests. The reason may be the non-heterogeneity of the delaminated surface. Although the nesting/shifting is controlled, other properties as local fibre-resin distribution, geometry variability, the lack of control of crack front position and inclusions are present in the material. Analyzing the results of mode I fracture toughness values of woven materials the next conclusions are obtained:

- There is fibre bridging effect at the crack front for 12K and not for 3K. Fibre bridging effect at the crack front in woven material depends on the unit cell size: bigger unit cell size leads to a higher amount of fibre bridging. It seems that there is a unit cell size limit for woven material, below this unit cell size the fibre bridging does not affect the fracture toughness values.
- The differences between A/B and C configurations cannot be explained by the fibre bridging: other phenomena must be taking part. For 12K material, fracture toughness values can be linked with nesting values: a higher nesting effect leads to a higher fracture toughness value. For 3K material the nesting values are similar for all configurations and the cause-effect relationship of the nesting is not clear to determine.

6. CHAPTER 6: NESTING EFFECT ON THE MODE II FRACTURE TOUGHNESS OF WOVEN LAMINATES

6.1 INTRODUCTION

In this chapter the mode II fracture toughness is evaluated for carbon fibre T700-epoxy reinforced woven laminates using the end notch flexure set-up. The analysed woven composites have a different tow size (3K/12K). Three different nesting/shifting configurations are applied to the plies at the fracture surface. Corrected Beam Theory with effective crack length method (CBTE) and Beam Theory including Bending rotations effects method (BTBE) are evaluated for obtaining mode II fracture toughness. During data post-processing, the importance of the bending angle of rotation and the test configuration is observed to be important. The results show that crack propagation under mode II is more stable if the matrix is evenly distributed on the surface. The nesting does not significantly affect mode II fracture toughness values, although a greater presence of matrix on the delaminated area increases its value.

6.2 TEST SET-UP AND DATA POST-PROCESSING

6.2.1 Material

The material is the carbon fibre (T700)-epoxy reinforced woven laminate made of 2/2 twill woven layers and manufactured from prepreg sheets in an autoclave (described in chapter 4.2). In a previous work, the author obtained the elastic, geometrical properties and mode I fracture toughness values [92] (Figure 37,Table 1, Table 11). By controlling

the nesting/shifting of the delaminated surface as a design parameter, three different configurations are manufactured: A, B and C (Figure 51) described in chapter 5.2.

6.2.2 End-notch flexure (ENF) test

In this work the three-point bending end notch flexure specimen (ENF) is selected for obtaining the fracture toughness values in mode II (Figure 60). The simplicity of the test set up and the fact that the friction effect is lower in this test are the reasons why it is selected for this research. During the test the load/displacement data from the central loading support are recorded. As the loading support is moving toward the sample, the specimen starts to bend until the crack starts propagating. The test terminates when the crack front reaches the middle of the sample. The samples dimensions are 250mm long, 3,5 mm thick and 25 mm wide. The general rule for a stable propagation in mode II tests is that the initial crack length must be at least 70% of the span ($a_0/L \geq 0{,}7$). The suitability of using this restriction in the material analysed is discussed further in section 3.1.

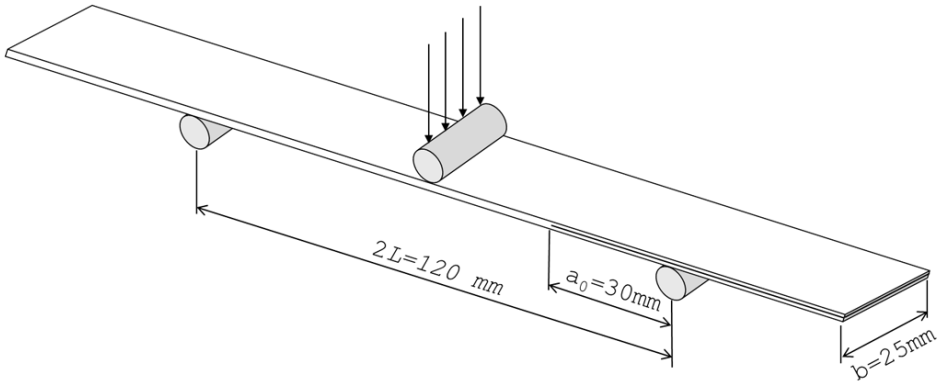

Figure 60: ENF test set up

6.2.3 Data Post-Processing

Corrected Beam Theory with effective crack length method (CBTE)

Due to the complexity of acquiring the crack tip position on woven material during the test, analytical prediction is done using a calculated effective crack length. The CBTE method is selected for the determination of the mode II fracture toughness [102]. The main reason is the simplicity: recording only the load/displacement data from the test is enough to obtain the R curve without any other extra test. From the compliance

calibration method (Eq. 17) a formula for G_{II} related to the equivalent crack length is obtained (Eq. 18).

$$G_{\mathrm{II}} = \frac{P^2}{2b}\frac{\mathrm{d}C}{\mathrm{d}a} \qquad \text{Eq. 17}$$

$$G_{\mathrm{II}} = \frac{9P^2a^2}{16b^2E_{\mathrm{f}}h^3} \qquad \text{Eq. 18}$$

b= Width [mm]

h= Half thickness [mm]

C = Compliance [mm/N]

a =Measured crack length [mm]

P = Load [N]

E_{f} = Apparent flexural modulus [N/mm^2]

Due to the difficulty in measuring the crack length (a) this method proposed to use the effective crack length (a_{e}) [103]. In order to include the effects of material degradation just near the crack tip and the shear, a correction is needed for compliance calculation ($\mathrm{C_c}$) [104] (Eq. 19)(Eq. 20).

$$C = \frac{2L^3+3a_{\mathrm{e}}^3}{8bE_{\mathrm{f}}h^3} + \frac{3L}{10G_{13}bh} \qquad \text{Eq. 19}$$

$$C_{\mathrm{c}} = C - \frac{3L}{10G_{13}bh} \qquad \text{Eq. 20}$$

L = Span [mm]

C_{c} = Corrected compliance [mm/N]

G_{13} = Shear modulus [N/mm^2]

This method does not require an initial test measurement for the apparent flexural modulus (E_{f}) , because it is calculated from the initial corrected compliance ($C_{0\mathrm{c}}$) and initial crack length (a_0) measured values. The effective crack length is obtained including the measured apparent flexural modulus (E_{f}) in the equation Eq. 19.

$$a_{\mathrm{e}} = \sqrt[3]{\frac{C_{\mathrm{c}}}{C_{0\mathrm{c}}}a^3 - \frac{2}{3}\left(\frac{C_{\mathrm{c}}}{C_{0\mathrm{c}}} - 1\right)L^3} \qquad \text{Eq. 21}$$

The final formula for fracture toughness in mode II is calculated replacing the effective crack length formula (Eq. 21) in equation (Eq. 18).

$$G_{\mathrm{IIc}} = \frac{9P^2C_{0\mathrm{c}}}{2b\left(2L^3+3a_0^3\right)}\left[\frac{C_{\mathrm{c}}}{C_{0\mathrm{c}}}a_0^3 - \frac{2}{3}\left(\frac{C_{\mathrm{c}}}{C_{0\mathrm{c}}} - 1\right)L^3\right]^{2/3} \qquad \text{Eq. 22}$$

At each data point the value of G_{IIc} is calculated and the R curve can be plotted with the effective crack length value ($\Delta a_{\mathrm{e}} = a_{\mathrm{e}} - a_0$). The initial propagation fracture energy is obtained when Δa_{e} crosses the zero value. The fracture toughness propagation is the flat G value that appears after stabilization of fracture evolution. This plateau zone is more clearly visible when the crack propagation is stable and where there are no jumps during the test (Figure 61).

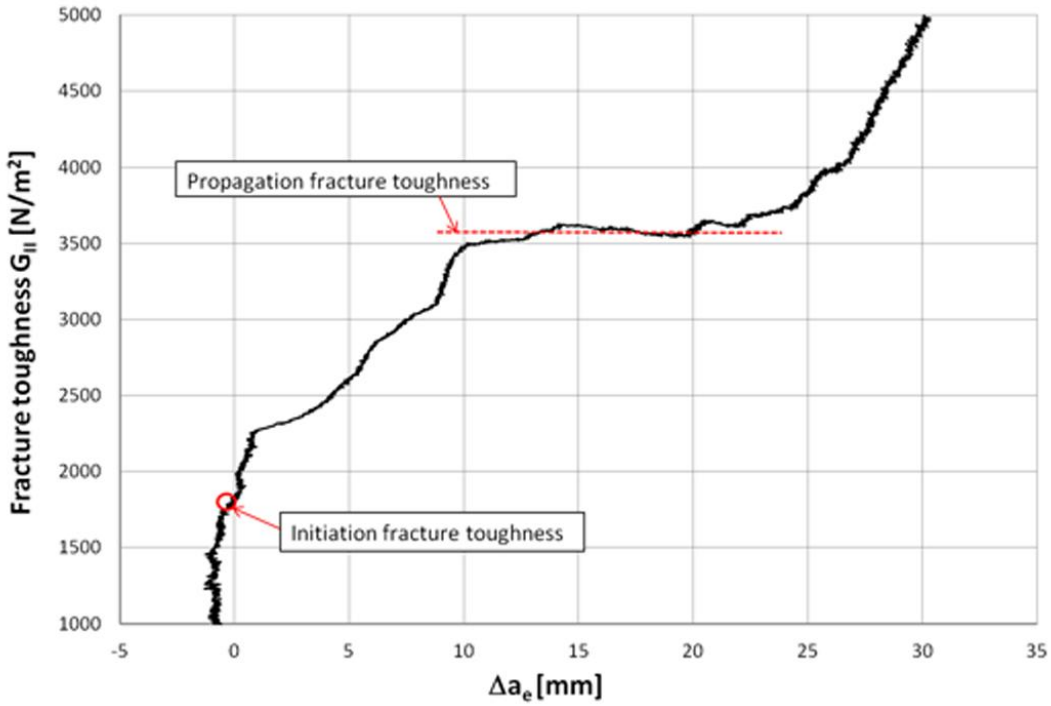

Figure 61: R curve for a 3K sample (CBTE method).

Beam Theory including Bending rotations effects method (BTBE)

Arrese [105] defined a non-linear approach for the BTBE method in cases when the compliance is not constant before crack propagation. The method includes shear, local deformations and bending rotations. It takes into account that due to the changes on contact angle values the span get shorter [106] (Figure 62). The new dimensions are calculated from geometrical changes on the test set-up. The displacement of the middle point is used for calculating the compliance value (Eq. 23) and correction factors due to bending rotations are taken into account (α_a, α_f, α_s) (Eq. 24)(Eq. 25)(Eq. 26).

$$C = \frac{\delta}{P} = \frac{1}{8E_f w h^3}(3(a)^3[1-3\alpha_a] + 2L_0^3)[1-\alpha_f] + \frac{3L_0}{10G_{13}wh}[1-\alpha_s] \qquad \text{(Eq. 23)}$$

$$\alpha_a = \frac{R}{2h}\frac{3P2L_0}{2E_f w(2h)^2}\frac{(-a_0^3+3a_0^2+1)}{a_0} \qquad \text{(Eq. 24)}$$

$$\alpha_f = \frac{3R}{2h}\frac{3P2L_0}{2E_f w(2h)^2}\frac{(4a_0^6-3a_0^5+3a_0^2+2)}{(2+3a_0^3)} \qquad \text{(Eq. 25)}$$

$$\alpha_s = \frac{R}{2h}\frac{3P2L_0}{2E_f w(2h)^2}\frac{(3a_0^2+2)}{2} \qquad \text{(Eq. 26)}$$

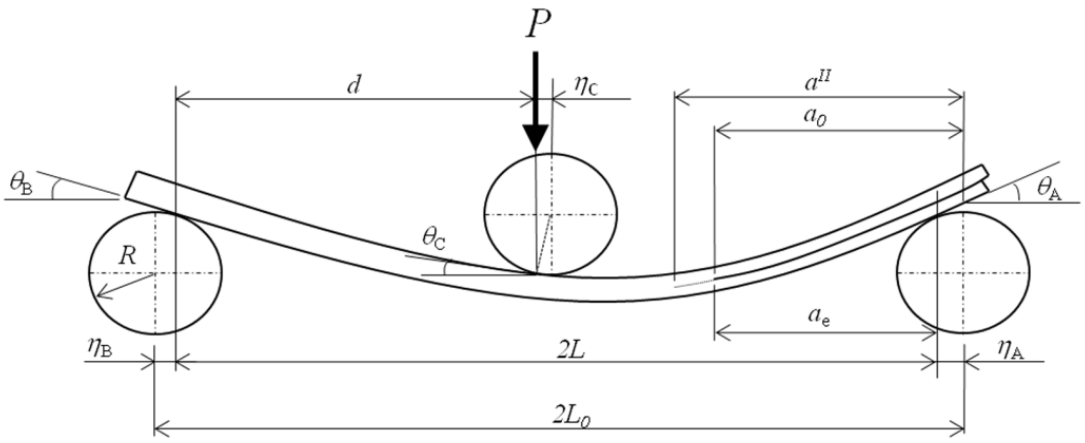

Figure 62: Span reductions in the deformed configuration

Crack length (Eq. 27) can be obtained from the formula of the compliance in equation (Eq. 23). Shear modulus (G_{13}) and flexural modulus (E_f) are calculated previously performing three point bending tests following the method described by Mujika [107] using different span values.

$$a = \sqrt[3]{\left[\left[\frac{E_f w(2h)^3}{3} C - \frac{(2L_0)(2h)^2}{10}\frac{E_f}{G_{13}}(1-\alpha_s)\right]\frac{1}{(1-\alpha_f)} - \frac{(2L_0)^3}{12}\right](1+3\alpha_a)} \qquad \text{(Eq. 27)}$$

Finally the energy release rate for mode II (G_{II}) is estimated in equation (Eq. 28) (χ is the correction factor for energy release rate formula). The results can be plotted in a R curve (similar to Figure 61).

$$G_{II} = \frac{9P^2a^2}{2E_f w^2(2h)^3}[1-\chi] \qquad \text{(Eq. 28)}$$

$$\chi = \frac{2R}{2h}\frac{P2L}{E_f w(2h)^2}\left[4a_0^3 - 5a_0^2 + 6a_0 + \frac{2}{a_0}\left(1+\frac{1}{5}\frac{E_f}{G_{13}}\left(\frac{h}{L_0}\right)^2\right)\right] \qquad \text{(Eq. 29)}$$

6.3 EVALUATION OF TWO METHODS AND DISCUSSION

6.3.1 Tests

Five tests per material type are carried out. As the samples have a length of 250mm, a maximum value of 100mm is defined for the L span value during ENF tests. Applying the restriction established for the initial position of the sample, an initial crack length (a_0) of 70mm is defined. Several tests were performed with this configuration, and in all samples a problem was identified: the samples slipped from one side of the supports (Figure 63). When the span is too large, the sample slips from the supports because of

the high contact angle changes. Several tests were performed in an attempt to avoid the slipping effect using sticky tape on the supports, but the result was always non satisfactory. The first idea to overcome this problem was the reduction of the span (L), but another difficulty arose immediately: reducing the span value and applying the restriction for the initial crack length ($a_0/L \geq 0{,}7$), the propagation length was not enough for obtaining a stable fracture toughness value. As an example, when a span value of 70 mm is defined, the minimum value of a_0 is 49 mm. The length for crack propagation stabilization is only 21 mm, not always enough for obtaining a stable and reliable value in the non-homogeneous material analysed in this research. For these textile materials, at least 25-30 mm of delaminated length is required for fracture energy stabilization. In addition it must be pointed out that due to the diameter size of the supports (20 mm), the test finishes before the crack reaches the middle of the sample. The load starts increasing at approximately ≈3-5mm before reaching the central position. This effect further reduces the length for the stabilization of the fracture toughness. For all these reasons, in this research the previously defined restriction is not applied and new test geometries are defined (L= 60 mm, a_0= 30 mm).

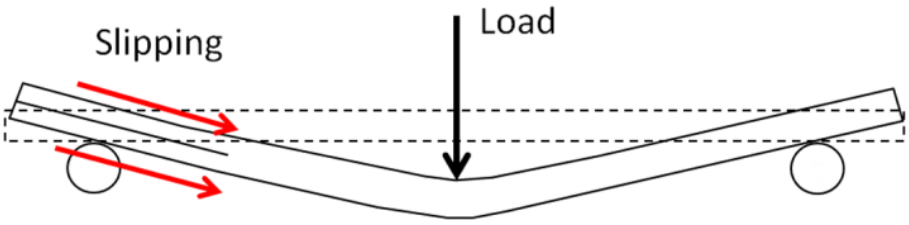

Figure 63: Slipping effect for large span values

Using the new test set-up geometry, the crack propagation for 3K material is smooth and a repetitive value for fracture toughness is obtained using both post processing methods. In mode I tests (DCB test) there were many jumps and sudden crack propagations for 3K material, but for mode II the results hardly show any discontinuous propagation (Figure 64). In the Figure 65 the evolution of fracture toughness value along the crack propagation length is plotted for a 3K material (CBTE method). The G_{II} stable area starts around 10 mm from the crack tip and finished near 20mm, 10mm of stable fracture toughness value is obtained.

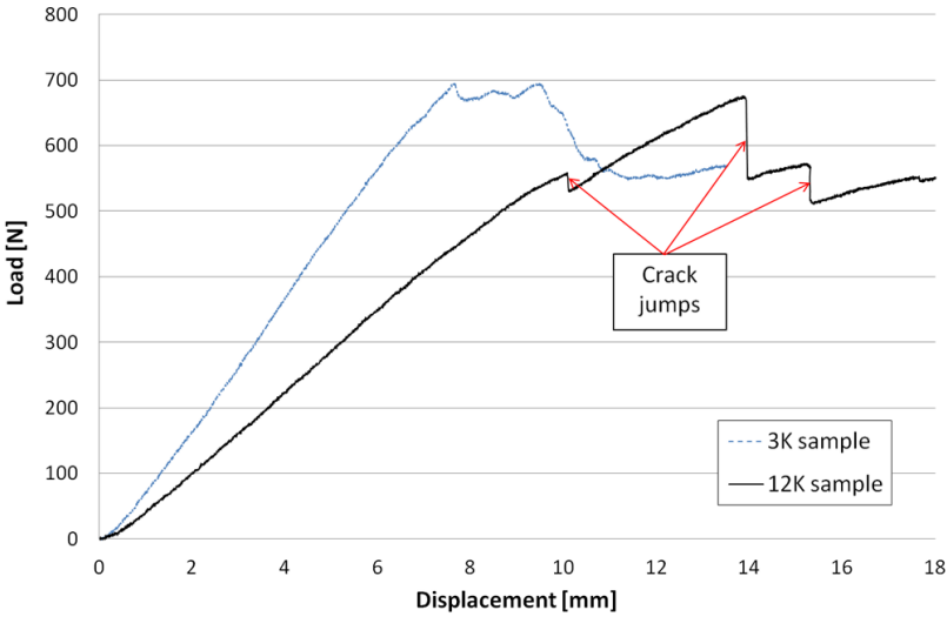

Figure 64: Load/displacement chart for 3K and 12K sample for ENF test

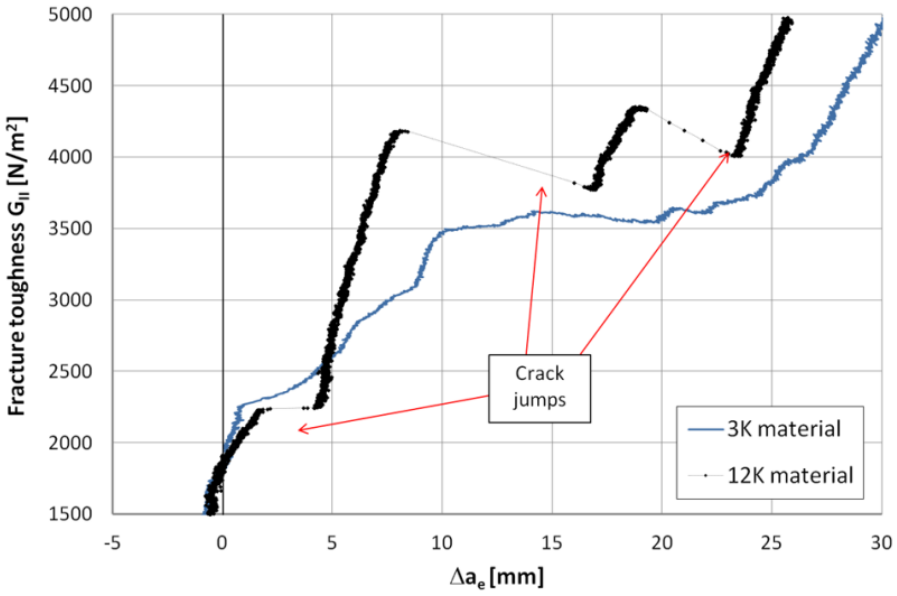

Figure 65: R chart for 3K and 12K sample for ENF test (CBTE method)

For 12K material the crack propagation is not smooth and big jumps appear during the tests; the plateau zone is not easy to determine. The sudden load reductions during crack jumps create also jumps in the R curve. Jump lengths do not follow a repetitive pattern; the jump values vary from 2-3mm to 10mm in some cases.

6.3.2 Crack length positioning verification

In order to evaluate the suitability of using the CBTE and BTBE method for calculating mode II fracture toughness in the material analyzed, the Digital Image Correlation technique is used as an independent reference. The specimen is randomly speckled with a dark-colored ink using an airbrush. The acquisition frequency is 1 image per second and the resolution of the test is 14 microns/pixel (recording camera resolution is 3384*2710 pixels, which correspond to a window of 45 mm*36 mm). The average error evaluated for the data acquisition measurements is 0.017 pixels (0.23 microns). After recording the images the post processing is done using the VIC2D-2009 software. Shear strains are evaluated and the crack front evolution is obtained from the analysis of the strain field propagation along the sample (Figure 66). After finishing the test the sample was removed and the position of the crack was measured: this position was the same as the last position measured using DIC.

The calculated effective crack length using method CBTE and the delamination length measured with the DIC are compared in Figure 67 (the initial compliance calculated for this material is 0,0165mm/N, defined as Compliance1). The difference between the calculated crack length and the measured one is 4-5mm. The calculated crack length using BTBE method is also evaluated in Figure 67; the difference between the data obtained using DIC and BTBE method is below 2 mm. The BTBE method describes the crack evolution along the delaminated surface better than the CBTE method.

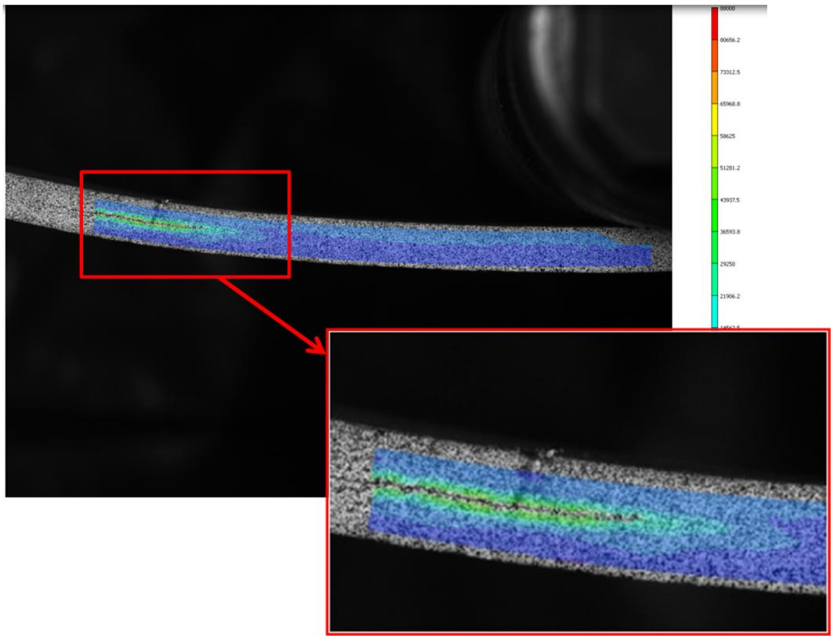

Figure 66: Crack front position for an ENF test using DIC

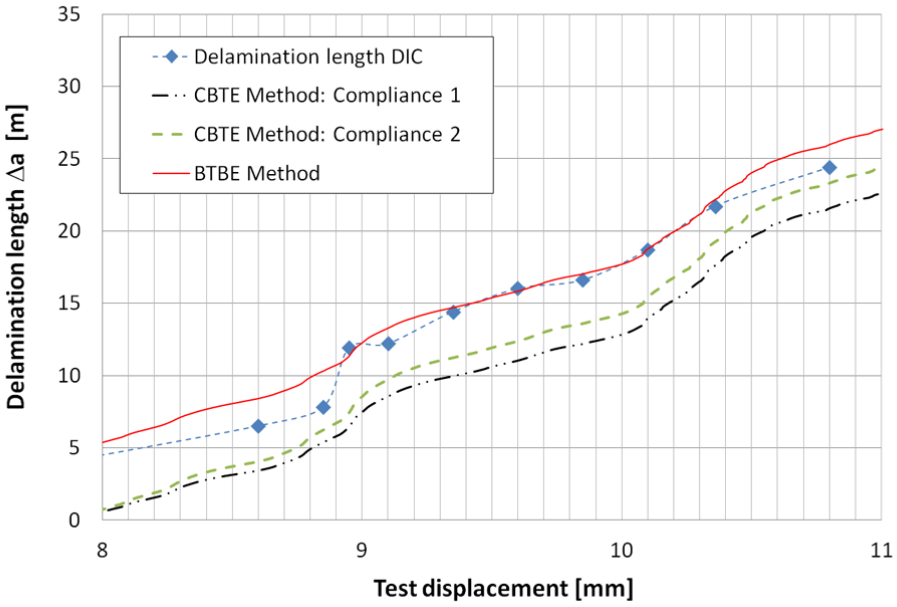

Figure 67: Comparison of delamination length evolution between DIC results and analytical methods

6.3.3 Discussion

The reasons for the differences in the delamination length evolution between CBTE and BTBE methods are discussed in this section.

Compliance: The assumption in method CBTE that the compliance is constant before crack propagation is not fulfilled by our samples: the compliance of the cracked beam decreases when the displacement is applied (Figure 68). This effect is observed for all sample types. The reason why the compliance value is changing can be the effect of large displacement on the test set-up [105]. As the load is applied on the sample the distances between support contact points decrease (the contact position is different) and consequently the compliance also decreases. This effect is more pronounced due to the large diameter dimension of the loading and supports (20 mm).

The sample tested for DIC correlation is used for the evaluation of the sensitivity of the initial compliance (C_0) in the CBTE method. Two initial compliances are defined for calculating the delamination length value; the compliance1 (minimum compliance value from the Figure 68) and the compliance2 (a 6% higher compliance than the minimum, arbitrary chosen). Figure 67 shows the results for crack evolution: the crack front position varied 1-2mm using one or the other compliance value. The obtained fracture toughness is 3,5% higher using the initial compliance1 instead of the compliance2

(Table 13). It is demonstrated that the sensitivity of the initial compliance for calculating the fracture toughness by CBTE method is high.

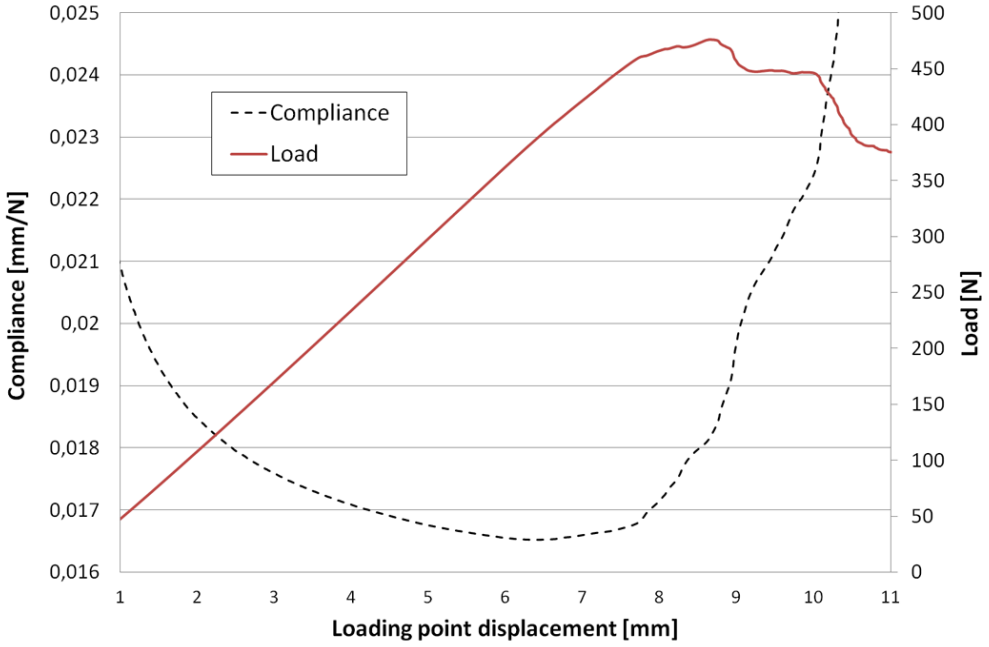

Figure 68: Compliance evolution during ENF test

Table 13: Initial compliances used and obtained fracture toughness values applying CBTE method

Initial Compliance1	Initial Compliance2	Difference
0,0165 mm/N	0,0175 mm/N	6%
G_{IIc}= 2322 N/m2	G_{IIc} =2244 N/m^2	3.5%

Table 14: Flexural modulus for 3K and 12K (five samples tested per material type)

	E_f average [MPa]	Standard deviation [MPa]	Deviation %	E_f supplier [MPa]	Shear modulus [MPa]
3K	50425	1769	3,5%	59000	1609
12K	48444	1393	2,9%	57000	1718

Flexural modulus: The CBTE method uses the initial compliance and the initial crack length as the input data value for calculating E_f and a_e. In addition to the fact that the initial compliance C_0 is difficult to determine, the a_0 value is also difficult to control; errors can be introduced during the positioning of the sample. The dispersion on the flexural modulus obtained using the analytical equation (6) can be significant: a range of values from 40 to 60 GPa are calculated. In order to evaluate the real scatter on the flexural modulus three point bending tests are carried out. The tests are performed in samples without crack or delamination and the positioning of the layers is random. The

methodology described by Mujika [107] is followed for obtaining reliable flexural and shear modulus. One sample from 3K and another sample for 12K are tested using five different span values (40/50/60/80/100mm) and flexural modulus and shear modulus are obtained. Four other samples are tested per material type for obtaining the average and deviation for each material property (Table 14). The results show a scatter below 4% on the flexural modulus and lower values than the ones defined by the supplier. The dispersion introduced using the formula (6) with the initial compliance is higher (10-15%) than the dispersion measured in the samples (below 4%).

The CBTE method can be appropriate when the sample´s compliance is more constant before crack initiation than in our textile material. The test set-up that we are using can be also the reason for this non-linearity: supporting cylinders have 20mm of diameter and the effect of large displacements is high. The flexural modulus values obtained using equations (6) are not inside the range calculated using three point bending test. For these reasons the BTBE is proposed for calculating mode II fracture toughness values [105]. The proposed method takes into account the span reduction due to large displacements, creating a reduction on the compliance.

6.4 RESULTS (BTBE method)

Initiation and propagation fracture toughness are calculated from the post processing of the data using the BTBE method (five samples per material type).

$G_{II\ initiation}$ values: The initiation fracture toughness value is calculated from the R curve when G_{II} crosses zero crack advance length [105] (Figure 61). Following this criterion in the tested samples, the scatter of the initiation value is quite high, in some cases more than 50%. The position of the curve is very sensitive to the E_f introduced for the calculation. In this research the averaged flexural modulus used is calculated previously (Table 14). The scatter of 3% of the flexural modulus creates small shift in the R curve and the initiation value is sensitive to these changes. This scatter, albeit small, leads to an inaccurate calculation of the fracture initiation value. The flexural modulus should be measured for each sample in the non-cracked zone using a three point bending test for a reliable initiation value. A better way for the definition of the initiation fracture energy value is described in Figure 69, plotting the compliance with the fracture energy. The $G_{II\ initiation}$ value is defined when the linear slope changes the trend. The scatter on the results in G_{II} initiation values calculated using this method is

12-30% (Table 15). The percentage difference between G_{II} average values of A/B and C configurations is 15-17%, close to the scatter for each configuration type individually. There is no clear tendency for different configurations. The average G_{II} initiation value for 3K (≈2027 J/m^2) is 15% higher than for 12K (≈1763 J/m^2).

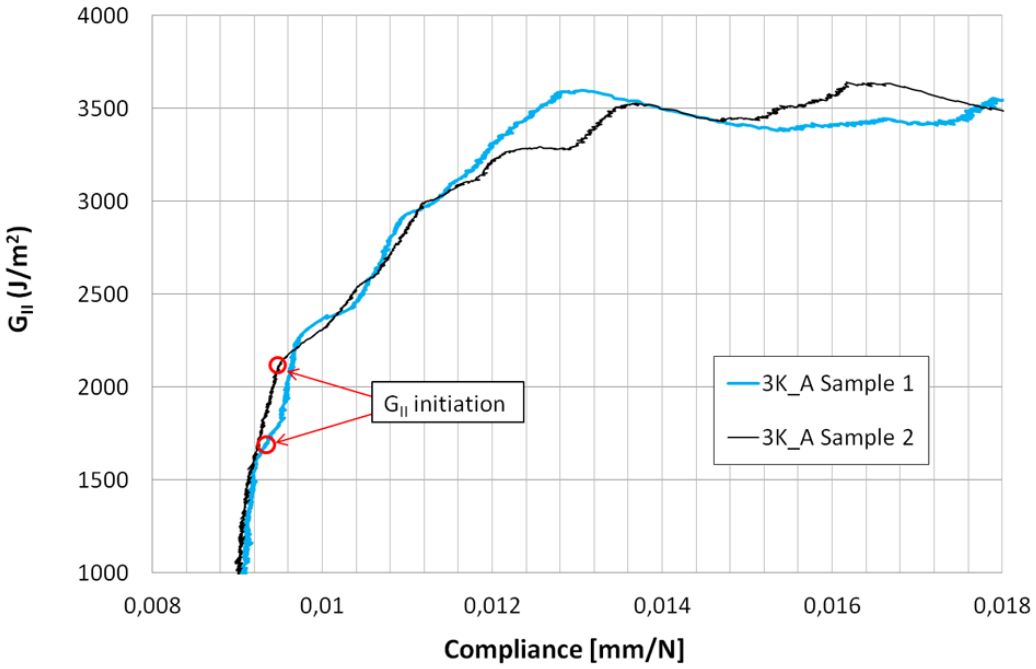

Figure 69: Two examples for fracture initiation value calculations using the compliance (BTBE method).

Table 15: G_{II} initiation and propagation (5 samples per material type) (BTBE method)

		3K			12K		
		A	**B**	**C**	**A**	**B**	**C**
INITIATION	Average (J/m^2)	2019	1869	2194	1661	2045	1583
	Standard deviation (J/m^2)	245	276	289	550	294	482
	Standard deviation [%]	12%	15%	13%	33%	14%	30%
	Median (J/m^2)	2078	1980	2179	1630	2054	1415
PROPAGATION	Average (J/m^2)	3613	3427	3537	2912	3048	3029
	Standard deviation (J/m^2)	194	206	282	214	244	469
	Standard deviation [%]	5,4%	6%	8%	7,4%	8%	15,5%
	Median (J/m^2)	3510	3493	3420	3006	3095	2990

$G_{II\ propagation}$ values: The stable propagation fracture energy value is obtained from the R curves. For 3K material, the stable zone is situated 15-25mm away from the initial crack position. The stable zone is easy to define for 3K material, but for 12K the jumps complicate the definition of the stable value (Figure 70). When sudden jumps appear during the tests, the same procedure described in a previous work for mode I is defined

here [journal paper send to Comp-Par A: under review]. Three stages may be observed: INST where the sudden crack growth starts, ARREST where the crack propagation is stopped and STABLE where a stable crack growth is observed. As 12K material does not have a STABLE crack propagation zone, the G_{II} value is calculated at INST positions. Otherwise, it is possible to underestimate the G_{II} value if ARREST positions are also evaluated. The propagation fracture toughness value for 12K is obtained averaging fracture energy values before unstable crack propagation (Eq. 30) (Figure 71). The scatter on the results in G_{II} propagation values (5-8%) are for almost all material types below the scatter obtained for mode I (above 10%). The percentage difference between G_{II} average values of A/B and C configurations is 5%, below the scatter for each configuration type. For mode II fracture toughness, the configuration type does not affect the result. Average G_{II} propagation value for 3K (≈3500 J/m^2) is 17% higher than for 12K (≈3000 J/m^2) (Table 15).

$$G_{IIpropagation} = \frac{\sum_{i=1}^{n} G_i}{n} \qquad n\text{= number of unstable crack propagations} \qquad \text{(Eq. 30)}$$

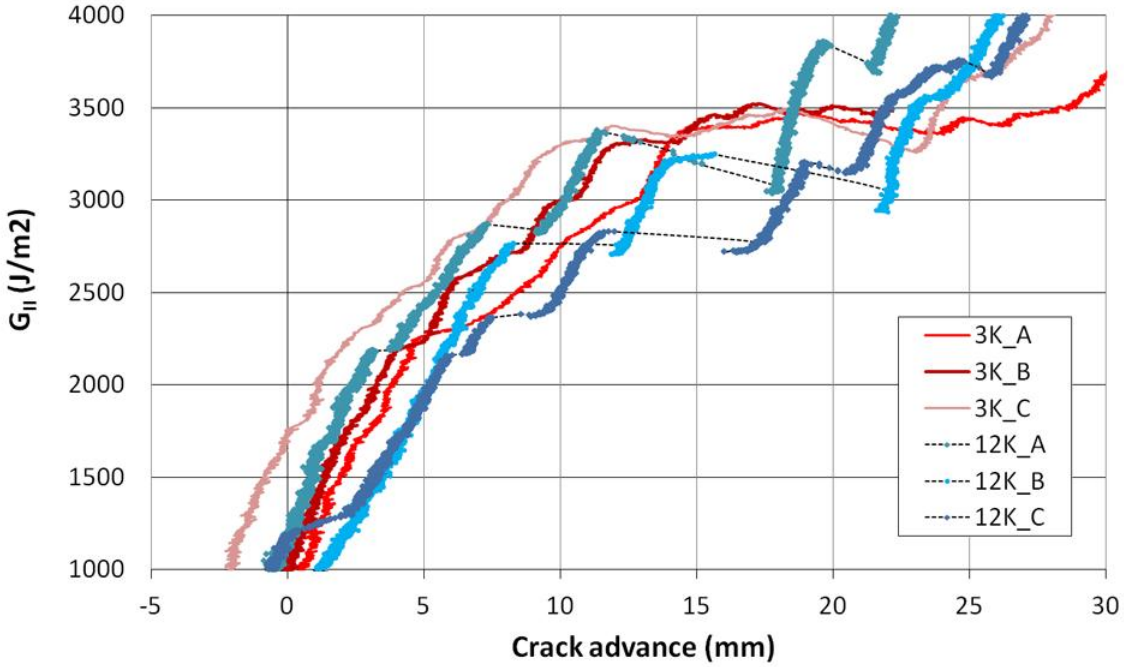

Figure 70: R curve for all material types (BTBE method).

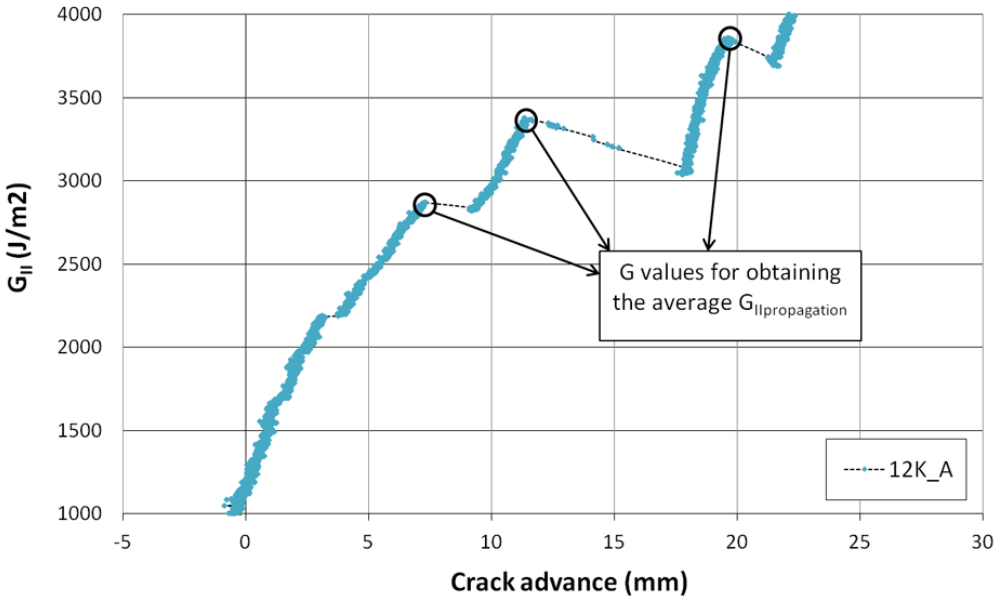

Figure 71: Fracture energy values before unstable crack propagation (BTBE method)

6.5 DISCUSSION

The CBTE method does not work properly with the material and test set-up defined in this research. It is verified that this method creates a delay on the crack front of 4-5 mm in the R curve. The compliance is not stable before crack propagation due to the large displacements and span reduction effects. The diameter of 20 mm of the supports contributes to reduce the span (by almost 10%) during the test. The BTBE method that takes into account bending effects seems to be more suitable when non-linearities appear during ENF tests.

The matrix distribution on the delaminated surface may be the reason why 3K materials show more stable crack propagation and higher fracture toughness under mode II than 12K. On the 3K material matrix pockets are located at almost every yarn crossing (yarn dimension is 2 mm) and the matrix is evenly distributed on the surface. On the 12K also material matrix pockets are located almost every yarn crossing, but as the yarn dimension is larger (5,5mm), the distribution of the matrix is not sufficiently spread. Visually analyzing the matrix amount and position on the delaminated surfaces it is not possible to distinguish the nesting type applied to each sample from images of the delaminated surface. Matrix pockets for A/B and C configurations are located in a very similar way and the matrix amount is also similar.

Optical images from one side reveal crack propagation length and the matrix pockets on the delaminated surface (Figure 72). Matrix pockets length percentage value can be measured in the warp direction:

- 3K: Matrix pockets on the 38% of the delaminated length.
- 12K: Matrix pockets on the 24% of the delaminated length.

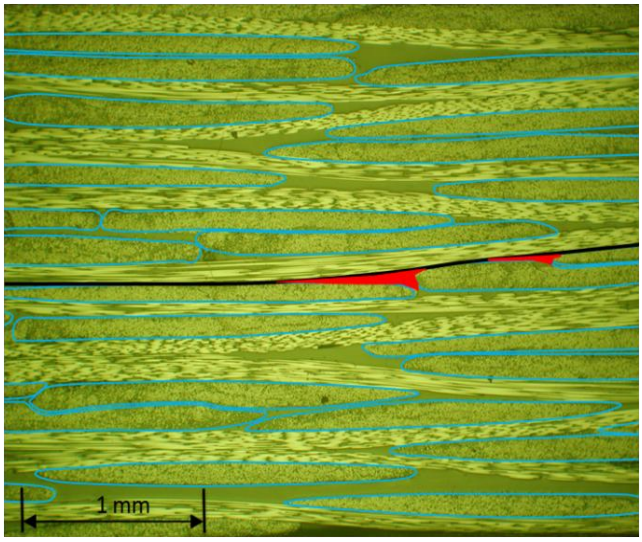

Figure 72: Matrix pockets (red areas) on the delaminated front (black line) from one side (3K material)

In previous measurements carried out by the author [92] it is determined that the delaminated surface in warp and weft direction is very similar in this material. For this reason it is possible to assume that 38% for 3K and 24% for 12K of the surface is covered by matrix material. The value of fracture toughness under mode II is higher when the matrix amount is higher on the surface. An increase on the matrix presence from 24 to 38% creates a 17% higher mode II fracture toughness. The results do not show differences for different nesting values.

6.6 CONCLUSIONS

The nesting does not significantly affect mode II fracture toughness values; the differences in waviness due to the nesting and differences between contact types (0/0, 0/90, 90/90) in the woven material do not affect the results. The higher variability value for initiation than for propagation value can be explained by the position of the crack front at the beginning of the test. Crack front may have higher or lower amount of matrix percentage depending the initial position.

Crack propagation under mode II is more stable if the matrix is evenly distributed on the surface. The distribution of the matrix can be linked with the unit cell size; smaller unit cell size show better matrix distribution than larger unit cell size. As the matrix pockets are located every crossing yarn, the even distribution of the matrix is inversely related to the yarn dimension. The value of fracture toughness under mode II is higher when the matrix amount is higher on the surface having the same fibre volume fraction.

The CBTE method can be appropriate when the compliance of the ENF test is stable before crack initiation. The set-up and specimen geometry affects highly the compliance; when large displacements and high contact angles appear on the supports the BTBE method is more suitable. It is advisable to measure the flexural modulus, shear modulus and the system stiffness previously by three point bending test; the effective flexural modulus obtained from compliance values may have higher deviation values.

7. CHAPTER 7: MODE I FATIGUE FRACTURE TOUGHNESS OF WOVEN LAMINATES: NESTING EFFECT

7.1 INTRODUCTION

This chapter evaluates the mode I fatigue delamination onset and growth for two carbon fibre T700-epoxy reinforced woven laminates with a different tow size (3K/12K). Three different nesting/shifting configurations are applied to the plies at the fracture surface. The nesting differences show little effect on the delamination onset fracture energy threshold limits, but normalised results show higher values for the smaller unit cell size. Analyzing the normalised Paris diagrams it is concluded that the unit cell size and the nesting configuration does not affect the slopes for the Paris plot. However a smaller unit cell size shifts the normalised Paris diagram to the right. The non-homogeneity of the delaminated surfaces of textile materials leads to irregular slopes.

7.2 TEST SET-UP AND DATA POST-PROCESSING

7.2.1 Material

The material is the carbon fibre (T700)-epoxy reinforced woven laminate made of 2/2 twill woven layers and manufactured from prepreg sheets in an autoclave (described in chapter 4.2). In a previous work, the author obtained the elastic, geometrical properties and mode I fracture toughness values [92] (Figure 37,Table 1, Table 11). By controlling the nesting/shifting of the delaminated surface as a design parameter, three different configurations are manufactured: A, B and C (Figure 51).

7.2.2 Test set-up and methodology

Fatigue delamination onset

For fatigue delamination onset of UD fibre reinforced polymer matrix composites the standard D6115 is defined [108], but there is no standard for textiles or other kind of laminates. In this work this standard is used for obtaining the fatigue delamination onset and consequently the G/N curve. The tests are done in a DCB test set-up where constant opening amplitude is applied to the samples at different G levels. The R ratio between the minimum and maximum peak displacement is 0,1 (3 – 0.3 mm). The tests are carried out at 5 Hz frequency value. This value is a compromise between avoiding temperature increases on the samples and a reduction of the tests time. An initial pre-crack is needed to avoid any previously created surface condition that may distort the fatigue delamination onset result. Load and displacement of the opening device is recorded during the test. The D6115 standard defines three methods for defining the cycle number when the delamination starts: number of cycles at visual detection of crack opening, when the compliance increases by 1% with respect to initial conditions and when the compliance increases by 5%. The crack opening is not easy to determine, visual definition of crack front is difficult to define in the woven material selected for this research. This visual method may overestimate the number of cycles needed for crack initiation, because the crack is probably propagated before the crack front is visually observed. The increase of 1% in the compliance is also a small change to be measured accurately, as the noise in the data can lead to a non real value. In consequence, 5% compliance increase is defined as the method used for measuring crack initiation.

The applied a_0 length is the initial parameter responsible for the maximum fracture toughness value applied on the sample (at the same maximum displacement value). Changing the initial crack length, the required maximum fracture toughness is obtained for the same opening displacement values (δ_{max} =3mm). From the required energy level (G) the initial fracture length ($a = a_0$) is calculated using the modified beam theory expression (Eq. 31) [93].

$$G_{Imax} = \frac{3P_{max}\,\delta_{max}}{2b(a+|\Delta|_{av})} \qquad \text{(Eq. 31)}$$

where b is the sample width, P_{max} is the maximun load

The averaged effective delamination extension ($|\Delta|_{av}$) defined to correct the rotation of DCB arms at delamination front are defined as the average value of the effective delamination extensions calculated from all static mode I tests carried out by the author [109]. For the calculation of the initial fracture length the average value is introduced to the formula (Table 16), although it must be pointed out that the dispersion obtained is very high for all material types.

Table 16: Length correction value obtained from static DCB tests (six samples/material type)

	Average value of $\|\Delta\|_{av}$ [mm]
3K_A	2,1 ± 1,8
3K_B	3,14 ± 1
3K_C	3,47 ± 2,1
12K_A	1,41 ± 1,6
12K_B	1,42 ± 1,9
12K_C	1,48 ± 1,3

The test is performed at different G levels in order to obtain an overall overview of the G/N curve for the delamination onset. As the number of cycles is increasing, the maximum fracture energy required for delamination initiation decreases from the static fracture toughness value to the fracture threshold value. From the maximum load (F_{max}) and maximum displacement (δ_{max}) recorded data the compliance (C) is calculated as follows:

$$C = \frac{\delta_{max}}{F_{max}} \qquad \text{(Eq. 32)}$$

and continuous compliance is afterwards plotted versus number of cycles. In order to reduce the noise appearing on the compliance chart, the moving average method is used for filtering the data. The number of cycles required for the onset of the crack propagation at the fracture energy level applied is afterwards defined when the compliance increases by 5%.

Fatigue delamination growth:

Three different stages may be identified when delamination propagation rates are obtained at different fatigue energy levels: a region where the delamination rate propagation is very low (threshold value), a stable crack propagation zone (linear zone) and the catastrophic failure (within one load cycle). The stable crack propagation zone is described using the Paris relation (Eq. 33)(Eq. 34) with the fitting parameters A and p:

$$\frac{\mathrm{d}a}{\mathrm{d}N} = A(\Delta G)^p \qquad \text{(Eq. 33)}$$

$$\Delta G = \frac{G_{\max}}{G_{\min}} \qquad \text{(Eq. 34)}$$

As for R=0,1 it is possible to define $\Delta G \approx G_{\max}$:

$$\frac{\mathrm{d}a}{\mathrm{d}N} = B(G_{\max})^m \qquad \text{(Eq. 35)}$$

The m value represents the slope in a log diagram for the stable crack propagation zone and B is a fitting parameter. The tests are carried out using the same test parameters as in the fatigue delamination onset evaluation: 5 Hz frequency and R=0,1. In order to record the complete behaviour of crack propagation of the samples in the same test, it is preferable to start applying a high percentage of the static fracture toughness value as the maximum value. The compliance along the cycles is obtained from the recorded load and displacement data. Every N number of cycles the test is stopped and the delamination length is measured. The procedure must be completed without removing the sample from the test set-up. As the DCB test is based on beam theory, a linear relationship between the crack length and the cubic root of the compliance is assumed. From this relationship and the compliance data along the number of cycles the delamination crack length is calculated (a vs. cycles). The crack growth rate ($\frac{\mathrm{d}a}{\mathrm{d}N}$) is obtained using the secant method, where the slopes of the straight line between adjacent data points are calculated as described in [110].

7.3 RESULTS

7.3.1 Fatigue delamination onset

Nine tests are carried out per material type. The tests are performed at different fracture toughness values to obtain the general tendency of the G/N chart. The points related to 12K material appear above the points related to 3K material (Figure 73). As 12K

material shows higher absolute fracture toughness values than 3K materials in mode I (**¡Error! No se encuentra el origen de la referencia.**), the results are normalised to compare the onset behaviour.

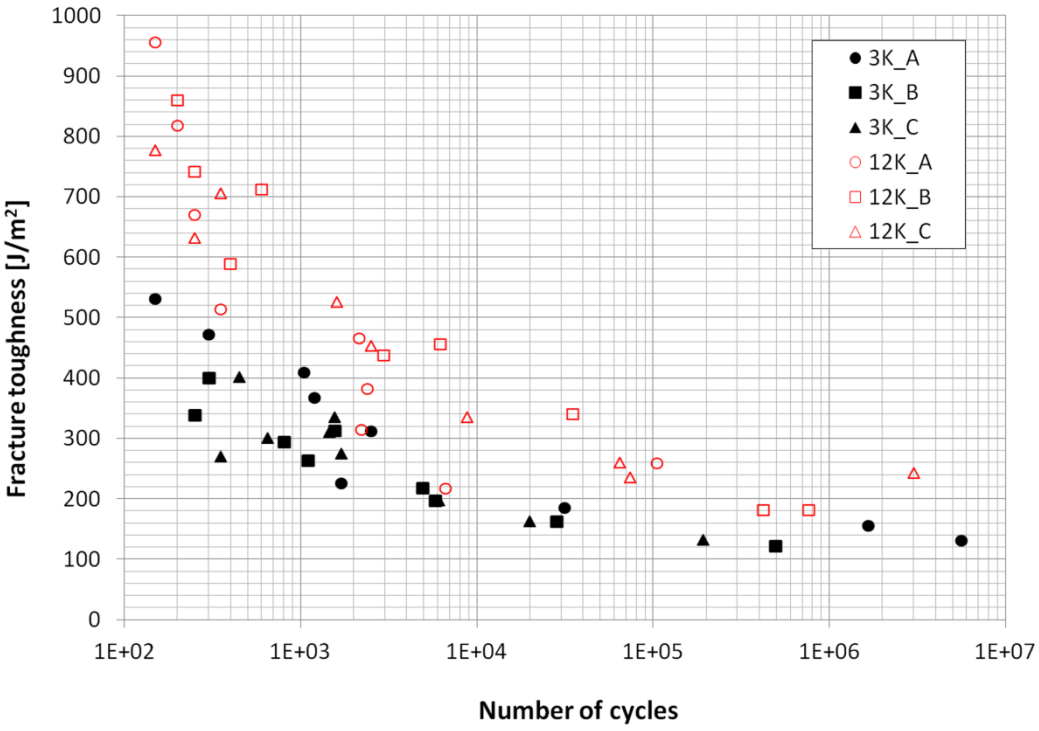

Figure 73: Non-normalised G/N curve for all samples

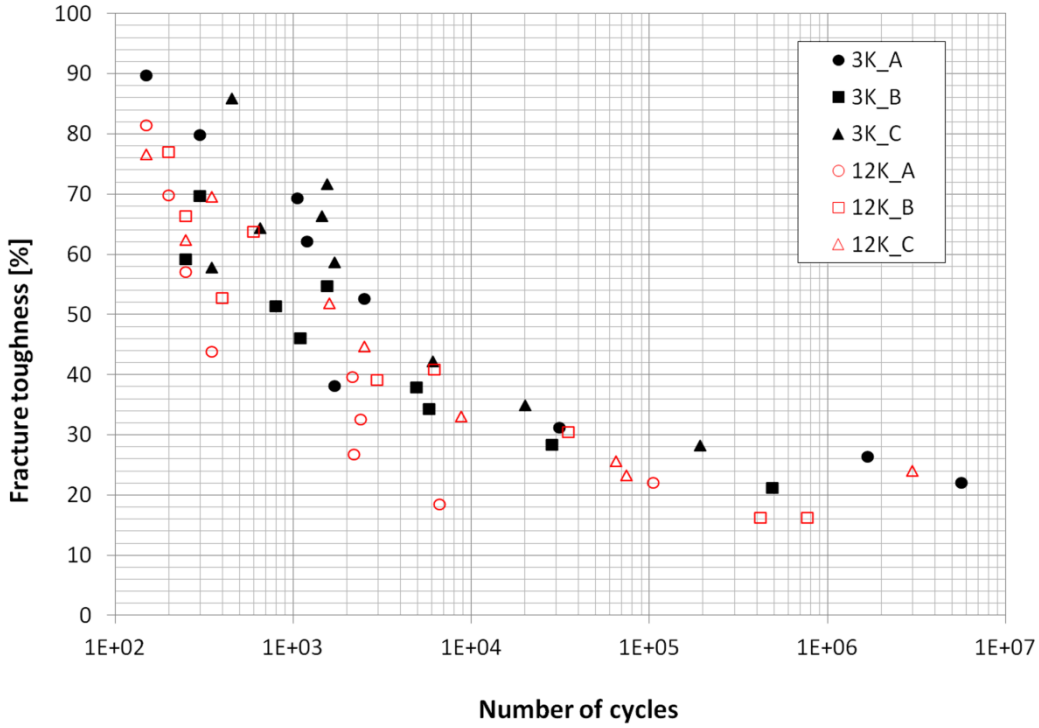

Figure 74: Normalised G/N curve for all samples

In the literature some authors, as Murri [111, 112] and Chen [113] have normalised the fatigue data using the R-curve obtained from the quasi-static delamination tests with the aim of taking into account the fibre bridging effect on the crack tip. Yao [114] put into question this normalisation and concluded that the fibre bridging created in fatigue delamination and in quasi-static delamination is different. From the results obtained by the author in [109] it was concluded that;

- For 3K material the fibre bridging effect does not appear; fracture initiation and propagation values are similar.
- For 12K material the fibre bridging effect is observed at the beginning of the static test (5mm from the crack tip). The question at this point is if the fibre bridging effect observed in a monotonous test is correct to be used also in a fatigue test. From loading-unloading static test it was verified that part of the fibre bridging was already eliminated when the sample is opening and closing repeatedly.

In order to compare the materials under fatigue delamination in this research, in the absence of a consensus, the fracture toughness values are normalised by the static propagation fracture toughness values (**¡Error! No se encuentra el origen de la referencia.**).

Figure 74 shows the normalised G/N diagrams for all material types. The decreasing tendency is similar for all configurations. The initial visual estimation shows that fracture toughness thresholds are between 15%-25% of the G_{Ic}. For a statistical analysis the following assumption is taken: the fatigue threshold for each material is obtained by assuming that crack initiation follows a Weibull distribution. Castillo [115] and Ruiz [116] developed a Weibull distribution model for predicting the probability of failure (p_{f}) at a certain stress level.

$$p_{\text{f}}(N,\Delta\sigma) = 1 - \exp\left[-\left(\frac{(\log N - B)(\log \Delta G - C) - E}{\delta}\right)^{\beta}\right] \qquad \text{(Eq. 36)}$$

For R=0,1 it is possible to define $\Delta G \approx G_{\max}$

$$p_f(N,\Delta\sigma) = 1 - \exp\left[-\left(\frac{(\log N - B)(\log G_{max} - C) - E}{\delta}\right)^{\beta}\right] \qquad \text{(Eq. 37)}$$

Where N: Number of cycles

G_{max}: Applied maximum fracture energy

B: Threshold parameter for fracture energy level

C: Threshold parameter lifetime

E: Parameter that defines the position of zero percentile (probability=0)

δ: Scale parameter for Weibull distribution

β: Shape parameter for Weibull distribution

The most suitable parameters for Weibull distribution are obtained using a free programme [117-119] developed by Castillo [115] for statistical analysis. The input data are the results from the fatigue tests carried out experimentally; the stress level and the lifetime (number of cycles of each test). If any sample is run-out without crack propagation it must be specified during data introduction. After calculation the programme predicts the best threshold lifetime (for an infinite life), the endurance limit and the median curve associated with all data points.

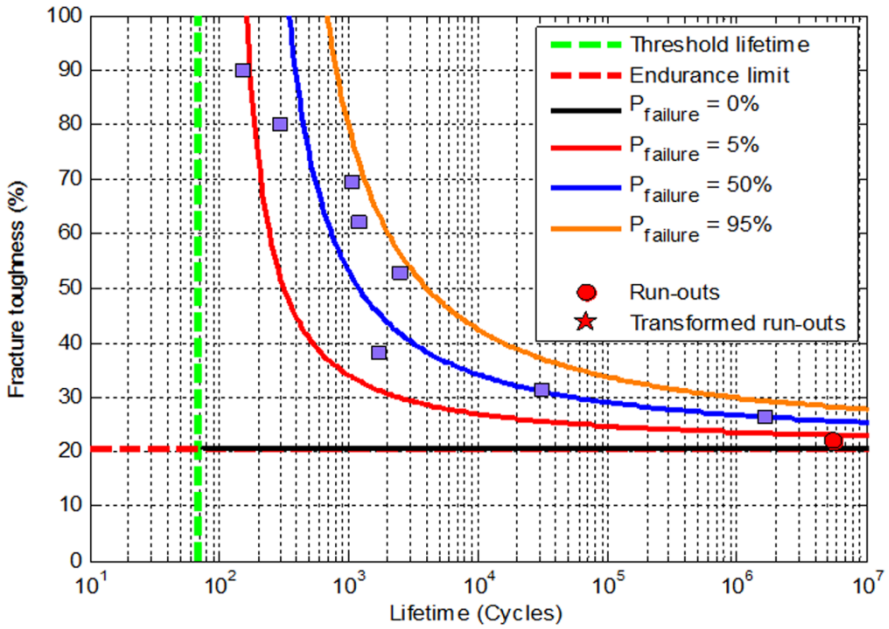

Figure 75: Estimated Weibull distributions using ProFatigue for different failure probabilities (3K-A material/nine data points)

The data points defined in Figure 75 are introduces to the programme and the obtained results are described in Table 17. Fatigue delamination threshold values calculated are higher for 3K material than for 12K material. The threshold value is calculated for an infinite life, but this assumption can underestimate the properties of the material. In a real application a fatigue limit at 10^7 cycles can be enough for a reliable behaviour during service life. In Table 17 the fatigue thresholds for 10^7 cycles with a 50% of failure probability are also included for each material and configuration type.

Table 17: Fatigue delamination thresholds from ProFatigue software

	3K			12K		
	3K_A	**3K_B**	**3K_C**	**12K_A**	**12K_B**	**12K_C**
Fatigue delamination threshold for an infinite life (% of G_{ic})	20,4	8,3	16,1	4	4,7	10,3
Fatigue delamination threshold for 50% of failure probability at 10^7 cycles (% of G_{ic})	20,4	15,5	16,1	9,2	11,5	18

7.3.2 Fatigue delamination growth

Five samples per material type are tested under mode I fatigue loading for obtaining the Paris plots following the specifications defined in a previous section. In Figure 76 the fatigue delamination behaviour for one sample per material type is plotted without normalisation of the fracture toughness. The curves for 12K materials are shifted to the right because the absolute static fracture toughness values are higher than for 3K material. When only the linear zone needs to be characterised, in the literature [120] the end of the test is defined when the crack growth rate of 10^{-6} mm/cycle is reached. In this research the tested final growth rates are lower (10^{-7} to 10^{-8} mm/cycle) because threshold values from fatigue life charts will later be compared to the ones obtained using G/N curves. The aim is to evaluate the effect of the crack tip status (fatigued or pre-cracked) on the threshold value.

For a better comparison of the results, the curves are normalised by the static fracture propagation average values obtained previously by the authors (G_{IC}) (Table 11). Figure 77 shows the results for one sample per material type after data normalization. The 12K materials are shifted to the left, showing lower threshold percentage values than 3K material. Under the same G_{IC} percentage, the 12K material shows higher delamination rate values than 3K material. For 12K material the delamination rate is not decreasing

linearly and wavy lines appear on the charts. Although slope changes are also appearing for 3K, the lines are smoother.

From each fatigue test the delamination rate slope is obtained applying the method of least squares for the linear regression approach. In order to avoid the values close to the threshold limit, data points above 25-30%G_{IC} are used for obtaining the linear slope. The results are summarised in Table 18.

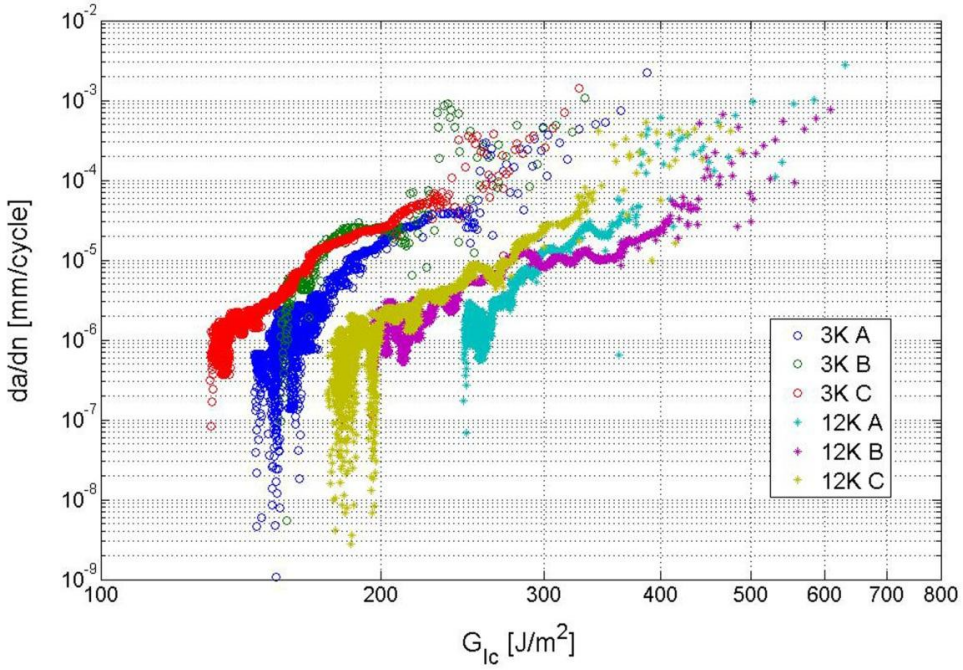

Figure 76: Fatigue delamination plot for 3K and 12K (one sample per material configuration type)

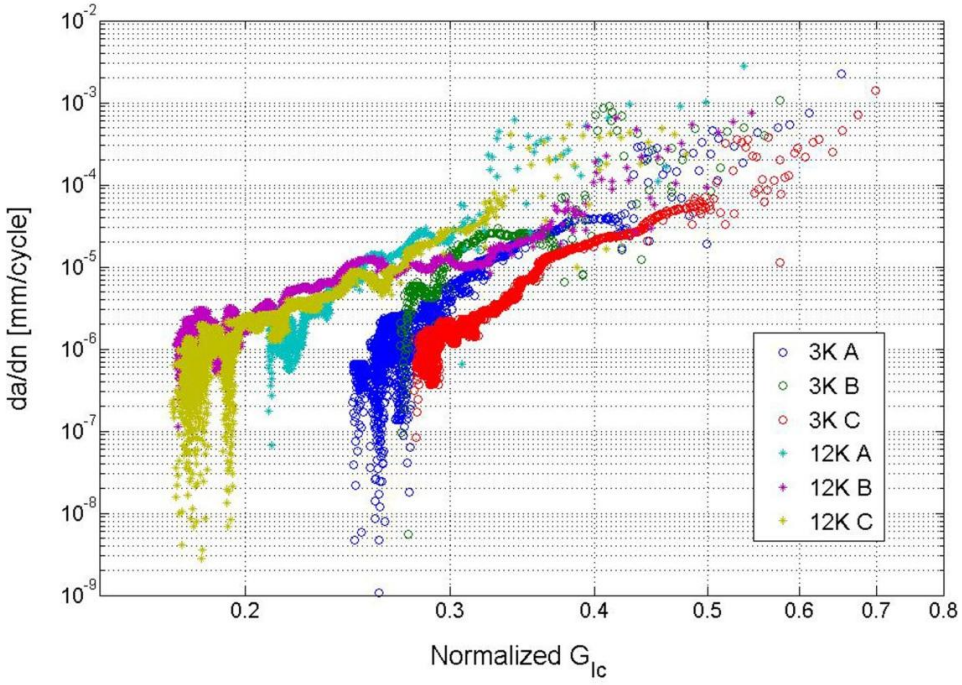

Figure 77: Normalised fatigue delamination plot for 3K and 12K (one sample per material configuration type)

Table 18: Slope values (m) for configuration type and unit cell size.

		3K			12K		
		A	**B**	**C**	**A**	**B**	**C**
5 samples/configuration	m [-]	6,5	7,1	7,9	6,9	7,6	6,7
	Standard dev. [-]	0,6	1,9	2,1	1,3	1,4	1,1
	Standard dev. [%]	11%	27%	27%	20%	20%	17%
	Median [-]	6,4	5,8	7,7	6,9	7,1	6,4
15 samples/unit cell size	m [-]	7			7,1		
	Standard dev. [-]	1,4			1,3		
	Standard dev. [%]	21			19		
	Median [-]	6,4			6,9		

The slopes for each material type are presented also in Figure 78. The median and the 25th and 75th percentiles (the median value is the line inside the box and the edges of the box are the 25th and 75th percentiles). The cross represents the outliers. From the data it is not possible to observe a tendency for different nesting/configurations. The lower limit for the slope value is similar for all material types; close to 5,7. The median

values seem to be similar for 12K samples regardless of the configuration type, but as the deviation is high (17-20%) it is not possible to establish any conclusion. The deviation of the tests is similar for 3K-B, 3K-C, 12K-A and 12K-B, and lower for 3K-A and 12K-C. In order to analyze the results from other point of view, the samples are going to be classified by the size of the unit cell; all 3K samples from one side and all 12K samples from the other side (Figure 79). The results are very similar for 3K and 12K, average slope values of 7 and 7,1 and a deviation of 19-21%.

The threshold values obtained from the fatigue life diagram are higher for 3K (22-28%) than for 12K (28-20%) (Table 19). The same tendency was observed previously from the data calculated using ProFatigue software (Table 17), the. The variability obtained in the results is close to the variability obtained for the static fracture toughness propagation value used for data normalization.

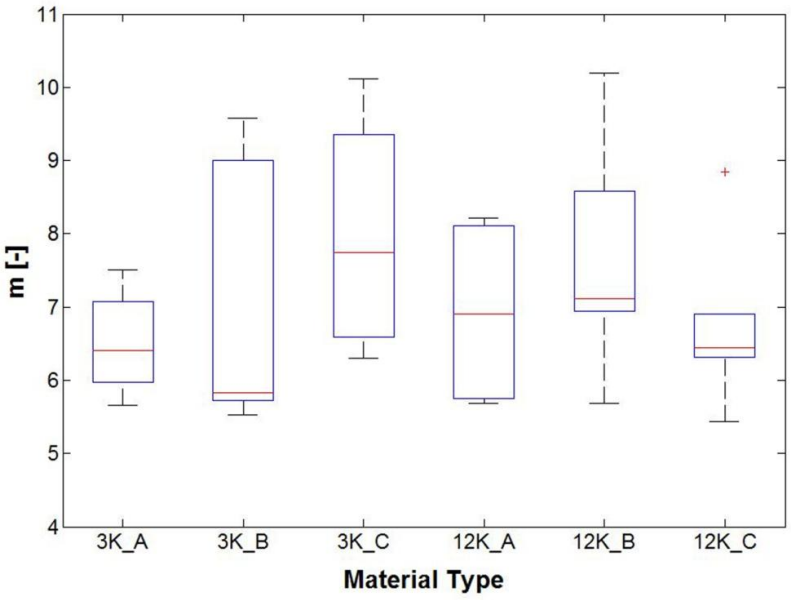

Figure 78: m slope results for each configuration type (5 samples/ material)

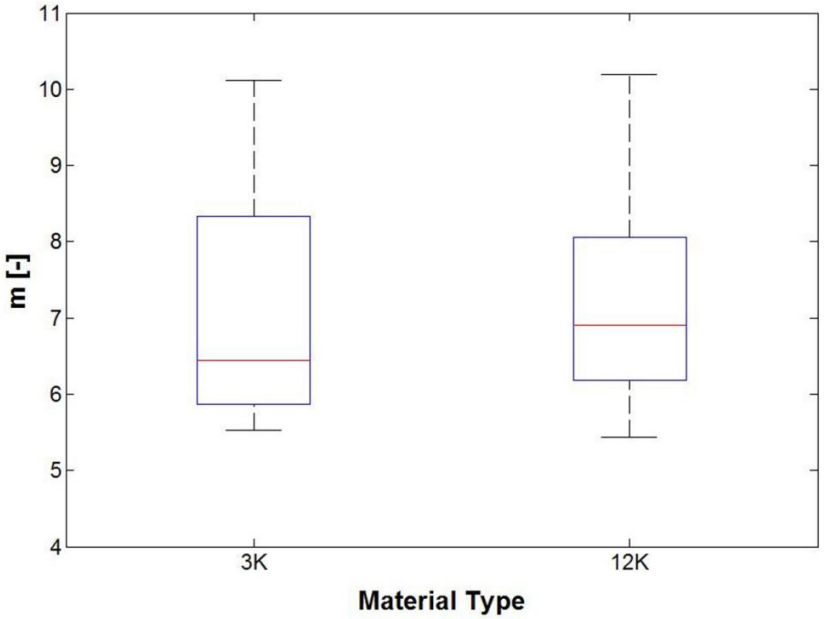

Figure 79: m slope results for each unit cellsize (15 samples/ material)

Table 19: Threshold values from fatigue life diagrams (5 samples per material)

	3K			12K		
	A	**B**	**C**	**A**	**B**	**C**
Normalised threshold [%]	24	22,5	27,5	19	20	18
Standard dev. [%]	2	4	1	2	4	3
Standard dev. [%]	8%	16%	5%	11%	18%	18%
Median [%]	25	23	28	20	18	18

7.4 DISCUSSION

From the normalised G/N curves it is observed that 3K material presents a higher fatigue delamination threshold value than 12K material. In the literature it is explained that the fibre bridging effect may delay the delamination onset in fibre reinforced composite materials. From our results this effect is not observed; although 12K material shows a higher fibre bridging effect than 3K material, the threshold value is lower. Another possible reason for these differences may be the matrix percentage on the delaminated surface. In a previous work [121] it was verified that for the 3K material the matrix pockets are spread evenly on the delaminated surface every 2 mm, covering the 38% of the delaminated surface. For 12K the matrix is not so well distributed every 5,5 mm on the 24% of the surface. The probability of having more matrix percentage at

the crack front is higher for 3K material, which may be the reason for the delay of the fatigue onset.

Analysing the nesting effect on the threshold values it is not possible to observe a repetitive tendency for different configurations types. Table 17 shows a higher threshold value for A configuration than B and C for 3K material. For 12K the higher threshold value is for C configuration. From the threshold values obtained using fatigue life diagrams in Table 19 also no conclusive results have been reached.

The effect of the crack tip status is evaluated: a fatigued crack tip increases the threshold value with respect to a pre-cracked one. The fatigue threshold values obtained from the fatigue life diagram are higher than the values obtained from the normalised G/N curves. Yao [114] linked this difference to the fibre bridging effect. The values obtained using the G/N curves are pre-cracked and there is no fibre bridging effect. On the other hand the values obtained from fatigue life diagrams are delaminated under fatigue and the delamination front may have fibre bridging. In this research this conclusion may work with 12K material because fibre bridging was observed from quasi static mode I tests. However, as in 3K material no fibre bridging was observed, another phenomenon, as matrix presence, must also be taking part.

In this work fatigue delamination rate plots are normalised by the static fracture propagation toughness values. 3K material shows higher fracture percentages than 12K for the same delamination rate. From another point of view, it means that under the same fatigue loading fracture toughness percentage, the delamination rate is lower for 3K than for 12K. The obtained Paris values are very similar for all material types; the delamination rate slope is close to seven. The slope for the stable crack propagation zone is not affected by the unit cell size nor by the nesting effect.

The slope of the fatigue delamination rate is not straight for the textile materials analysed and fluctuations appear on the charts. The non-homogeneous delaminated surface may be the reason for these slope changes. The properties of the delaminated crack front are different depending on the position; matrix pockets, fibrous contacts, nesting differences, etc. During fatigue tests the delaminated length is close to one unit cell for 3K and a third of the unit cell size for 12K ($\Delta a \approx$8-10 mm). In order to verify if these wavy Paris plots are related to the unit cell or tow size, the delamination rate values versus the delaminated length are plotted for each unit cell size (Figure 80). The

wavelengths are in both unit cell materials smaller than the yarn thickness values and not constant. In consequence these wavelengths cannot be linked to the unit cell dimensions. However, it can be assumed that the materials non-homogeneity at the delaminated front may be primarily responsible for these fluctuations.

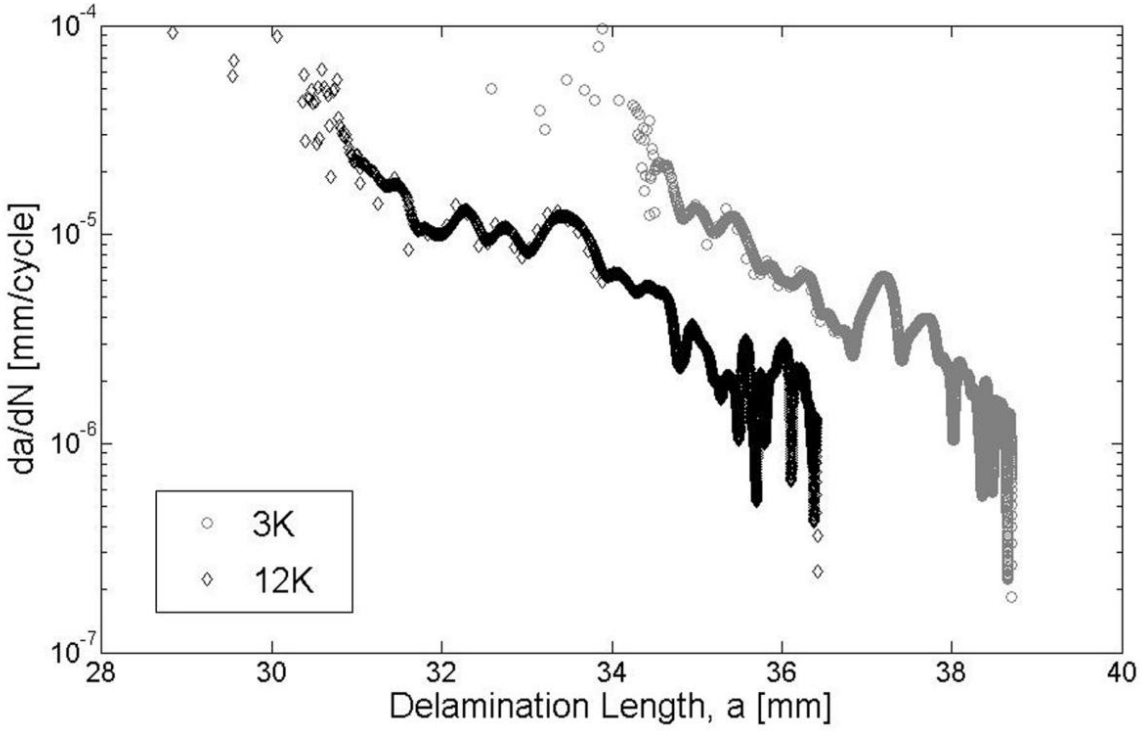

Figure 80: Delamination rate versus the delaminated length

7.5 CONCLUSIONS

In this work fatigue delamination threshold and growth in mode I are tested for two woven materials with different nesting values. The methodology proposed for the data acquisition and post processing are appropriate for carrying out fatigue tests in textile materials. From G/N charts fatigue delamination onset values are obtained under different fracture energy levels. Statistical analysis is crucial while few specimens are tested per material type. When normalised values are compared and the Weibull distribution is assumed the following conclusions are obtained:

- The higher matrix percentage at the crack front may delay the fatigue onset. 3K material presents a higher fatigue delamination threshold value than 12K material.

- The nesting differences do not show noticeable changes in the G/N curves.
- From a practical point of view the threshold for an infinite life is too restrictive and values at 10^7 cycles may be enough for a reliable design.

From fatigue life diagrams the following conclusions are obtained:

- For woven materials the unit cell size and configuration type do not affect the delamination rate slope. All material types present very similar Paris values.
- A smaller unit cell size shifts the normalised Paris diagram to the right. Comparing normalised charts, the 3K materials are shifted to the right respect to 12K materials. It means that at the same fracture toughness percentage under fatigue loading, 3K delaminates more slowly than 12K material.
- The non-homogeneity of the delaminated surfaces of textile materials can lead to wavy slopes. For the textile materials analysed the stable crack propagation zone is not quite linear and fluctuations appear. The wavelength in this material cannot be linked directly to the textile geometry dimensions.
- From G/N curves lower threshold values are obtained than for fatigue life diagrams. In addition to the effect of fibre bridging, another factor as matrix presence must be responsible for the differences.

8. MAIN CONCLUSIONS

This part of the manuscript summarises the main conclusions and achievents of the dissertation. The milestones defined in section 1.3 are divided into the ***three main objectives*** at the beginning of the research: experimental analysis of the internal structure, static and dynamic fracture toughness measurements of textile materials.

a) Experimental analysis of the internal structure of textile materials.

- The internal geometry variability is higher as the unit cell size increases due to the scale effect. The influence of this variability in the statistical numerical model was investigated and it was revealed that compared to the measured experimental variability, the influence is low.
- Sensitivity analysis shows that the laminate thickness and orientation are the largest contributors to the stiffness dispersion. These parameters should be defined as the most important to be controlled during the manufacturing process in order to reduce the scatter on the mechanical properties.
- The damage evolution inside the material is different during tensile tests depending on the unit cell size. Larger unit cell size showed higher density of intra-yarn cracks at similar loading tensile conditions. These cracks, if they developed up to the interlaminar surface, can accelerate the delamination failure.

b) Static facture toughness measurements of textile materials and the effect of the internal geometry

Fracture toughness in MODE I:

- After comparing different methodologies, the proposed method for post-processing the fracture toughness results for textile composite materials under mode I (DCB test) is the ASTM standard method. Only critical points (just before sudden crack propagation) on the force-displacement curve must be taken into consideration to calculate fracture toughness average values.
- From the experimental test performed using DCB test set up it was concluded that the delamination length of the samples must be defined depending on the unit cell size: at least more than 2 unit cell size dimension must be defined. When the unit cell size is large, the minimum delamination length should be longer than the dimensions proposed in the standards for UD material.
- The scale factor changes the fracture behaviour of the woven material: abrupt crack advancement and the fibre bridging effect at the crack front are linked to bigger unit cell sizes and higher fracture toughness values. Smoother crack advancement and almost no fibre bridging effect are observed for smaller unit cell sizes and lower fracture toughness values in mode I.
- The fracture toughness value differences in mode I between different configurations can be linked with nesting values for large unit cell sizes: a higher nesting effect leads to a higher fracture toughness value. The nesting parameter can be used as a design parameter for improving the fracture toughness values for the components.
- This cause-effect relationship between nesting and fracture toughness in mode I was not clear for smaller unit cell sizes.
- If static mode I fracture toughness needs to be improved for components made of woven composite material, a larger unit cell size and the A configuration should be defined at the delaminated surfaces (0/90 yarns in contact between layers).

Fracture toughness in MODE II:

- The ENF test set-up defined during this research leads to large displacements and large contact angles on the supports, which affects highly the compliance during the tests. In order to take into consideration these effects the proposed method for post-processing the results is the BTBE method.
- Smaller support diameters should be considered for the test set-up. After carrying out all the measurements for this research a new standard was released [52], where the diameter of the supports is recommended to be smaller to the ones used here.
- The stable or non-stable crack propagation behaviour is affected by the matrix distribution on the delaminated surface: crack propagation under mode II is more stable if the matrix is evenly distributed on the surface. As a smaller unit cell size shows better matrix distribution than larger unit cell size, the propagation is smoother for smaller unit cell sizes.
- The results showed a correlation between the amount of matrix material on the delaminated surface and the fracture toughness value in mode II: a higher amount of matrix material on the surface leads to higher fracture toughness.
- The fracture toughness values in mode II is not affected by the nesting parameter.
- If static mode II fracture toughness needs to be improved for components made of woven composite material, special attention must be paid for increasing the matrix percentage at the delaminated surface.

c) Dynamic fracture toughness measurements and the effect of the internal geometry.

- The selected methodology and data post-processing are suitable for measuring fatigue fracture toughness onset and growth in mode I for textile materials. As fatigue tests are highly time consuming, few specimens are tested, and statistical analysis is required for data evaluation.
- When normalized fatigue onset values are compared, the main conclusion is that a higher matrix percentage at the crack front delays the delamination initiation.
- The fatigue fracture toughness onset values in mode I is not affected by the nesting

parameter.

- The unit cell size and nesting parameter do not affect the delamination rate slope, but a smaller unit cell size shifts to the right the Paris diagram. The main effect of the textile on the fatigue behaviour is the delamination rate changes during the delamination evolution. These rate fluctuations are linked with the non-homogeneous surfaces of the material.

Journal papers published during this thesis

In the Figure 81 the topics covered in this research are described and the relationships between different concepts are described graphically. The journal papers published in this research are summarized here:

I. Olave, M., Vanaerschot, A., Lomov, S. V. and Vandepitte, D., Internal geometry variability of two woven composites and related variability of the stiffness. ***Polym Compos***. Volume 33, Issue 8, Pages: 1335-1350, 2012

II. Olave M., Vara I., Usabiaga H., Aretxabaleta L., Lomov S.V. and Vandepitte D., Nesting effect on the mode I fracture toughness of woven laminates, ***Composites Part A*** (2015), 10.1016/j.compositesa.2015.03.017

III. Olave M., Vara I., Usabiaga H., Aretxabaleta L., Lomov S.V. and Vandepitte D., Nesting effect on the mode II fracture toughness of woven laminates, ***Composites Part A*** (2015), 10.1016/j.compositesa.2015.03.020

IV. Olave M., Vara I., Usabiaga H., Aretxabaleta L., Lomov S.V. and Vandepitte D., Mode I fatigue fracture toughness of woven laminates: nesting effect, ***Composite Structures*** (2015), 10.1016/j.compstruct.2015.07.073

In Figure 82, Figure 83, Figure 84 and Figure 85 the topics covered at each journal paper is described graphically.

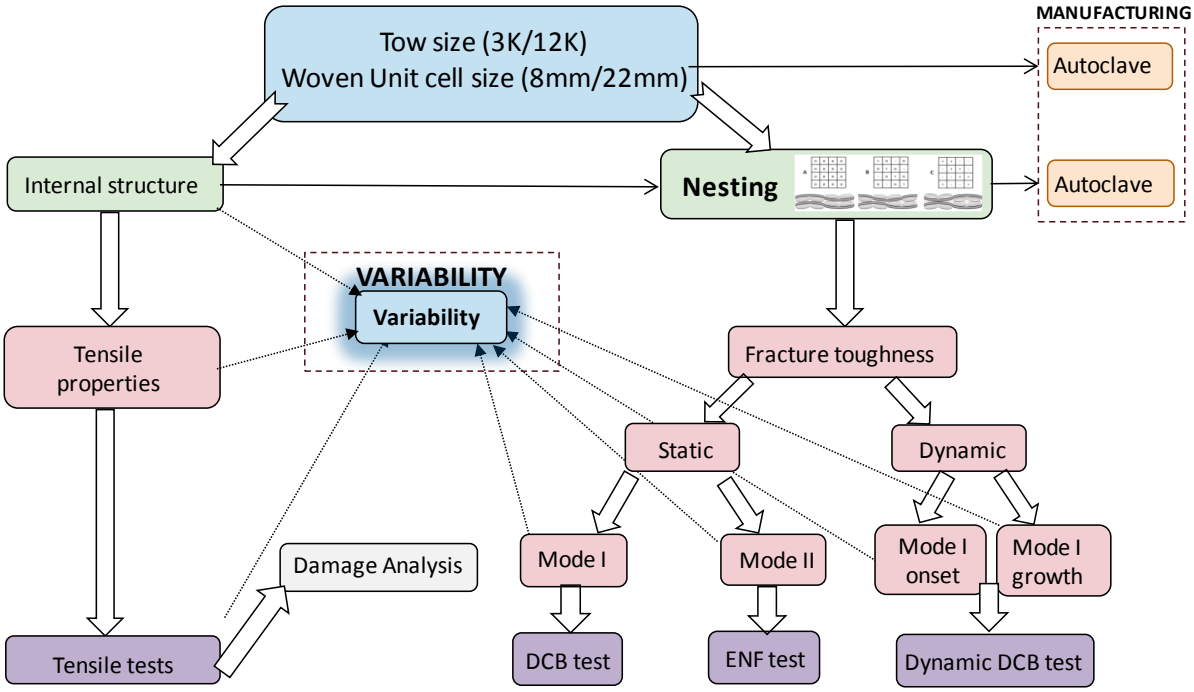

Figure 81: Topics covered during this dissertation

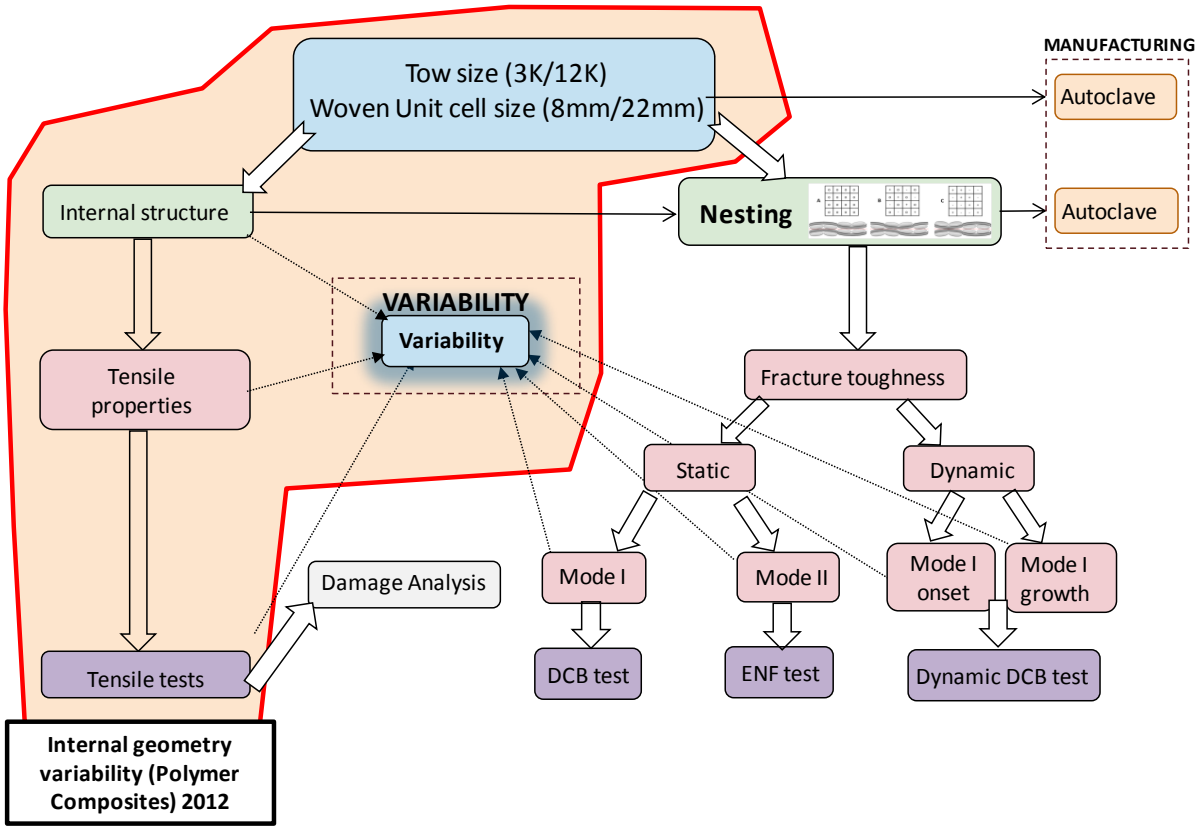

Figure 82:Topics covered in paper I

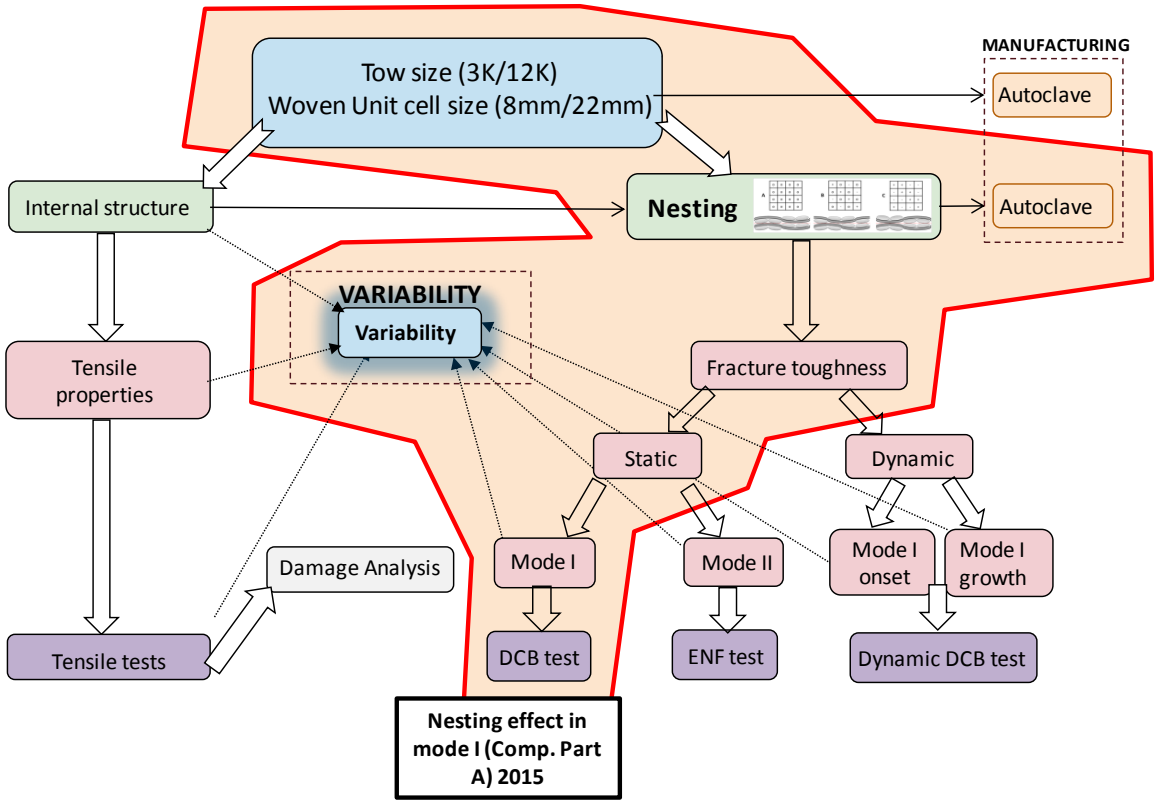

Figure 83:Topics covered in paper II

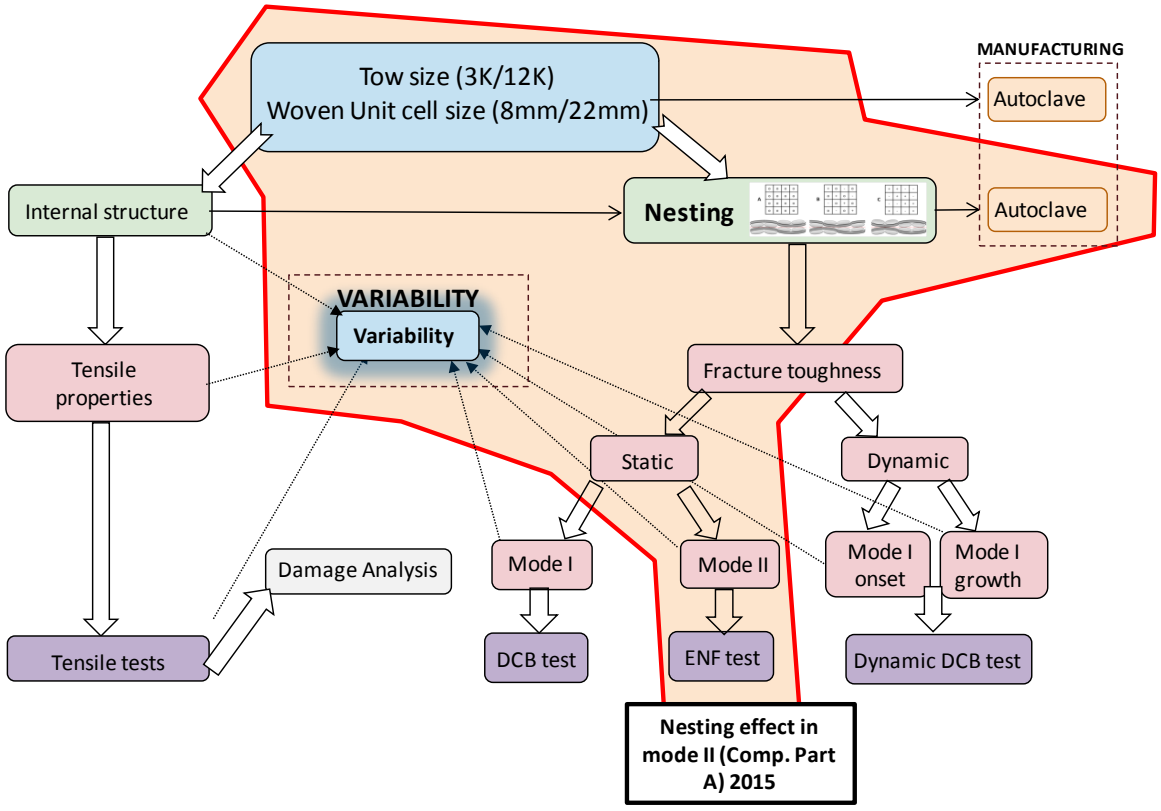

Figure 84 :Topics covered in paper III

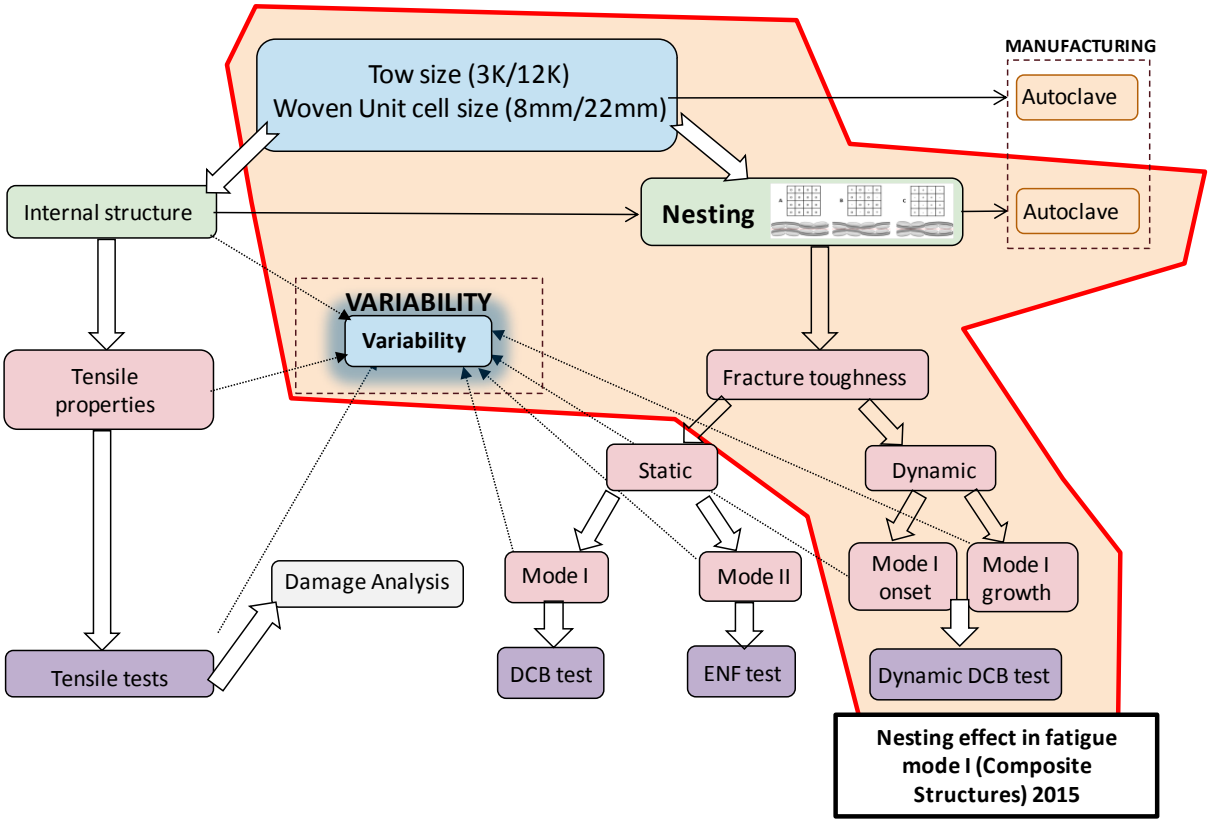

Figure 85: :Topics covered in paper IV

9. FUTURE WORK

The research carried out in this thesis work shows that the fracture behaviour of woven textile composite material changes depending on the internal structure. The obtained conclusions covered the experimental analysis of fracture properties in Mode I and Mode II. There are, however, still important gaps in knowledge to understand the behaviour of this textile material under all static and fatigue fracture loading conditions. The future work related to this dissertation should include next topics:

- *Developing standards for measuring fracture toughness values for textile composite material.*
- *Perform static mixed mode fracture toughness measurements in the textile material selected for this research.*
- *Perform fracture toughness measurements under fatigue in mixed mode and mode II (onset and growth) in the textile material selected for this research.*
- *Investigate other geometrical variables that can affect the fracture toughness properties.*
- *Include wavy surfaces and geometrical variability in numerical models.*
- *Expand the work done in this dissertation to other textile structures.*
- *After the general tendencies and sensitivities have been investigated, attention should be paid to identify scatter with each of these mechanisms*

There is a need of defining *specific standard tests for measuring fracture toughness values for textile composite materials*: the current standards (focused on UD materials)

are limited to smooth delamination propagation, and from the measurements carried out in this research proves that jumpy delamination propagation is a common behaviour. In this dissertation some advices and recommendations are defined for mode I and mode II fracture toughness tests: post-processing methodologies, minimum test lengths, etc. But there are still many factors that should be analysed for obtaining a common standard for different textile configurations.

Static mixed mode fracture toughness measurements should be carried out to analyse how the transitition from pure mode I to pure mode II. In this research it was concluded that for large unit cell sizes the nesting affects the fracture toughness value in mode I, but not for mode II. From the results obtained in mixed mode fracture toughness measurements, it will be possible to evaluate from which mode II/mode I ratio value the nesting affects.

Fracture toughness measurements under fatigue conditions should be performed to understand the overall behaviour of the textile material selected in this research. The effect of the nesting and the unit cell size in fatigue conditions under mode II and mixed mode has not yet been analysed. The results will help to design textile composite structures with improved toughness properties under fatigue conditions.

From the *manufacturing point of view*, the placement of the prepeg layers is at this point a challenging issue, because manual positioning does not have enough accuracy for the correct positioning. The placement of the prepeg layers should be done by new manufacturing processes with the lowest error in warp and weft directions. By application of the optimal nesting position between the layers at specific locations in a component, the fracture toughness value can be improved locally increasing the overall performance.

The *numerical modelling of wavy delaminated surfaces* should be included in numerical models, linking fracture surface geometry with fracture toughness values.

This research has focused on woven textile structures, and other textile structures were not considered. For future work, the repetition of the same analysis in other 2D or 3D textile geometries (satin, braided, etc) will help to generate more general conclusions in relation to textile materials: the *work done in this dissertation should be expanded to other textile structures*.

BIBLIOGRAPHY

1. Chawla, K., *Composite materials: Science and engineering*. 1987, New York: Springer-Verlag.
2. Miravete, *Materiales Compuestos*. 2007.
3. ASM, *ASM Handbook*. 2001.
4. *The Boeing Company*. 2014; Available from: www.boeing.com.
5. *LM Brade Manufacturer*. Available from: www.lmwindpower.com/Blades/Products.aspx.
6. Tong, Mouritzen, and Bannister, *3D fibre reinforced polymer composites*, ed. f. edition. 2002, Oxford: Elsevier.
7. Tan, P., L. Tong, and G. Steven, *Modelling for Predicting the Mechanical Properties of Textile Composites ¾ A Review.* Composites Part A, 1997. **28A**: p. 903-922.
8. Mouritz, A., C. Baini, and I. Herszberg, *Mode I interlaminar fracture toughness properties of advanced textile fibreglass composites.* Composites: Part A, 1999. **30**: p. 12.
9. Lomov, S., et al., *Nesting in textile laminates: geometrical modelling of the laminate.* Composite Science and Technology, 2003. **63**: p. 993-1007.
10. Hoes, K., et al., *Study of nesting induced scatter pf permeability values in layered reinforcement fabrics.* Composites: Part A, 2004. **35**: p. 12.
11. Endruweit, A., et al., *Influence of stochastic fibre angle variations on the permeability of bi-directional textile fabrics.* Composites Part A, 2006. **37**: p. 10.
12. Bickerton, S., et al., *Fabric structure and mold curvature effects on preform permeability and mold filling in the RTM process. Part II. Predictions and comparisons with experiments.* Composites: Part A, 2000. **31**: p. 20.

13. Comas-Cardona, S., et al., *Influence of textile architectures on the compaction and saturated permeability spatial variations*, in *TexComp9*. 2008: Delaware.

14. Skordos, A. and M. Sutcliffe, *Stochastic simulation of woven composites forming.* Composites Science and Technology, 2008. **68**.

15. John, S., I. Herszberg, and F. Coman, *Longitudinal and transverse damage taxonomy in woven composite components.* Composites Part B, 2001. **32**: p. 659–668.

16. Vallons, K., et al., *Loading direction dependence of the tensile stiffness, strength and fatigue life of biaxial carbon/epoxy NCF composites.* Composites Part A: Applied Science and Manufacturing, 2011. **42**: p. 6.

17. Pinho, S., L. Ianucci, and P. Robinson, *Formulation and implementation of decohesion elements in an explicit finite element code.* Composites part A,-Applied Science Manufacturing, 2006. **37**: p. 778-789.

18. Loendersloot, R., *THE STRUCTURE – PERMEABILITY RELATION OF TEXTILE REINFORCEMENTS*. 2006, Universiteit Twente.

19. Liu, K., *Origins of shear strength of polymers and reinforces polymers*. 1997, University of Toronto: Canada.

20. Desplentere, F., et al., *Micro-CT Characterization of Variability in 3D Textile Architecture.* Composites Science and Technology, 2005. **65**(13): p. 1920-1930.

21. Charpis, D., G. Schueller, and M. Pellissetti, *The need for linking micromechanics of materials with stochastic finite elements: A challenge for materials science.* Computational Materials Science, 2007. **41**: p. 10.

22. Gao, F., et al., *Damage accumulation in woven-fabric CFRP laminates undertensile loading: part 1: observations of damage accumulation.* Composite Science and Technology, 1999. **59**(1): p. 123-136.

23. Gao, F., et al., *Damage accumulation in woven-fabric CFRP laminates under tensile loading: Part 2. Modelling the effect of damage on macro-mechanical properties.* Composites Science and Technology, 1999. **59**: p. 137-145.

24. Ernst, G., et al., *Multiscale progressive failure analysis of textile composites.* Composites Science and Technology, 2010. **70**: p. 61-72.

25. Karahan, M. and S. Lomov, *Internal geometry evaluation of non-crimp 3D orthogonal woven carbon fabric composite.* Composites Part A, 2010. **41**(9): p. 1301–1311.

26. Lomov, S., et al., *Experimental methodology of study of damage initiation and development in textile composites in uniaxial tensile test.* Composites Science and Technology, 2008. **68**(12): p. 2340–2349.

27. Daggumati, S., et al., *Local damage in a 5-harness satin weave composite under static tension: part I - Experimental analysis.* Composites Science and Technology, 2010. **70**(13): p. 1926-1933.

28. Daggumati, S., et al., *Local damage in a 5-harness satin weave composite under static tension: part II - Meso-FE modelling.* Composites Science and Technology, 2010. **70**(13): p. 1934-1941.

29. Karkkainen, R. and B. Sankar, *A direct micromechanics method for analysis of failure initiation of plain weave textile composites.* Composites Science and Technology, 2006. **66**: p. 137–150.

30. Naik, N. and V. Ganesh, *An analytical method for plain weave fabric composites.* 1995. **26**(4): p. 281-289.

31. Woo, K. and Y. Suh, *An analytical and experimental study of strength and failure behaviour of plain weave composites.* Journal of composite Technology and research, 2001. **23**(4): p. 239-246.

32. Vaidya, U., et al., *Non destructive evaluation and characterization of microfibers modified textile carbon-phenolic and carbon-carbon composites.* Journal of reinforced plastics and composites, 1997. **16**(11): p. 968-1001.

33. Bolotin, V., *Delaminations in composite structures: its origin, buckling, growth and stability.* Composites Part B, 1996. **27**(2): p. 129-145.

34. Harper, P. and S. Hallet, *A fatigue degradation law for cohesive interface elements – Development and application to composite materials.* International Journal of Fatigue, 2010. **32**: p. 1774-1787.

35. Obreimoff, *The splitting strength of mica.* Proceedings of the Royal Society of London A, 1930: p. 8.

36. Kinloch, A. and R. Young, *Fracture behaviour of polymers*. 1983, Amsterdam: Elsevier.

37. Bucknall, C., *Toughened Plastics*, ed. E.a. science. 1977, London.

38. Williams, J., *Fracture mechanics of Polymers*. 1984, Chichester: Ellis Horwood.

39. Scott, J. and D. Phillips, *Carbon fibre composites with rubber toughened matrices.* Journal of Materials Science, 1975. **10**: p. 551-562.

40. Hunston, D., et al., *Youghened composites.* ASTM STP 937, 1987: p. 21.

41. Ogihara, S. and M. Katsuhiro, *Evaluation of mode III interlaminAr fracture toughness of laminated composites*, in *16th International Conference on Composite Materials*. 2007: Kyoto.

42. Blackman, B. and A. Brunner, *The determination of the mode II fracture resistance, Gii, of unidirectional fibre-composites using the calibrated end loaded split test and an effective crack length apporach*. 2008.

43. international, A.A.S.f.t.a.m., *D5528 Standard test method for mode I interlaminar fracture toughness of unidirectional* in *D 5528*. 1994.

44. International organization for Standardisation, I., *ISO-15024 Fibre-reinforced plastic composites – determination on mode I interlaminar fracture toughness, GIC, for unidirectionally reinforced materials*. 2001.

45. International, A., *6115 Standard test method for Mode I fatigue delamination growth onset of unidirectional fiber-reinforced polymer matrix composites*. 2004.

46. Andersons, J., M. Hojo, and S. Ochiai, *Empirical model for stress ratio effect on fatigue delamination growth ratese in composites laminates.* International Journal of Fatigue, 2004. **26**(6): p. 597-604.

47. Shivakumar, K., et al., *A total fatigue life model for mode I delaminated composite laminates.* International Journal of Fatigue, 2006. **28**(1): p. 33-42.

48. Gregory, J. and S. Spearing, *A fibre bridging model for fatigue delamination in composite materials.* Acta Materialia, 2004. **52**(19): p. 5493-5502.

49. Blanco, N., *Variable Mixe-mode delamination in composite laminate under fatigue conditions: testing and analysis*. 2004, Unievrsitat de Girona.

50. Brunner, A., B. Blackman, and P. Davies, *A status report on delamination resistance testing of polymer-matrix composites.* Engineering fracture mechanics, 2008. **75**: p. 2779-2794.

51. Tay, T., *Characterization and analysis of delamination fracture in composites: An overview of developments from 1990 to 2001.* Applied Mechanics Reviews, 2003. **58**(1): p. 31.

52. *ASTM D7905-14 Standard Test Method for Determination of the Mode II Interlaminar Fracture Toughness of Unidirectional Fiber-Reinforced Polymer Matrix Composites*. 2014.

53. *ISO 15114:2014 Fibre-reinforced plastic composites -Determination of the mode II fracture resistance for unidirectionally reinforced materials using the calibrated end-loaded split (C-ELS) test and an effective crack length approach*. 2014.

54. Martin, R. and B. Davidson. *Mode II fracture toughness evaluation using a four point bend end notch flexure test*. 1997. Manchester, Institute of materials.

55. Beghini, M., L. Bertini, and P. Forte, *Experimental investigation on the influence of crack front to fibre orientation on fatigue delamination growth rate under mode II.* Composites Science and Technology, 2006. **66**(2): p. 240-247.

56. Shindo, Y., *Delamination growth mechanisms in woven glass fiber reinforced polymer composites under Mode II fatigue loading at cryogenic temperatures.* Composite Science and Technology, 2009. **69**: p. 1904-1911.

57. Shindo, Y., *Cryogenic delamination growth in woven glass/epoxy composite laminates under mixed-mode I/II fatigue loading.* Composite Science and Technology, 2011. **71**: p. 647-652.

58. international, A.A.S.f.t.a.m., *D6671/D6671m Standard test method for mixed-mode I-mode II interlaminar fracture toughness of unidirectional fiber-reinforced polymer-matrix composites* 2006.

59. Davijani, A.B., M. Hajikhani, and M. Ahmadi, *Acoustic emission based on sentry function to monitor the initiation of delamination in composite materials,.* Materials and Design, 2011. **31**: p. 3059-3065.

60. Ndiaye, I., A. Maslouhi, and J. Denault, *Characterization of interfacial properties of composite materials by acoustic emission,.* Polymeric composites, 2000. **21**(4).

61. Loutas, T., et al., *Damage evolution in center-holed glass/polyester composites under quasi-static loading using time/frequency analysis of acoustic emission monitored waveforms.* Composites Science and Technology, 2006. **66**: p. 1366-1375.

62. Stutz, S., J. Cugnoni, and J. Botsis, *Studies of mode I delamination in monotonic and fatigue loading using FBG wavelength multiplexing and numerical analysis.* Composites Science and Thecnology, 2011. **71**: p. 443-449.

63. Sorensen, L., et al., *Delamination detection and characterization of bridging tractions using FBG optical sensors.* Composites Part A, 2007. **38**: p. 2087-2096.

64. Sans, D., et al., *Characterization of mixed mode delamination fracture with embedded long FBG sensors and numerical simulations*, in *Comptest 11*. February 2011: Laussane.

65. Briscoe, B., *The Effects of Fabric Weave and Surface Texture on the Interlaminar Fracture Toughness of Aramid/Epoxy Laminates.* Composites Science and Technology, 1993. **47**: p. 261-70.

66. Alif, N., *The efefct of weave pattern and crack propagation direction on mode I delamination resistance of woven glass and carbon composites.* Composites Part B, 1998. **29**(5): p. 603-611.

67. Kim, J., *Impact and delamination failure of woven-fabric composites.* Composites Science and Technology, 2000. **60**: p. 745-761.

68. Gill, A., P. Robinson, and S. Pinho, *Effect of variation in fibre volume fraction on modes I and II delamination behaviour of 5HS woven composites manufactured by RTM.* Composites Science and Technology, 2009. **69**(14): p. 2368-2375.

69. Espinosa, H., *Modelling impact induced delamination of woven fiber reinforced composites with contact/cohesive laws.* Computer Methods in Applied Mechanics and Engineering, 2000. **183**: p. 259-290.

70. Zavattieri, P., L. Hector, and A. Bower, *Determination of the effective mode I toughness of a sinusoidal interface between two elastic solids.* International Journal of fracture, 2007. **145**(3): p. 167-180.

71. Zavattieri, P., L. Hector, and A. Bower, *Cohesive zone simulations of crack growth along a rough interface between two elastic-plastic solids.* Engineering Fracture Mechanics, 2008. **75**: p. 4309-4332.

72. Lu, X., *The sinusoidal crack.* Engineering Fracture Mechanics, 1989. **34**: p. 649-656.

73. Gao, Y. and A. Bower, *A simple technique for avoiding convergence problems in finite element simulations of crack nucleation and growth on cohesive interfaces.* Modelling and Simulation in Materials Science and Engineering, 2004. **12**(3): p. 453-463.

74. Li, B., et al., *Numerical study on the effects of hierarchical wavy interface morphology on fracture toughness.* Computational materials Science, 2011.

75. Benzerga, D., *A mixed-mode damage model for delamination growth applied to a new woven composite.* Computational Materials Science, 2008. **41**: p. 515-521.

76. Hexcel. *Composite manufacturer*. Available from: www.hexcel.com.

77. Coleman, R., *The need for linking micromechanics of materials with stochastic finite elements: A challenge for materials science*. 1984, Duke University: Massachusetts.

78. Karahan, M., et al., *Internal geometry evaluation of non-crimp 3D orthogonal woven carbon fabric composite.* Composites Part A, 2010. **41**: p. 10.

79. Verpoest, I. and S. Lomov, *Virtual textile composiets software Wisetex: integration with micro-mechanical, permeability and structural analysis.* Composite Science and Technology, 2005. **65**: p. 12.

80. Hivet, G. and P. Boisse, *Consistent mesoscopic mechanical behaviour model for woven composite reinforcements in biaxial tension.* Composites Part B, 2008. **39**: p. 16.

81. Hivet, G., et al., *Modelling strategies for fabrics unit cell geometry application to permeability.* Int J Mater Form, 2010. **3**: p. 4.

82. Lomov, S., et al., *Carbon composites based on multi-axial multi-ply stitched preforms. Part 1: Geometry of the preform.* Composites part A, 2002. **33**(9): p. 1171-1183.

83. Saunders, R., C. Lekakou, and M. Bader, *Compression and microstructure of fibre plain woven cloths in the processing of polymer composites.* Composites Part A, 1998. **29**: p. 12.

84. Summerscales, J. and P. Russell, *Observations on the fibre distribution abd fibre strain in a woven fabric reinforcement.* Advanced composites Letters, 2004. **13**(3): p. 6.

85. Koissin, V., et al., *Fibre distribution inside yarn of textile composites: geometrical and FE modelling*, in *TexComp: 8th International Conference on Textile Composites*. 2006: Nottingham, United Kingdom.

86. Yurgatis, S., *Measurement of small angle fiber misalignment in continuous fiber composites.* Composite Science and Technology, 1987. **30**: p. 15.

87. Kratmann, K. and M. Sutcliffe, *A novel image analysis procedure for measuring fibre misalignmebt in unidirectional fibre composites.* Composite Science and Technology, 2009. **69**(2): p. 11.

88. Mlekusch, B., E. Lehner, and W. Geymayer, *Fibre orientation in short fibre reinforced thermoplastics. Contrast enhancement for image analysis.* Composite Science and Technology, 1999. **59**: p. 3.

89. Sun, C., *Mechanics of Aircraft Structures*. 2006: John Wiley and Sons.

90. Mori, T. and K. Tanaka, *Average stress in matrix and average elastic energy of materials with misfitting inclusions.* Acta Metallurgica, 1973. **21**(6): p. 4.

91. Curtis, G., J. Milne, and W. Reynols, *Non-Hookean behaviour of strong carbon fibres* Nature, 1968. **220**: p. 2.

92. Olave, M., et al., *Internal geometry variability of two woven composites and related variability of the stiffness.* Polymer composites, 2012. **33**(8): p. 16.

93. *ASTM D5528 Standard test method for mode I interlaminar fracture toughness of unidirectional fiber-reinforced polymer matrix composites*. 1994.

94. *ISO-15024 Fibre-reinforced plastic composites – determination on mode I interlaminar fracture toughness, GIC, for unidirectionally reinforced materials*. 2001, International organization for Standardisation, ISO.

95. Vanaerschot, A., et al., *Stochastic framework for quantifying the geometrical variability of laminated textile composites using micro-computed tomography.* Composites: Part A, 2013. **44**: p. 10.

96. Davies, P. and D. Moore, *Glass Nylon-6.6 composites-delamination resistance testing.* Composite Science and Technology, 1990. **38**: p. 7.

97. Dharmawan, F., et al., *Mixed mode fracture toughness of GFRP composites.* Composite Structures, 2006. **75**: p. 11.

98. Blake, S.P., K.A. Berube, and R.A. Lopez-Anidp, *Interlaminar fracture toughness of woven E-glass fabric composites.* Journal of composite materials, 2012. **46**(13): p. 10.

99. Baere, I.D., et al., *Study of the Mode I and Mode II interlaminar behaviour of a carbon fabric reinforced thermoplastic.* Polymer Testing, 2012. **31**: p. 11.

100. AIRBUS, *AITM 1.0005: Carbon Fibre reinforced plastics, Determination of interlaminar fracture toughness energy*. 1994.

101. Argüelles, A., et al., *Fatigue delamination, initiation and growth under mode I and mode II of fracture in a carbon-fiber epoxy composite.* Polymer composites, 2010. **31**(4): p. 7.

102. Moura, M.F.d. and A.B. Morais, *Equivalent crack based analyses of ENF and ELS tests.* Engineering fracture mechanics, 2008. **75**: p. 13.

103. Blackman, B., A. Kinloch, and M. Paraschi, *The determination of the mode II adhesive fracture resistance, GIIC, of structural adhlesive joints: an effective crack length method.* Engineering fracture mechanics, 2005. **72**: p. 21.

104. Wang, J. and P. Qiao, *Novel beam analysis of end notched flexure specimen for mode II fracture.* Engineering fracture mechanics, 2004. **71**: p. 13.

105. Arrese, A., et al., *A new method for determining mode II R-curve by the End-Notched flxure test.* Engineering fracture mechanics, 2010. **77**: p. 20.

106. Arrese, A. and F. Mujika, *Influence of bending rotations on three and four-point bend end notched flexure tests.* Engineering fracture mechanics, 2008. **75**: p. 13.

107. Mujika, F., *On the effect of shear and local deformation in three-point bending test.* Polymer Testing, 2007. **26**: p. 9.

108. *ASTM D6115 Standard test method for mode I fatigue delamination growth onset of unidirectional fibre reinforced polymer-matrix composites*. 1997.

109. Olave, M., et al., *Nesting effect on the mode I fracture toughness of woven laminates.* Composites Part A, 2015.

110. *ASTM E647 - 11e1 Standard Test Method for Measurement of Fatigue Crack Growth* 2011.

111. Murri, G. *Effect of data reduction and fiber-bridging on mode I delamination characterization of Unidireccional composites*. in *26th Annual technical conference of the American Society for composites*. 2011. Montreal.

112. Murri, G., *Evaluation of Delamination Onset and Growth Characterization Methods under Mode I Fatigue Loading*. 2013, NASA Langley Research Center: Hampton, VA, United States.

113. Chen, H., K. Shivakumar, and F. Abali, *Application of total fatigue life model to T700 carbon/vivyl ester composite.* Composites: Part B, 2008. **39**: p. 6.

114. Yao, L., et al., *Bridging effect on mode I fatigue delamination behaviour in composite laminates.* Composites Part A, 2014. **63**: p. 7.

115. Castillo, E., et al., *A fatigue model with local sensitivity analysis.* International journal of fatigue, 2007. **30**: p. 20.

116. Ruiz, M., *A Statistical fatigue model covering the tension and compression Wöhler fields and allowing damage accumulation*, in *Departamento de Matemática aplicada y ciencias de la computación* 2008, Universidad de Cantabria: Santander.

117. *Profatigue code.* . Department of Contruction and Manufacturing Engineering, University of Oviedo. Free-use software.

118. Castillo, E. and A. Fernandez-Cantelli, *A unified statistical methodology for modeling fatigue damage*. 2009: Springer.

119. Argüelles, A., et al., *Influence of temperature on the delamination process under mode I fracture and dynamic loading of two carbon–epoxy composites.* Composites Part B, 2015. **68**: p. 8.

120. Stelzer, S., et al., *Mode I delamination fatigue crack growth in unidirectional fiber reinforced composites: Development of a standarized test procedure.* Composite Science and Technology, 2012. **72**: p. 6.

121. Olave, M., et al., *Nesting effect on the mode II fracture toughness of woven laminates.* Composites Part A, 2015.

CURRICULUM VITAE

Education

- PhD in Mechanical Engineering, Katholieke Universiteit Leuven (KUL), Belgium, 2010-present.
- 2003- 2004: Master in materials: POLYMERS & COMPOSITES (KULeuven).
- 2004: Master thesis KULeuven "Analysis of acoustic absorption".
- 1997-2002: Mechanical engineering (Mondragón unibertsitatea, Spain)

Published journal papers

1. Olave M., Vara I., Usabiaga H., Aretxabaleta L., Lomov S.V. and Vandepitte D., Mode I fatigue fracture toughness of woven laminates: nesting effect, ***Composite Structures*** (2015), 10.1016/j.compstruct.2015.07.073
2. Olave M., Vara I., Usabiaga H., Aretxabaleta L., Lomov S.V. and Vandepitte D., Nesting effect on the mode I fracture toughness of woven laminates, ***Composites Part A*** (2015), 10.1016/j.compositesa.2015.03.017

3. Olave M., Vara I., Usabiaga H., Aretxabaleta L., Lomov S.V. and Vandepitte D., Nesting effect on the mode II fracture toughness of woven laminates, ***Composites Part A*** (2015), 10.1016/j.compositesa.2015.03.020
4. Xu, J., Lomov, S.V., Verpoest, I., Daggumati, S., Van Paepegem, W., Degrieck, J., Olave, M., A progressive damage modelo of textile composites on meso-scale using finite element method: static damage analysis, ***Journal of Composite Materials***, 2013, doi:10.1177/0021998313507008
5. Olave, M., Vanaerschot, A., Lomov, S. V. and Vandepitte, D., Internal geometry variability of two woven composites and related variability of the stiffness. ***Polym Compos***. Volume 33, Issue 8, Pages: 1335-1350, 2012
6. Olave M, Sagartzazu X, Damian J, Serna A, Load distribution in a four contact-point slewing bearing taking into account the stiffness of the rings and the supporting structures, ***Journal of Mechanical Design***, Volume 13, Issue 2, 2010.
7. Mujika F, Pujana J, Olave M, On the determination of out-of-plane elastic properties of honeycomb sandwich panels, ***Polymer Testing***, Volume 30, Issue 2, Pages: 222-228, 2010

Conference papers

1. Olave M, Vara I, Usabiaga H, Aretxabaleta L, Lomov SV, Vandepitte D, Does unit cell size affect? an overview of mechanical properties of woven laminates, ICCM20, Copenhagen, Denmark, July 2015

2. Olave M, Vara I, Usabiaga H, Aretxabaleta L, Lomov SV, Vandepitte D, Mode II fracture toughness of woven laminates: unit cell size efefct, Comptest2015, Madrid, April 2015

3. Olave M, Vara I, Aretxabaleta L, Lomov SV, Vandepitte D, Nesting and size effect on the mode I fatigue fracture toughness of woven laminates, ECCM16, Seville, June 2014
4. Vara I, Olave M, Fracture characterization in Modo I and modo II of a textil material, MATCOMP, Algeciras, Spain, July 2013

5. Olave M, Aretxabaleta L, Stepan S, Vandepitte D, Modelling of nesting effect on the delaminated surface for woven structures, ECCM15, Venice, Italy, June 2012.
6. Vanaerschot, A., Olave, M., Lomov, S., Vandepitte, D., A stochastic multi-scale framework for textile composites to evaluate the stiffness tensor. AIAA Non-deterministic approaches conference. Honolulu, Hawai, 23-26 April 2012.
7. Olave M, Xu J, Lomov S, Vandepitte D, Mechanical behaviour and damage initiation comparison between textile materials with the same architecture but different tow size, ECCOMAS Composites 2011, Hannover, Germany, September 2011.
8. Olave M, Xu J, Lomov S, Vandepitte D, Internal geometry variability evaluation of two woven structures, ICCS16 International conference in composite structures, Porto, Portugal, June 2011.
9. Olave M, Xu J, Lomov S, Vandepitte D, Mechanical property and internal geometry variability evaluation in woven materials, MATCOMP, Girona, Spain, July 2011.
10. Joseba Pujana, M. Olave, F. Mujika, Characterization of Unsymmetrical sandwich panels by three point bending tests, TestComp, Laussane (Switzerland), 2011.
11. Jian XU, Mireia Olave, Subbareddy Daggumati, Stepan V. Lomov, Ignaas Verpoest, Wim Van Paepegem, Joris Degrieck, Damage analysis of twil-weave carbon//epoxy composites subjected to quasi-static loading: materials characteriation and FEM modeling, Texcomp10, Lille (France), 2010.
12. M. Olave, J. Iriondo, M. Aguirre, Modelling of an aluminium skin and pp honeycomb core sandwich material under low energy impact, ECCM14 European Conference on Composite Materials, Budapest, 2010.
13. Villarreal, M. Rivas, L. Rodriguez-Martinez, L. Otaegi, A. Zabala,N. Gomez, M. Alvarez, I. AnteparaN. Arizmendiarrieta, J. Manzanedo, M. OlaveA. Urriolabeitia, N. Burgos, F. Castro and A. Laresgoiti, Tubular Metal Supported SOFC Development for Domestic Power Generation, Solid Oxide Fuel Cells, Eleventh International Symposium (SOFC-XI), Viena, 2009.